



FRP Shear Strengthening of Concrete Beams

by

KAGAN SOGUT

A thesis submitted to the University of Birmingham

for the degree of

DOCTOR OF PHILOSOPHY

Department of Civil Engineering

School of Engineering

College of Engineering and Physical Sciences

University of Birmingham

January 2022



University of Birmingham Research Archive

e-theses repository

This unpublished thesis/dissertation is copyright of the author and/or third parties. The intellectual property rights of the author or third parties in respect of this work are as defined by The Copyright Designs and Patents Act 1988 or as modified by any successor legislation.

Any use made of information contained in this thesis/dissertation must be in accordance with that legislation and must be properly acknowledged. Further distribution or reproduction in any format is prohibited without the permission of the copyright holder.

ABSTRACT

The necessity of strengthening concrete beams appears in cases where concrete beams are subjected to deterioration mainly instigated by heavier traffic loads, poor initial design, aggressive exposure conditions, natural or man-made extreme events, and steel reinforcement corrosion. All these circumstances may lead to catastrophic consequences unless immediate precautions are taken. Many cost-effective, practical, and durable fibre reinforced polymer (FRP) shear strengthening solutions have emerged in response to the increasing number of shear-deficient concrete structures. Both the externally bonded (EB) and near-surface mounted (NSM) FRP shear strengthening systems have been demonstrated to enhance the shear resistance of existing reinforced concrete (RC) beams. However, these systems require laborious surface preparation and, unless properly anchored, debond prematurely from the concrete. The Deep Embedment (DE), also known as the embedded through-section (ETS), shear strengthening technique has been developed to eliminate the shortcomings of these techniques. Previous research studies proved the effectiveness of the DE technique. However, the effects of steel-to-FRP shear reinforcement ratio, presence of existing holes, beam size, and shear span-to-effective depth (a/d) ratio on the DE FRP-strengthened behaviour have not yet been fully understood. In particular, the effects of tension reinforcement ratio and embedded length of FRP bars on the DE FRP-strengthened behaviour have not yet been identified. The DE shear strengthening technique used in this study consisted of glass FRP (GFRP) or carbon FRP (CFRP) bars embedded into the concrete core to act as additional shear reinforcement. The fifteen RC T-beams, which comprised the experimental programme of this research, were designed, fabricated, and tested at the University of Birmingham Structural Engineering Laboratory. Test parameters

were steel-to-FRP shear reinforcement ratio, tension reinforcement ratio, presence of existing holes, embedded length of FRP bars, and a/d ratio. Moreover, beam size was also considered as a parameter for the investigation. The results from the experimental programme demonstrated that the concrete and DE FRP reinforcement contributions to shear resistance as well as total shear force capacity all decreased with increasing steel-to-FRP shear reinforcement ratio. The total shear force capacity of strengthened beams decreased by up to 33.7% with increasing steel-to-FRP shear reinforcement ratio from 1.35 to 3.82. The DE FRP and concrete contributions to the shear resistance also decreased by up to 39.2% and 62.8%, respectively, when steel-to-FRP shear reinforcement ratio was increased from 1.35 to 3.82. The tension reinforcement influenced the failure mode of tested beams but had an insignificant impact on shear strength enhancement. Existing holes instigated premature shear failure in RC T-beams before reaching their nominal shear force capacity. The shear strength reduction due to existing holes ranged from 7 to 22%. The embedded length of FRP bars had a clear effect on shear resistance. Both the DE FRP reinforcement contribution and the total shear resistance increased by up to 197.8% and 91.1%, respectively, with increasing embedded length from 262.5 to 300 mm. The concrete contribution to the shear resistance and total shear force capacity increased with decreasing a/d ratio, whereas the contribution of DE FRP reinforcement decreased with decreasing a/d ratio. Experimental results also suggested that DE FRP reinforcement significantly mitigated the size effect in the strengthened beams. The reduction in shear stress at failure of the unstrengthened and strengthened beams was 50% and 18%, respectively. The corresponding values for deep beams were 26% and 10%, respectively.

Moreover, a nonlinear finite element (FE) model was developed, validated, and used to conduct parametric studies. The crucial parameters impacting the shear behaviour of

strengthened beams were examined numerically after validating the FE model by comparing experimental results reported in this study and published literature with numerical predictions. Limitations in current shear strengthening design guidance and existing design models were also identified, and new design equations were proposed and demonstrated to give accurate predictions.

DEDICATION

This thesis is dedicated to:

The memory of my grandmother

My mother and father

My Wife

ACKNOWLEDGEMENTS

First of all, I would especially like to express my innermost gratitude to my supervisor, Dr Samir Dirar, who always encourages, helps, and guides me. I will always be proud of being his PhD student. I also want to thank my co-supervisors, Dr Marios Theofanous and Dr Asaad Faramarzi, for their support throughout my PhD research.

I am grateful to the Ministry of National Education of Turkey for sponsoring my PhD research.

My sincere thanks also go to the technicians at the University of Birmingham Structural Engineering Laboratories for their help and support.

Last but not least, I want to express heartfelt gratitude to my parents, brother, cousins, aunt and aunt`s husband for their unending support. My special thanks and love also go to my wife for her unwavering support and tremendous patience throughout my PhD research.

TABLE OF CONTENTS

ABSTRACT	I
DEDICATION	IV
ACKNOWLEDGEMENTS	V
TABLE OF CONTENTS	VI
LIST OF FIGURES	X
LIST OF TABLES	XV
CHAPTER 1: INTRODUCTION	1
1.1. Background	1
1.2. Research significance	4
1.3. Aim and Objectives	5
1.4. Thesis structure	6
1.5. List of publications	7
CHAPTER 2: LITERATURE REVIEW	9
2.1. General	9
2.2. Shear in reinforced concrete beams	9
2.2.1. Shear in uncracked beams	10
2.2.2. Shear in cracked beams without shear links	10
2.2.2.1. Shear transfer mechanisms	13
2.2.2.2. Significant parameters governing shear behaviour	16
2.2.3. Function of shear links in an RC beam	18
2.3. Shear resistance models for cracked beams	19
2.3.1. Analytical models	19
2.3.2. The Modified Compression Field Theory (MCFT) and Disturbed Stress Field Model (DSFM)	23
2.4. Shear strengthening with fibre-reinforced polymer (FRP) composites	27
2.4.1. General properties of FRP composites	27

2.4.2. RC beams strengthened in shear with FRP composites	29
2.4.2.1. Externally bonded (EB) FRP systems	29
2.4.2.2. Near-surface mounted (NSM) technique	31
2.4.2.3. Deep Embedment (DE) technique	31
2.5. Previous studies on DE shear strengthened RC beams.....	33
2.5.1. Existing unfilled holes	33
2.5.2. DE bar type	34
2.5.3. DE bar spacing, diameter, and inclination angle	36
2.5.4. Steel shear link ratio	37
2.5.5. a/d ratio	38
2.5.6. Size effect	40
2.5.7. Corroded shear links	41
2.5.8. Anchorage system and Prestressed DE bar	42
2.6. Summary and conclusions	44
CHAPTER 3: EXPERIMENTAL PROGRAMME	48
3.1. General	48
3.2. Preparation of beams	49
3.2.1. Description of beams	50
3.2.2. Fabrication of specimens	56
3.2.3. Strengthening process	57
3.3. Material properties	59
3.3.1. Concrete	59
3.3.2. Steel reinforcement	62
3.3.3. Fibre reinforced polymer and epoxy resin	62
3.4. Test setup and instrumentation	63
3.5. Summary and conclusions	68
CHAPTER 4: EXPERIMENTAL RESULTS AND DISCUSSION	70
4.1. General	70
4.2. Experimental observations and measurements	71
4.2.1. Unstrengthened beams	71
4.2.2. Strengthened beams	75

4.2.2.1. First group of strengthened beams	75
4.2.2.2. Second group of strengthened beams	80
4.2.2.3. Third group of strengthened beams	84
4.3. Discussion	88
4.3.1. Shear strength	88
4.3.2. Components of Shear Resistance	92
4.3.2.1. Unstrengthened beams	92
4.3.2.2. Strengthened beams	95
4.3.3. Effect of steel-to-FRP shear reinforcement ratio	99
4.3.4. Size effect	102
4.3.5. Effect of shear span-to-effective depth ratio (a/d)	106
4.3.6. Effect of FRP bar depth	107
4.3.7. Effect of holes	109
4.4. Summary and conclusions	110
CHAPTER 5: FINITE ELEMENT MODELLING	112
5.1. General	113
5.2. FE model	113
5.2.1. Geometric modelling, element, and mesh details	114
5.2.2. Material modelling	117
5.2.2.1. Concrete	117
5.2.2.2. Steel and FRP reinforcement	120
5.2.3. Solution algorithm	122
5.3. Validation	123
5.3.1. Overall response	123
5.3.2. Unstrengthened beams	125
5.3.3. Strengthened beams	127
5.4. FE modelling of beams in published literature	130
5.4.1. Experimental programme	131
5.4.1.1. Mofidi et al. (2012a)	131
5.4.1.2. Jemaa et al. (2015)	133
5.4.2. Validation	134
5.5. Summary and conclusions	139

CHAPTER 6: PARAMETRIC STUDY AND DESING OF DE FRP STRENGTHENED RC BEAMS.....	140
6.1.General	140
6.2.Parametric study	141
6.2.1. Size effect	141
6.2.2. Tension reinforcement ratio	143
6.2.3. Shear span-to-effective depth ratio (a/d)	145
6.2.4. Interaction between existing steel shear links and FRP bars	146
6.3.Design models	151
6.3.1. Existing design models	151
6.3.2. Proposed design models	155
6.3.2.1. Proposed design framework	155
6.3.2.2. Proposed shear design equations for beams with low existing steel shear reinforcement ratios	157
6.3.2.3. Proposed shear design equations for beams with high existing steel shear reinforcement ratios	159
6.3.3. Comparison between existing and proposed design models	160
6.4.Summary and conclusions	163
CHAPTER 7: CONCLUSIONS AND RECOMMENDATIONS	170
7.1. General	170
7.2. Conclusions	171
7.3. Recommendations in support of future work	173
REFERENCES	175

LIST OF FIGURES

Figure 2.1. Kani`s concrete teeth model (Kani, 1964)	11
Figure 2.2. Kani`s valley diagram (redrawn from Kani, 1964)	12
Figure 2.3. Shear transfer mechanisms (redrawn from ASCE-ACI Committee 426, 1973)	14
Figure 2.4. Ritter- Mörsch truss model (Subramanian, 2013)	20
Figure 2.5. Equations proposed for the MCFT (Bentz et al., 2006)	23
Figure 2.6. Comparison of different types of FRP to steel	28
Figure 2.7. Various configurations of the EB FRP system (ACI 440.2R-17, 2017)	30
Figure 2.8. Configuration of an embedded FRP bar	32
Figure 2.9. Tested beams (Dirar and Theofanous, 2017)	39
Figure 2.10. Test setup (Qin et al., 2015)	42
Figure 2.11. Mechanically anchored GFRP bar (Bui et al., 2020a)	43
Figure 3.1. Details of slender beams; (a) cross-section of beams (b) elevation of beams (c) FRP and steel reinforcement details (units in millimetres)	54
Figure 3.2. Details of deep beams; (a) cross-section of beams (b) elevation of beams (units in millimetres)	55
Figure 3.3. Fabrication of specimens; (a) steel reinforcement cage (b) wood formwork (c) casting concrete	57
Figure 3.4. Embedding FRP bars; (a) PVC rods (b) a thin layer adhesive on an FRP bar (c) Embedded FRP bars	59

Figure 3.5. Experimental setup of slender and deep beams (a) schematic view of slender beams (b) schematic view of deep beams (c) slender beam before testing (d) deep beam before testing (units in units in millimetres)	64
Figure 3.6. Positions of strain gauges (a) Deep beams (b) Slender beams with 6 FRP bars (c) Slender beams with 3 FRP bars (units in millimetres)	66
Figure 3.7. Strain gauges (a) on tension reinforcement (b) on 4 mm diameter steel shear link (c) on GFRP bar with protective coating (d) on tension reinforcement with protective coating	68
Figure 4.1. Crack patterns of the unstrengthened slender beams at failure	71
Figure 4.2. Crack pattern of the unstrengthened deep beam at failure	72
Figure 4.3. Shear force vs deflection for the unstrengthened beams	73
Figure 4.4. Shear force vs strain in the steel shear links of the unstrengthened beams	74
Figure 4.5. Crack patterns at failure (slender beams strengthened with 3 FRP bars)	76
Figure 4.6. Shear force vs deflection for the strengthened slender beams with 3 FRP bars..	77
Figure 4.7. Shear force vs strain in steel shear links of the strengthened slender beams with 3 FRP bars	78
Figure 4.8. Shear force vs strain in the FRP bars of the strengthened slender beams with 3 FRP bars	79
Figure 4.9. Crack patterns at failure (strengthened slender beams with 6 FRP bars)	80
Figure 4.10. Shear force vs deflection for the strengthened slender beams with 6 FRP bars	81
Figure 4.11. Shear force vs strain in the steel shear links of the strengthened slender beams with 6 FRP bars	82
Figure 4.12. Shear force vs strain in the longitudinal reinforcement of S/S/2.0/G6-325	83

Figure 4.13. Shear force vs strain in the FRP bars of the strengthened slender beams with 6 FRP bars	84
Figure 4.14. Crack patterns at failure (strengthened deep beams with 2 FRP bars)	85
Figure 4.15. Shear force vs deflection for the strengthened deep beams with 2 FRP bars ...	86
Figure 4.16. Shear force vs strain in the steel shear links of the strengthened deep beams with 2 FRP bars	87
Figure 4.17. Shear force vs strain in the FRP bars of the strengthened deep beams with 2 FRP bars	87
Figure 4.18. Components of shear resistance (a) U/S/2.0 (b) U/S/2.7 (c) U/S/2.7/H3-325, (d) U/S/2.0/H6-325 (e) U/D/2.7	94
Figure 4.19. Components of shear resistance (a) S/S/2.0/G3-325, (b) S/S/2.7/G3-325, (c) S/S/2.7/G6-262.5, (d) S/S/2.7/G6-325, (e) S/S/2.7/C3-325, (f) S/D/2.7/G2-325, (g) S/D/2.7/C2-325	98
Figure 4.20. Experimental variations of V_c and V_f vs. steel-to-FRP shear reinforcement ratio: (a) V_c , (b) V_f ,	101
Figure 4.21. Effect of size on shear strength for slender beams	103
Figure 4.22. Components of shear stress for slender beams at failure	104
Figure 4.23. Effect of size on shear strength for deep beams	105
Figure 4.24. Experimental variations of V_c and V_f vs. a/d ratio: (a) V_c , (b) V_f ,	107
Figure 4.25. Effect of FRP bar depth on (a) V_t (b) V_f	108
Figure 4.26. Shear stress at failure vs. A_n/A_t	109
Figure 5.1. FE model (a) slender beam (b) deep beam	113
Figure 5.2. Rectangular plane stress element (Vector2 & Formworks User`s Manual, 2013)	114

Figure 5.3. Comparison of different mesh sizes	115
Figure 5.4. Truss element (Vector2 & Formworks User`s Manual, 2013)	116
Figure 5.5. Experimental and FE-predicted shear force-deflection curves for the un strengthened beams	125
Figure 5.6. Experimental and FE-predicted crack patterns at failure for the unstrengthened beams	126
Figure 5.7. Experimental and FE-predicted shear force-deflection curves for strengthened beams	128
Figure 5.8. Experimental and FE-predicted crack patterns at failure for the strengthened beams	130
Figure 5.9. Elevation and cross-sections of the beams tested by Mofidi et al. (2012a) (dimensions in millimetres)	132
Figure 5.10. Cross-section and elevation of tested beams (Jemaa et al., 2015) (dimensions in millimetres)	134
Figure 5.11. FE modelling (a) Mofidi et al. (2012a) (b) Jemaa et al. (2015)	135
Figure 5.12. Experimental and FE-predicted shear force-deflection curves for the beams tested by Mofidi et al. (2012a) and Jemaa et al. (2015)	138
Figure 6.1. Normalised shear stress vs. $\log(d)$	143
Figure 6.2. Effect of tension reinforcement ratio	144
Figure 6.3. Effect of a/d ratio on predicted (a) Shear force capacity (b) Shear force gain provided by FRP bars	146
Figure 6.4. Components of shear resistance for the beams tested by Qin (2016)	147
Figure 6.5. Components of shear resistance for the tested beams	148

Figure 6.6. Effect of steel-to-FRP shear reinforcement ratio for DE FRP-strengthened beams with low existing steel shear reinforcement ratios	149
Figure 6.7. Effect of steel-to-FRP shear reinforcement ratio for DE FRP-strengthened beams with high existing steel shear reinforcement ratios	150
Figure 6.8. FRP-to-steel shear resistance ratio vs. steel-to-FRP shear reinforcement ratio for DE FRP-strengthened beams with low existing steel shear reinforcement ratios	158
Figure 6.9. $V_f / (V_c + V_f)$ vs. steel-to-FRP shear reinforcement ratio for DE FRP-strengthened beams with high existing steel shear reinforcement ratios	159

LIST OF TABLES

Table 2.1. Summary of previous studies on RC beams strengthened with the DE technique	47
Table 3.1. Details of tested beams	51
Table 3.2. Concrete mixture	60
Table 3.3. Average concrete compression test result for each specimen	61
Table 3.4. Material properties of steel reinforcement bars	62
Table 4.1. Experimental results	90
Table 4.2. Axial rigidity of the FRP bars and steel shear links	91
Table 5.1. Summary of FE model	122
Table 5.2. Comparison between experimental results and FE predictions	124
Table 5.3. Material properties of the RC T-beams tested by Mofidi et al. (2012a)	132
Table 5.4. Material properties of the RC T-beams tested by Jemaa et al. (2015)	134
Table 5.5. Experimental results and FE predictions for the beams tested by Mofidi et al. (2012a) and Jemaa et al. (2015)	137
Table 6.1. Details of RC T-beams	142
Table 6.2. Details of DE FRP shear-strengthened RC beams with low existing steel shear reinforcement ratios	166
Table 6.3. Comparison between existing and proposed design models for DE FRP shear-strengthened RC beams with low existing steel shear reinforcement ratios	167

Table 6.4. Details of DE FRP shear-strengthened RC beams with high existing steel shear reinforcement ratios	168
--------------------------------------------------------------------------------------------------------------------	-----

Table 6.5. Comparison between existing and proposed design models for DE FRP shear-strengthened RC beams with high existing steel shear reinforcement ratios	169
--------------------------------------------------------------------------------------------------------------------------------------------------------------------	-----

CHAPTER 1: INTRODUCTION

1.1. Background

A significant number of concrete infrastructures exhibit substandard conditions mainly instigated by heavier traffic loads, poor initial design, aggressive exposure conditions, natural or man-made extreme events, and steel reinforcement corrosion (Valerio and Ibell 2003; Valerio et al., 2009; Dirar et al., 2013a; Thermou et al., 2019; Sogut et al., 2021). The shear strength of existing reinforced concrete (RC) beams can be deteriorated by all these circumstances. Thus, replacement or repair of existing shear deficient RC beams can become a necessity. Many cost-effective, practical, and durable shear strengthening techniques have emerged to counteract brittle and sudden shear failures in structurally deficient RC beams. For example, externally bonded (EB) and near-surface mounted (NSM) fibre reinforced polymer (FRP) shear strengthening techniques have been verified to enhance shear resistance of existing RC beams (Triantafillou, 1998; De Lorenzis and Nanni, 2001; Rizzo and De Lorenzis, 2009; Rahal and Rumaiah, 2011; Dirar et al., 2012; Qin et al., 2015). In addition to these techniques, fibre-reinforced cementitious matrix (FRCM) systems were also introduced to eliminate the shortcomings emerging from using epoxy (e.g., Triantafillou and Papanicolaou, 2006; Gonzalez-Libreros et al., 2017; Thermou et al., 2019). Some of these shortcomings include its higher cost, lower fire resistance, and difficulty of applying to wet surfaces (Triantafillou and Papanicolaou, 2006; Gonzalez-Libreros et al., 2017; Thermou et al., 2019). Based on the textile type, the FRCM systems are designated as textile-

reinforced mortar (TRM), poliparafenilen benzobisoxazole fibre-reinforced cementitious matrix (PBO-FRCM) and steel-reinforced grout (SRG) (e.g., Triantafillou and Papanicolaou, 2006; D'Ambrisi et al., 2013; Tetta et al., 2015; Gonzalez-Libreros et al., 2017; Thermou et al., 2019) However, the efficacy of the EB, NSM, and FRCM shear strengthening techniques is governed by the bond behaviour between concrete and textiles or reinforcement. Moreover, EB, NSM, and FRCM strengthening systems require laborious surface preparation and, unless properly anchored, debond prematurely from the concrete (Sogut et al., 2021; Sogut et al., 2022). To eliminate these shortcomings, the deep embedment (DE) technique (Valerio and Ibell, 2003), also known as the embedded through-section (ETS) technique (Chaallal et al., 2011), has emerged as an alternative shear strengthening solution for existing shear-deficient RC beams. In this technique, FRP and/or steel bars are inserted into epoxy-filled holes drilled throughout the entire depth of the beam, thereby connecting the compression chord to the tension chord and ensuring that truss action can be fully developed. The DE technique is also advantageous where the flange and/or web are inaccessible (Valerio and Ibell 2003; Valerio et al., 2009; Sogut et al., 2022). It is acknowledged that it might be difficult to drill holes in RC beams with existing steel reinforcement. However, it is worth noting that existing shear-deficient RC beams have a relatively low shear reinforcement ratio. The locations of existing steel bars can be obtained from as-built drawings and/or by using cover metres. This process helps to ensure the position of the vertical and/or inclined holes. The embedded length of FRP and/or steel bars may also play an important role in the effectiveness of this technique. The reduction in the embedded length of FRP and/or steel bars may not allow connection of the compression chord to the tension chord.

Previous research work on DE FRP shear strengthening provided valuable findings with regard to the effects of the presence of existing unfilled holes and internal steel shear

reinforcement (Valerio and Ibell, 2003; Valerio et al., 2009; Mofidi et al. 2012a). The effect of the presence of existing unfilled holes on the behaviour of RC beams was investigated by performing a test on a rectangular concrete beam (Valerio and Ibell, 2003). However, it is also necessary to carry out an experimental study to investigate this effect on the behaviour of RC T-beams. Previous studies have shown that the presence of existing shear reinforcement significantly decreases the effectiveness of the DE technique (e.g., Chaallal et al., 2011; Mofidi et al. 2012a, Breveglieri et al., 2015). It has therefore been recognised that the steel-to-FRP shear reinforcement ratio is one of the main parameters governing the strengthened behaviour. However, experimental and numerical research examining the effect of steel-to-FRP shear reinforcement ratio is limited (Breveglieri et al., 2015; Qapo et al., 2016). The effects of the DE bar diameter and spacing, shear link corrosion level and moment-shear interaction were also examined (Mofidi et al., 2012a; Qin, 2015; Raicic et al., 2017). However, the effects of other parameters that may also influence the strengthened behaviour have not yet been fully understood (Sogut et al. 2021). For example, tension reinforcement ratio has been demonstrated to influence the behaviour of EB FRP-strengthened beams (Dirar et al. 2012). However, the effect of tension reinforcement ratio on the behaviour of DE FRP-strengthened beams has not yet been identified (Sogut et al. 2021). Moreover, a significant number of experimental tests were performed on DE FRP-strengthened beams with relatively small cross-section dimensions compared to strengthened beams with large cross-section dimensions (Valerio and Ibell, 2003; Mofidi et al., 2012a; Qin et al., 2015; Breveglieri et al., 2015, Bui et al., 2020a). This is of particular concern as size effect in RC beams instigates a reduction in shear strength and a transition from ductile to brittle behaviour with the increase in beam size (Kani, 1967; Bažant, 1997). It is therefore important to quantify size effect in DE FRP-strengthened beams. However, the sole experimental research involving two geometrically similar DE FRP-strengthened

beams was carried out by Brindley (2018) to investigate the effect of beam size. Further experimental research is therefore needed to fill the knowledge gap with regard to the size effect in RC beams strengthened in shear with embedded FRP bars. It is a well-known issue that the shear span-to-effective depth (a/d) ratio has a significant impact on the behaviour of RC beams (Kani, 1964; Kani 1967). However, the effect of a/d ratio on the DE strengthened behaviour has received less attention. Similar to the effect of beam size, current literature includes only one experimental study, which was conducted by Dirar and Theofanous (2017). As mentioned previously, the embedded length of FRP bars may influence the strengthened behaviour. However, the effect of embedded length of the FRP bars on the behaviour of DE FRP-strengthened beams has not yet been reported. Analytical models for predicting the contribution of the DE bars to the shear strength were also proposed (Valerio and Ibell, 2003; Mofidi et al. 2012a; Rahman et al., 2018; Raicic, 2019). However, it has emerged that the existing DE FRP-shear strengthening design models in the published literature give conservative predictions (Qapo et al., 2015; Dirar and Theofanous, 2017; Raicic, 2019; Sogut et al., 2021). New design equations which can adequately estimate shear force capacity of the DE FRP-strengthened beams are therefore required.

1.2. Research significance

Shear strengthening of existing RC structures with embedded FRP bars is an area with great potential, particularly in situations when the flange and/or web are inaccessible. The embedded FRP bars are less susceptible to debonding issues when compared with unanchored EB and NSM shear strengthening systems. Yet, the main parameters influencing the strengthened behaviour are not fully understood as discussed in Section 1.1. This PhD study provides valuable insights into the effect of main parameters on the strengthened

behaviour. The investigated parameters are given in the following section. Moreover, it identifies limitations in current shear strengthening design guidance and existing design models and presents new design equations that have been demonstrated to give better predictions.

1.3. Aim and Objectives

The aim of this PhD research is to develop a better understanding of the behaviour of RC T-beams strengthened in shear with DE FRP bars.

The following is a list of research objectives:

- To quantify the effects of the existing steel-to-embedded FRP shear reinforcement ratio and shear span-to-effective depth (a/d) ratio on the shear behaviour of DE FRP-strengthened RC beams.
- To examine size effect in DE FRP-strengthened RC beams.
- To explore the effect of tension reinforcement ratio on the behaviour of DE FRP-strengthened RC beams.
- To determine the effect of existing holes on the shear behaviour of RC T-beams.
- To investigate the influence of the embedded length of FRP bars on the DE FRP-strengthened behaviour.
- To conduct a finite element (FE) parametric study of RC T-beams strengthened in shear with embedded FRP bars by making use of the validated FE model.
- To review the accuracy of existing design models to strengthen RC beams in shear with the DE FRP strengthening system and propose new design equations for DE FRP-strengthened beams.

1.4. Thesis structure

This thesis including experimental and numerical research on DE FRP-strengthened beams consists of seven chapters as follows:

Chapter 1 provides brief background, research significance, and aim and objectives of the thesis.

Chapter 2 overviews the shear behaviour of uncracked and cracked concrete beams. This chapter also includes general properties of FRP composites with benefits emerging from their usage and addresses previous studies on RC beams strengthened in shear with the DE technique.

Chapter 3 details an experimental programme conducted at the University of Birmingham Structural Engineering Laboratory. The details on fabrication process and DE shear strengthening scheme of fifteen RC beams together with material properties and experimental setup are given in this chapter.

Chapter 4 presents experimental observations and measurements, including shear force capacity, deflection, failure mode, and strain in the steel shear links and FRP bars. The experimental results are also discussed in this chapter.

Chapter 5 introduces a nonlinear FE predictive tool to numerically simulate tested beams reported in Chapter 4 and DE FRP-strengthened beams reported in the literature.

Chapter 6 presents a parametric study of DE FRP-strengthened beams. The investigation of crucial parameters impacting the strengthened behaviour and the evaluation of the accuracy of existing design models together with proposed new design equations are included in this chapter.

Chapter 7 summaries main findings of this study. Recommendations for future work are also given in this chapter.

1.5. List of publications

Some of content presented in this thesis has already been published in some of following journal and conference papers.

Sogut K., Dirar S., Theofanous M., Faramarzi A. and Nayak A. N. (2021). Effect of transverse and longitudinal reinforcement ratios on the behaviour of RC T-beams shear strengthened with embedded FRP bars, *Composite Structures*, 113622.

Sogut K., Dirar S., Theofanous M. and Faramarzi A. (2022). Effect of FRP bar type on the behaviour of shear-strengthened reinforced concrete T-beams, In: Ilki A., Ispir M., Inci P. (eds), *10th International Conference on FRP Composites in Civil Engineering, CICE 2021*, Lecture Notes in Civil Engineering, vol 198.

Sogut K., Dirar S., Nayak A. N., Theofanous M. and Faramarzi A. (2020). Cyclic behaviour of reinforced concrete T-beams strengthened in shear with embedded GFRP bars, *fib Symposium 2020*, Shanghai, China, November 22-24, 2020.

Sogut K., Dirar S., Theofanous M. and Faramarzi A. (2019). Size effect in shear-deficient reinforced concrete T-beams strengthened with embedded FRP bars, *The 14th International Symposium on Fiber-Reinforced Polymer Reinforcement for Concrete Structures, (FRPRCS-14)*, Belfast, UK, June 4-7, 2019.

Sogut K., Dirar S., Theofanous M. and Faramarzi A. (2019). Effect of existing steel-to-embedded FRP shear reinforcement ratio on the behaviour of reinforced concrete T-beams,

The 9th International Conference on Advanced Composites in Construction, (ACIC 2019),
Birmingham, UK, September 3-5, 2019.

Dutta B., Sogut K., Dirar S., Nayak A. N., Nanda B., Theofanous M. and Faramarzi A.
(2019). Nonlinear finite element analysis of reinforced concrete beams strengthened in shear
with embedded steel bars, *The 9th International Conference on Advanced Composites in*
Construction, (ACIC 2019), Birmingham, UK, September 3-5, 2019.

CHAPTER 2: LITERATURE REVIEW

2.1. General

The behaviour of both uncracked and cracked RC beams in shear and the use of FRP materials to strengthen RC beams in shear are described in this chapter. Section 2.2 considers the shear behaviour of RC beams before or after the appearance of cracks, as well as important parameters governing the behaviour of a cracked beam. Section 2.3 provides a framework for existing models developed to shed light on identifying the shear behaviour of RC beams with steel shear links. The general properties of FRP composites with benefits emerging from their usage and FRP shear strengthening techniques for RC beams are described in Section 2.4. Section 2.5 addresses previous studies on shear-strengthened RC beams with the Deep Embedment (DE) technique. This chapter concludes with Section 2.6 with a particular focus on the arising knowledge gap.

2.2. Shear in reinforced concrete beams

There is no doubt that substandard design of RC beams against shear compared to their substandard flexural design results in catastrophic impacts as shear failure occurs in a brittle and sudden manner (Subramanian, 2013). The flexural design of RC beams is based on Bernoulli-Euler beam theory, also referred to as classical beam theory, which assumes

“plane sections remain plane” (Subramanian, 2013). This approach brings a simplicity into flexural design of RC beams rather than the shear design of RC beams (Subramanian, 2013). In this section, the aim is to provide a framework for the shear behaviour of RC beams before and after the development of cracks, and the parameters influencing the shear behaviour of cracked beams.

2.2.1. Shear in uncracked beams

It is worth noting that shear in RC beams can be characterised by considering three distinct mechanisms (Subramanian, 2013). The first of such considers the case where cracks do not appear in the beam, whilst the second and third mechanisms include examining the behaviour of the beam without and with steel shear links after the development of cracking. The principal stresses, namely principal tension stress and principal compression stress, are instigated by the concurrent action of flexural and shear stresses. The cracks begin to appear by following the direction of the principal compression stresses, and this means the direction of the cracking in the beam is represented by compressive stress trajectories (Subramanian, 2013). It is a well-known issue that the principal stress equations based on flexural and shear stresses cannot be used in the instance where cracking in the beam has started to appear (Subramanian, 2013).

2.2.2. Shear in cracked beams without shear links

The shear behaviour of RC beams without shear links has been presented using the notion of concrete teeth by Kani (1964). As shown in Figure 2.1, the flexural cracks instigated by the load acting on the simply supported RC beam are expected to make the RC beam a comb-like structure. In Kani’s model, one end of each concrete tooth is clamped in the compression zone, while the other end is free in the tension zone where it is exposed to longitudinal stress.

Hence, the concept of a cantilever with a small length can be used to identify the behaviour of each concrete tooth (Kani, 1964). It is worth noting that shear transfer mechanisms such as aggregate interlock and dowel action, which are detailed in the next subsection, were ignored in Kani's model (Taylor 1971). Reineck (1991, cited in ASCE-ACI Committee 445, 1998 p. 1397) conducted additional research to present a tooth model in which each shear transfer mechanism is considered a parameter.

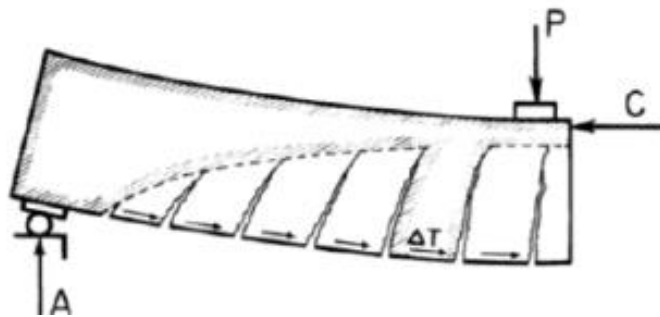


Figure 2.1. Kani's concrete teeth model (Kani, 1964)

The findings reported by Kani (1964) shed light on two possible mechanisms that can take place in the comb-like structure scheme. These mechanisms were identified as the beam action and arch action mechanisms. The occurrence of the arch action mechanism is expected to appear in the case where the capacity of the concrete teeth is deteriorated by the load acting on the beam, whereas the occurrence of beam action relies on the condition where the capacity of concrete teeth does not the failure capacity (Kani, 1964).

The behaviour of RC slender beams with a/d ratios higher than the critical ratio of 2.5 is controlled by the beam action mechanism, while the arch action mechanism appears in RC deep beams with a/d ratios of less than the critical ratio of 2.5 (Kani, 1964); thus, the

behaviour of RC beams is mainly controlled by the a/d ratio (Kani, 1964; Kani, 1967). The valuable findings reported by Kani (1967) showed that the shear stress at failure decreased by approximately 82.1% with an increase in a/d ratio from 1.03 to 5.92 for small-scale beams. The reduction in shear stress at failure for large-scale beams was about 55.3% with an increase in a/d ratio from 2 to 8 (Kani, 1967). One recent piece of research involving RC beams without shear links also proved that the shear stress at failure exhibited a significant decrease of 61% when the a/d ratio increased from 1.6 to 3.6 (Tetta et al., 2018). The considerable increase in the shear resistance of deep beams can be explained by the arch action mechanism, by which the shear force can be directly delivered to the support (ASCE-ACI Committee 445, 1998).

Figure 2.2, known as Kani's valley diagram in the literature, demonstrates the variation between moment capacity of the rectangular beam at shear failure (M_u) over the ultimate flexural capacity (M_f) of the rectangular beam and a/d ratio.

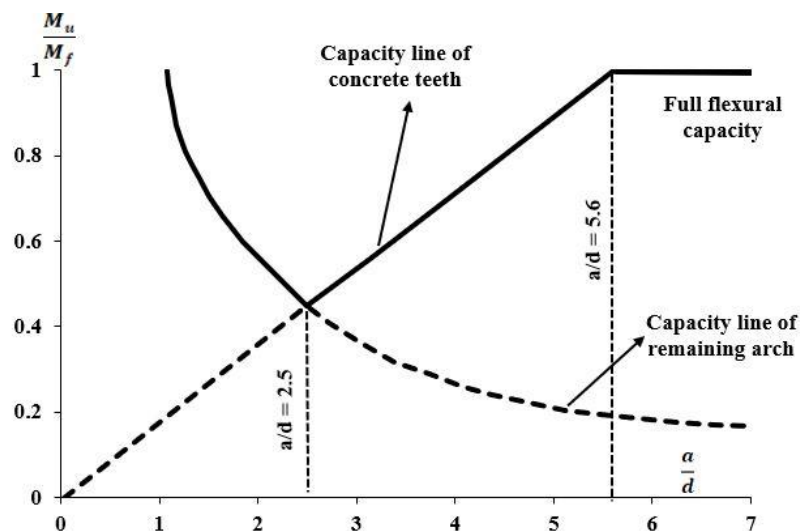


Figure 2.2. Kani's valley diagram (redrawn from Kani, 1964)

Kani's valley diagram comprises three regions (Kani, 1964). The beam behaviour together with the failure mode according to these regions can be categorised as follows:

Region I ($1 < a/d < 2.5$): The arch action in RC beams is expected to be followed until the critical a/d ratio of 2.5. The occurrence of failure is characterised by exceeding the arch capacity (Kani, 1964). The shear-tension failure is mainly initiated by the development of an inclined crack parallel to the tension reinforcement towards the direction of support (ASCE-ACI Committee 426, 1973; Hawkins et al., 2005). This is followed by a separation of the concrete, and so failure consequently arises (ASCE-ACI Committee 426, 1973; Hawkins et al., 2005). Another failure, namely shear-compression failure, is expected under condition in which the crushing of concrete takes place in the region between where an inclined crack reaches and the load (ASCE-ACI Committee 426, 1973).

Region II ($2.5 < a/d < 5.6$): The beam action mechanism appears in Region II and the failure is subject to the concrete teeth capacity (Kani, 1964). Failure is not observed as long as the capacity of the concrete teeth does not reach its ultimate capacity (Kani, 1964). A brittle shear failure instigated by a diagonal shear crack arises after the capacity of the concrete teeth is surpassed (Kani, 1964). A diagonal tension failure, as initiated by turning flexural cracks developing at the soffit of the beam into flexure-shear cracks, is expected (ASCE-ACI Committee 426, 1973; Hawkins et al., 2005).

Region III ($5.6 < a/d$): The RC beam is only expected to fail in flexure with reaching its full flexural capacity if the a/d ratio exceeds 5.6 (Kani, 1964).

2.2.2.1. Shear transfer mechanisms

The shear transfer mechanisms developed in a RC beam without shear links were initially emphasised by Fenwick (1966), Taylor (1971) and ASCE-ACI Committee 426 (1973). The

initial components, involving uncracked compression zone, dowel action, and aggregate interlock, are depicted in Figure 2.3. It should be noted that the residual tensile stresses are later included as a shear transfer mechanism by ASCE-ACI Committee 445 (1998).

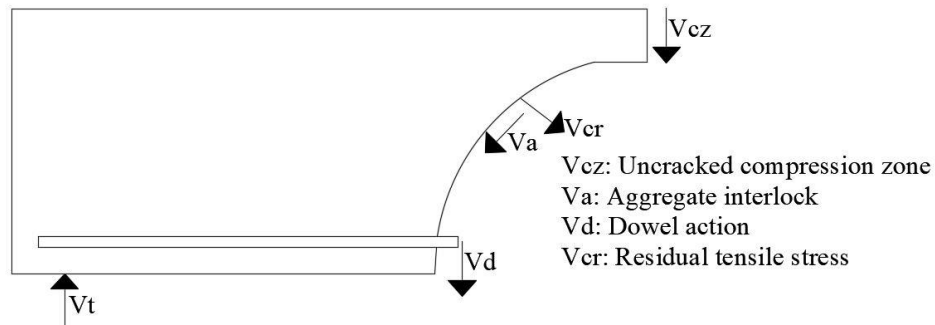


Figure 2.3. Shear transfer mechanisms (redrawn from ASCE-ACI Committee 426, 1973)

Uncracked compression zone: One of the mechanisms providing the transmission of shear is the uncracked compression zone. The compression zone height has the potential to increase or decrease the shear resistance gain due to the uncracked compression zone (Hawkins et al. 2005). The compression zone has little impact on shear strength enhancement in slender beams that are not loaded by axial compression (Taylor, 1974, and Reineck, 1991, cited in ASCE-ACI Committee 445, 1998 p. 1395; Hawkins et al., 2005). This can be attributed to an increase in the compression zone height due to the applied prestressing force (Hawkins et al. 2005). According to experimental findings reported by Fenwick (1966), the contribution of this mechanism was 20%. Smith and Fereig (1977) found that the contribution of the compression zone was about 29%, and 35% for RC deep beams without any web reinforcement.

Dowel action: The load acting on the beam can be carried by flexural reinforcement following the development of shear cracks in the tension zone of the beam (Hawkins et al.,

2005). The shear resistance gained due to the dowel action in RC beams lightly reinforced in tension is strongly reliant on the amount of shear reinforcement since the concrete surrounding the longitudinal bars is governed by the concrete tensile strength in the absence of shear reinforcement (ASCE-ACI Committee 445, 1998). According to Fenwick (1966) and Taylor (1971), the dowelling action of tension reinforcement occurring in RC beams without shear links can contribute to the shear resistance by up to 20% and 25%, respectively. Kim et al. (2018) pointed out that the contribution of dowel action in RC beams without shear links was in the range of 25% to 30% of the total shear resistance. Moreover, the gain in shear resistance due to this mechanism was obtained between 18% and 22% in RC beams with shear links (Sonnenberg and Al-Mahaidi, 2007).

Aggregate interlock: This mechanism includes the interaction between uneven crack planes that appear following the development of shear cracks, where this interaction tends to produce a counteraction to prevent slippage (ASCE-ACI Committee 445, 1998; Hawkins et al., 2005). Both crack width and aggregate size play a vital role in terms of the shear resistance gain offered by this mechanism (Hawkins et al., 2005). A decrease in crack openings or the presence of coarse aggregates in concrete has a positive influence on the contribution to shear resistance (Hawkins et al., 2005). Fenwick (1966) demonstrated that the most significant component contributing to shear resistance was aggregate interlock, and the shear resistance due to this mechanism was about 60%. Taylor (1971) also conducted experimental research on concrete blocks and precracked beams to examine this mechanism. Experimental results suggested that the contribution of this mechanism to the total shear resistance varied between 33% and 60% (Taylor, 1971). This result has been validated by recent experimental research conducted by Schmidt et al. (2021). According to experimental

results, this mechanism carries approximately 40% of the total shear resistance (Schmidt et al., 2021).

Residual tensile stresses: As indicated previously, ASCE-ACI Committee 445 (1998) has considered residual tensile stresses as a shear transfer mechanism since 1998. There is no immediate failure that can be observed following the appearance of cracks in the beam since the peak tensile strength of concrete does not rapidly diminish to zero (ASCE-ACI Committee 445, 1998). The transmission of tensile stresses can therefore exist until a certain level of crack width in the cracked concrete (ASCE-ACI Committee 445, 1998; Hawkins et al., 2005). This level is stated to be 0.15 or 0.16 mm, which indicates that a small crack width has a positive influence on the gain in shear resistance due to this mechanism (ASCE-ACI Committee 445, 1998; Hawkins et al., 2005). Moreover, the larger cracks that develop in large-scale beams are highly likely to mitigate the impact of this mechanism, whereas the narrower cracks that develop in small-scale beams tend to enhance the shear resistance gain obtained from this mechanism (Kuchma and Collins, 1998; Hawkins et al., 2005).

2.2.2.2 Significant parameters governing shear behaviour

Some of the most significant parameters governing the shear behaviour of RC beams without shear links are the size effect, a/d ratio, tension reinforcement, and axial force, as stated in ASCE-ACI Committee 445 (1998). The effect of the a/d ratio has already been given in Section 2.2.2. The axial tension results in cracks that occur nearly parallel to the vertical axis of the beam (ASCE-ACI Committee 445, 1998). Thus, the presence of axial tension diminishes the shear resistance (ASCE-ACI Committee 445, 1998; Hawkins et al. 2005).

Size effect: Previous research findings clearly indicate that size effect causes a decrease in the shear strength with increasing beam depth (Kani, 1967; Bažant and Kim, 1984; Bažant,

1997). The experimental findings for concrete beams with an a/d ratio of 3 reported by Kani (1967) revealed that the relative beam strength significantly decreased from 0.65 to 0.385 with an increase in the effective depth from 5.35 inches to 42.8 inches. However, the size effect is yet to be properly understood and opinions regarding the explanation of the size effect have differed, although it has been widely acknowledged that the wider cracks that develop in large-scale beams compared to those that develop in small-scale beams play a crucial role in the occurrent size effect (ASCE-ACI Committee 445, 1998; Kuchma and Collins, 1998; Hawkins et al., 2005). For instance, Bažant and Kim (1984) shed light on the variation of nominal shear stress with beam depth in reference to fracture mechanics, emphasising a reduction formula based on the released energy due to cracking. A decrease or an increase in the shear stress against the beam size is, on the other hand, attributed to the aggregate interlock mechanism, which is significantly influenced by both crack spacing and width (ASCE-ACI Committee 445, 1998; Kuchma Collins, 1998). Fenwick (1966) also stated that a decrease in the shear stress obtained by increasing beam size was reasoned by no increase in aggregate size. A recent experimental study involving geometrically similar small- and large-scale beams without shear links was carried out by Benzeguir et al. (2019), the experimental results of which demonstrated that shear stress at failure decreased by about 45% with increasing beam size. The corresponding reduction for beams with shear links was about 28%, and this demonstrated that shear links mitigated the size effect (Benzeguir et al., 2019; Yu and Bažant, 2011). The effect of beam size in deep beams was investigated by Birrcher et al. (2014). According to their experimental results, an increase in the beam depth resulted in a decrease in the normalised shear stress at failure. However, the test results for RC deep beams without shear links reported by Godat et al. (2010) revealed that an increase in the beam depth from 200 to 600 mm did not instigate a decrease in the shear stress at failure. For instance, the tested small-, medium-, and large-scale deep beams had shear

stresses of 4.82, 5.37, and 5.44 MPa at failure. According to Zhang and Tan (2007), the size effect in deep beams can be mitigated by scaling width of loading and support plates proportional to beam size.

Tension reinforcement: The dowel action and crack opening are governed by the tension reinforcement ratio (Hawkins et al., 2005). The dowel action is directly proportional to the tension reinforcement ratio, whereas crack growth has an inverse relation to the tension reinforcement ratio (Hawkins et al., 2005). Moreover, Collins and Kuchma (1999) (cited in Hawkins et al., 2005, p. A4-A5) stated that the additional strength gain can be obtained by increasing the number of tension reinforcement layers. Sogut et al. (2021) demonstrated that an increase in the number of tension reinforcement layers from two to three instigated an increase in total shear strength by about 15% for beams lightly reinforced in shear. Jeong et al. (2017) pointed out that an increase in tension reinforcement ratio resulted in a considerable enhancement in the total shear force capacity for beams without shear links. The gain due to the higher tension reinforcement ratio was about 105% and 31% for small- and large-scale beams, respectively (Jeong et al., 2017).

2.2.3. Function of shear links in an RC beam

According to Park and Paulay (1975), shear links effectively convert each concrete tooth into a tied concrete tooth. Moreover, shear links contribute to the development of truss action (Park and Paulay, 1975), which is detailed in the next section.

The shear resistance provided by the shear links can be outlined as follows:

1. Crack growth is prevented by the shear links. This instigates an increase in shear resistance gain due to the aggregate interlock mechanism (Park and Paulay, 1975).

2. The longitudinal tension reinforcement is enclosed by shear links. This results in an increase in shear resistance provided by dowel action and mitigates the possibility of anchorage failure (Park and Paulay, 1975).
3. The steel shear links can mitigate size effect in RC beams (Yu and Bažant, 2011)

2.3. Shear resistance models for cracked beams

The truss models developed for RC beams are presented in this section. In addition to these analytical models, the Modified Compression Field Theory (MCFT) and Disturbed Stress Field Model (DSFM), which also enable the prediction of the complete nonlinear behaviour of RC beams, are also incorporated.

2.3.1. Analytical models

The necessity to understand and determine the behaviour of RC beams with shear reinforcement led to research being carried out on the truss model at the end of the 19th century (Hawkins et al., 2005). Research studies were first conducted by Ritter (1899) (cited in Subramanian, 2013, p. 238) to shed light on calculations for the shear resistance capacity of RC beams via the 45° truss model. Further research studies were carried out by Mörsch (1909) (cited in Subramanian, 2013, p. 238) to expand the knowledge of the truss model. The components of this model are demonstrated in Figure 2.4. The stirrups are expected to act as transverse ties by connecting the compression chord to the tension chord in the truss, while tension reinforcement and the compression zone of the beam contribute to developing the truss by acting as tension and compression chords, respectively (Hawkins et al., 2005; Subramanian, 2013). It is worth noting that tensile stresses instigated by the load acting on

the truss are only able to be carried by steel stirrups and tension reinforcement (Subramanian, 2013).

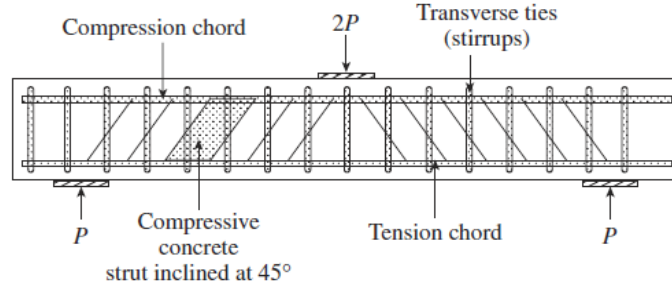


Figure 2.4. Ritter-Mörsch truss model (Subramanian, 2013)

The equations for the 45° truss model are given in Equation 2.1 (Hawkins et al., 2005).

$$f_2 = \frac{2V}{b_w j d} \quad (2.1)$$

where f_2 and V are the principal compressive stress and shear force; and $b_w j d$ is the effective web area (i.e., width of beam web multiplied by the lever arm).

The tension reinforcement and stirrups should carry the horizontal and vertical component of the diagonal force, respectively, as stated in Equations 2.2 and 2.3 (Hawkins et al., 2005).

$$N_v = V \quad (2.2)$$

$$\frac{A_{sw} f_y}{s} = \frac{V}{j d} \quad (2.3)$$

where A_v , f_y , and s are the cross-sectional area of the stirrup, yield stress of the stirrup, and spacing between stirrups, respectively.

The Ritter-Mörsch truss model suffers from certain disadvantages. For instance, it was recognised that the Ritter-Mörsch truss model did not tend to appropriately calculate the shear strength of RC beams reinforced in shear (Hawkins et al., 2005). In addition to this, the beam depth did not appear as a parameter in calculating the shear force capacity (Subramanian, 2013). The revision of the Ritter-Mörsch truss model consequently turned into an appeal to researchers (Subramanian, 2013). The revised model, namely the variable angle truss model, attempts to consider the inclination angle of the concrete strut as a variable rather than a strict assumption of 45°. The equations for the variable angle truss model can be obtained in similar way as described above for the 45° truss model (Hawkins et al., 2005).

$$f_2 = \frac{V}{b_w j d} (\tan\theta + \cot\theta) \quad (2.4)$$

$$N_v = V \cot\theta \quad (2.5)$$

$$\frac{A_{sw} f_y}{s} = \frac{V}{j d} (\tan\theta) \quad (2.6)$$

It should be noted that the assumption of a flatter angle for the strut angle reduces the number of stirrups required and increases the horizontal component of diagonal force, which should be carried by the tension reinforcement (Subramanian, 2013). Design codes of Eurocode 2 and ACI 318 utilise the variable angle truss model and 45° degree truss model, respectively (EN 1992-1-1, 2004; ACI 318, 2014).

Total shear force capacity as a function of concrete and steel contributions can be calculated based on the recommendations given in ACI 318 (2014), as follows:

$$V_t = \left(0.17\sqrt{f_c}b_wd + \frac{A_{sw}}{s}df_y\cot\theta \right) \quad (2.7)$$

where d and f_c are effective depth and concrete compressive strength; the inclination angle (θ) of the shear crack is 45° .

According to EN 1992-1-1, 2004, the steel contribution is given by Equation 2.8:

$$V_s = 0.78 \frac{A_{sw}}{s} df_y \cot\theta \quad (2.8)$$

where the inclination angle (θ) of the shear crack varies between 21.8° and 45° .

The shear strength of RC beams may be limited by crushing struts, as given in Equation 2.9.

$$V_{Rd,max} = \frac{\alpha_{sw}0.9dv_1f_{cd}}{\cot\theta + \tan\theta} \quad (2.9)$$

where α_{sw} is the coefficient considering the stress in the compression chord (taken as 1 for non-prestressed beams); v_1 is the strength reduction factor concrete cracked in shear (taken as 0.6 for $f_{ck} \leq 60$ MPa; $(0.9-(f_{ck}/200))$ otherwise).

2.3.2. The Modified Compression Field Theory (MCFT) and Disturbed Stress Field Model (DSFM)

The compression field theory (CFT) was initially established for RC members subject to pure torsion (Mitchell and Collins, 1974), which was followed by the implementation of the theory for RC members under shear (Collins, 1978). The CFT was mainly inspired by the tension field theory (TFT), which was first established by Wagner (1929). For the first time, the MCFT was proposed by Vecchio and Collins (1986) to offer a new insight into the shear behaviour of RC members by incorporating tensile stresses occurring in cracked concrete. Bentz et al. (2006) suggested further modifications to bring simplicity to the MCFT. Of note is that the simplified MCFT is incorporated into the Canadian code of practice to calculate shear resistance of RC beams (CSA A23.3, 2019).

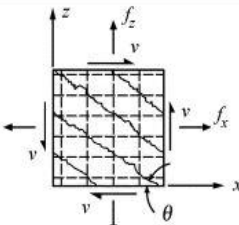
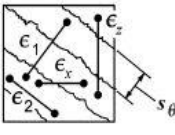
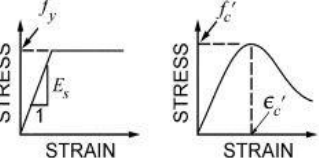
 <p>Equilibrium: Average Stresses:</p> $f_x = \rho_x f_{sx} + f_1 - v \cot \theta \quad (1)$ $f_z = \rho_z f_{sz} + f_1 - v \tan \theta \quad (2)$ $v = (f_1 + f_2) / (\tan \theta + \cot \theta) \quad (3)$ <p>Stresses at Cracks:</p> $f_{sxcr} = (f_x + v \cot \theta + v_{ci} \cot \theta) / \rho_x \quad (4)$ $f_{szcr} = (f_z + v \tan \theta - v_{ci} \tan \theta) / \rho_z \quad (5)$	 <p>Geometric Conditions: Average Strains:</p> $\tan^2 \theta = \frac{\epsilon_x + \epsilon_z}{\epsilon_y + \epsilon_2} \quad (6)$ $\epsilon_1 = \epsilon_x + \epsilon_z + \epsilon_2 \quad (7)$ $\gamma_{xz} = 2 (\epsilon_x + \epsilon_z) \cot \theta \quad (8)$ <p>Crack Widths:</p> $w = s_\theta \epsilon_1 \quad (9)$ $s_\theta = 1 / \left(\frac{\sin \theta}{s_x} + \frac{\cos \theta}{s_z} \right) \quad (10)$	 <p>Stress-Strain Relationships: Reinforcement:</p> $f_{sx} = E_s \epsilon_x \leq f_{yx} \quad (11)$ $f_{sz} = E_s \epsilon_z \leq f_{yz} \quad (12)$ <p>Concrete:</p> $f_2 = \frac{f_c'}{0.8 + 170 \epsilon_1} \left[2 \frac{\epsilon_2}{\epsilon_c'} - \left(\frac{\epsilon_2}{\epsilon_c'} \right)^2 \right] \quad (13)$ $f_1 = 0.33 \sqrt{f_c'} / \left(1 + \sqrt{500 \epsilon_1} \right) \text{ MPa} \quad (14)$ <p>Shear Stress on Crack:</p> $v_{ci} \leq \frac{0.18 \sqrt{f_c'}}{0.31 + \frac{24 w}{a_g + 16}} \text{ MPa, mm} \quad (15)$
-----------------------------------------------------------------------------------------------------------------------------------------------------------------------------------------------------------------------------------------------------------------------------------------------------------------------------------------------------------------------------------------------------------------------------------------------------------------------------------------------------------	--------------------------------------------------------------------------------------------------------------------------------------------------------------------------------------------------------------------------------------------------------------------------------------------------------------------------------------------------------------------------------------------------------------------------------------------------------------------------------------------------------------------------------------	---------------------------------------------------------------------------------------------------------------------------------------------------------------------------------------------------------------------------------------------------------------------------------------------------------------------------------------------------------------------------------------------------------------------------------------------------------------------------------------------------------------------------------------------------------------------------------------------------------------------------------------------------------------------------

Figure 2.5. Equations proposed for the MCFT (Bentz et al., 2006)

Three principal mechanisms are embedded in this model (Vecchio and Collins, 1986; Vector2 & Formworks User's Manual, 2013). These mechanisms, namely compatibility conditions, equilibrium conditions, and constitutive relationships, are used for several reasons, such as computing average stresses and strains in concrete and reinforcement, together with considering constitutive models proposed for cracked concrete and steel reinforcement (see Figure 2.5) (Vecchio and Collins, 1986; Vector2 & Formworks User's Manual, 2013; Subramanian, 2013).

The two-dimensional non-linear FE software, VecTor2, based on the Disturbed Stress Field Model (DSFM) (Vecchio, 2000), an improved version of the MCFT (Vecchio and Collins, 1986), emerged in response to the estimation of the structural behaviour of RC members (Vector2 & Formworks User's Manual, 2013). The crack shear slip deformations play a vital role in describing this improvement. In the MCFT, the orientations of the principal stress and principal strain are expected to change in a compatible manner with each other (Vecchio, 2000). However, the MCFT gives conservative predictions with an overestimated shear force capacity for RC members reinforced in shear with a low reinforcement ratio (Vector2 & Formworks User's Manual, 2013). This is attributed to a rotational lag between the principal stress and strain orientations occurring in these members in which crack shear slip deformations play a crucial role (Vector2 & Formworks User's Manual, 2013). Moreover, the MCFT tends to give conservative results with an underestimated shear force capacity for RC members where principal stress and strain are not allowed to fully rotate (i.e., the case where RC members are overly reinforced in the vertical and horizontal directions) (Vecchio, 2000; Vector2 & Formworks User's Manual, 2013). The concept of a smeared delayed rotating crack model has emerged in the DSFM since orientations of principal stress and strain are expected to be separated (Vector2 & Formworks User's Manual, 2013).

Shear slip deformations are incorporated into total strains in the DSFM, as given below equations (Vector2 & Formworks User's Manual, 2013).

$$\varepsilon_x = \varepsilon_{cx} + \varepsilon_x^s \quad (2.10)$$

$$\varepsilon_y = \varepsilon_{cy} + \varepsilon_y^s \quad (2.11)$$

$$\gamma_{xy} = \gamma_{cxy} + \gamma_{xy}^s \quad (2.12)$$

where ε_x and ε_y are total axial strains in the x - and y -directions, respectively, while γ_{xy} is the total shear strain; ε_{cx} and ε_{cy} are average net concrete axial strains in the x - and y -directions, respectively, while γ_{cxy} is the average net concrete shear strain; ε_x^s and ε_y^s are, respectively, average axial strains in the x - and y -directions due to shear slip, while γ_{xy}^s is the average shear strain due to shear slip (Vector2 & Formworks User's Manual, 2013).

The equilibrium relationships for average stresses are given in the equations below (Vector2 & Formworks User's Manual, 2013). It is worth noting that the stresses below are identical to those in the MCFT (Vector2 & Formworks User's Manual, 2013)

$$\sigma_x = f_{cx} + \rho_{sx} * f_{sx} \quad (2.13)$$

$$\sigma_y = f_{cy} + \rho_{sy} * f_{sy} \quad (2.14)$$

$$\tau_{xy} = \nu_{cxy} \quad (2.15)$$

where σ_x and σ_y are applied axial stresses in the x - and y -directions, respectively, while τ_{xy} and ν_{cxy} are the applied shear stress and average concrete shear stress, respectively; f_{cx} and f_{cy} are the average concrete axial stresses in the x - and y -directions, respectively; ρ_{sx} and ρ_{sy} are the reinforcement ratios in the x - and y -directions, respectively; while f_{sx} and f_{sy} are average reinforcement stresses parallel to the x - and y -directions, respectively (Vector2 & Formworks User`s Manual, 2013). The average and local stresses at crack are given in the equations below (Vector2 & Formworks User`s Manual, 2013).

$$f_{c1} = \rho_x(f_{scrx} - f_{sx})\cos^2\theta_{nx} + \rho_y(f_{scry} - f_{sy})\cos^2\theta_{ny} \quad (2.16)$$

$$\nu_{ci} = \rho_x(f_{scrx} - f_{sx})\cos\theta_{nx}\sin\theta_{nx} + \rho_y(f_{scry} - f_{sy})\cos\theta_{ny}\sin\theta_{ny} \quad (2.17)$$

where f_{c1} and ν_{ci} are the average principal concrete tensile stress and local concrete shear stress at crack, respectively; f_{scrx} and f_{scry} are local reinforcement stresses at crack parallel to the x - and y -directions, respectively; f_{sx} and f_{sy} are average reinforcement stresses parallel to the x - and y -directions, respectively; and θ_{nx} and θ_{ny} are the angles between the normal to the crack and reinforcement, respectively (Vector2 & Formworks User`s Manual, 2013). It is important to note that the tensile stress is not expected to suffer from restriction due to shear stresses at the crack, indicating a difference between the MCFT and DSFM (Vector2 & Formworks User`s Manual, 2013). As previously mentioned, the DSFM is an improved version of the MCFT and thus can provide more accurate predictions (Vecchio, 2000; Vector2 & Formworks User`s Manual, 2013).

2.4. Shear strengthening with fibre-reinforced polymer (FRP) composites

The initial interest in FRP composites appeared in various industries rather than in structural engineering (Amaechi et al., 2020 cited in Krauklis et al., 2021, p.2; ISIS Canada, 2007). The use of FRP composites in different industries can be explained by initial restrictions such as the expensive of FRP composites or experimental difficulties (Emmons et al., 1998 cited in Wu and Eamon, 2017, p.2). The further developments in structural engineering encouraged the use of FRPs for strengthening RC members in the 1980s. The FRP strengthening scheme, as an alternative to the strengthening scheme involving the use of conventional materials, was initially considered by Meier in 1984 (Teng et al., 2003). This attempt shed new light on the use of FRP composites in structural engineering and stimulated further related research. FRP composites, which are relatively more sustainable, have higher strength with lighter weight, are resistant to corrosion, and have effortless implementation (Teng et al., 2003; Pešić and Pilakoutas, 2003; Jemaa et al., 2015; Wu and Eamon, 2017; ACI 440.2R-17, 2017). All these can be counted as the main advantages of FRP composites compared to conventional materials. The aim of this section is to give a framework for the general properties of FRP composites and FRP shear strengthening solutions for RC beams.

2.4.1. General properties of FRP composites

FRP composites are mainly made up of two components, known as fibres and the polymeric matrix (Wu and Eamon, 2017). While fibres play a role in carrying the applied load, a polymeric matrix is expected to assemble the fibres in order to offer preservation against any damage (Wu and Eamon, 2017). The fibres can be manufactured in various mechanical properties. The tensile strengths of various fibre materials, from highest to lowest, can be ranked as follows: carbon, aramid, basalt, and glass. As can be seen in Figure 2.6, all fibres

have a linear-elastic behaviour until the point of rupture without a yield plateau, unlike high-strength and carbon steel.

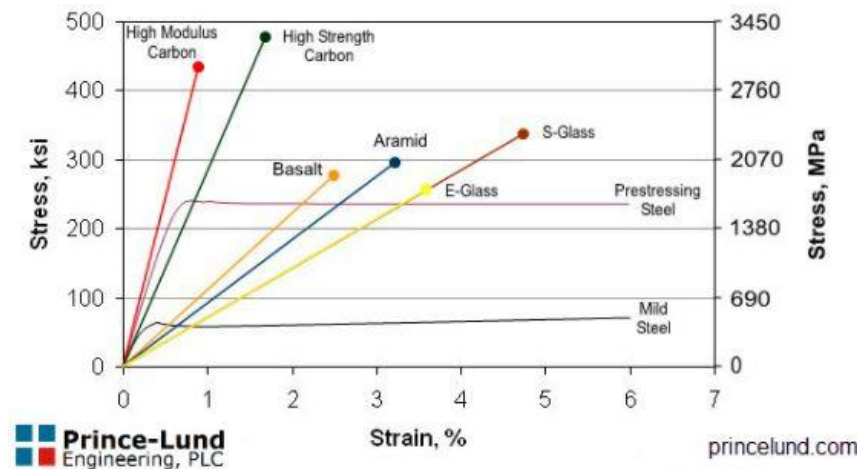


Figure 2.6. Comparison of different types of FRP to steel

(<https://www.princelund.com/frp-reinforcement.html>)

The Glass FRP composites have relatively lower stiffness compared to those in other FRP composites, high-strength, and carbon steel, whereas they can achieve a higher strain value at rupture compared to that by carbon, basalt, or aramid FRP composites, as shown in Figure 2.10. The CFRP composites, which went on sale later than GFRP composites, have higher durability, together with better performance under cyclic loading and extreme environmental conditions (Wu and Eamon, 2017). The alkaline resistance of FRP composites, from lowest to highest, can be ranked as GFRP, AFRP, and CFRP composites, respectively (Machida, 1993 cited in Byars et al., 2003 p. 31). BFRP composites can be considered an alternative to CFRP composites in structural engineering applications due to their well-known properties (i.e., chemical, and thermal resistance), together with their lower market price (Wu and Eamon, 2017). The lower market price of GFRP composites and the higher durability of CFRP composites have resulted in the potential usage of GFRP and CFRP composites in structural engineering applications (Elanchezhian et al., 2014; Abbood et al., 2021).

2.4.2. RC beams strengthened in shear with FRP composites

FRP composites have achieved a reputation for enhancing the shear force capacity of RC beams as well as altering the failure mode of shear-deficient RC beams from brittle to ductile (Chaallal et al., 2011; Sogut et al., 2021). The subsections below summarise the external shear strengthening techniques as well as the deep embedment (DE) technique, also referred to as the embedded through-section (ETS) technique.

2.4.2.1. Externally bonded (EB) FRP systems

Strengthening of existing shear-deficient RC beams with the EB FRP systems has become a desirable approach for the construction industry over the last three decades (Chaallal et al., 2011). The improvements in shear strength attained by using EB FRP sheets or laminates has been verified by numerous researchers (e.g., Triantafillou, 1998; Ianniruberto and Imbimbo, 2004; Zhang et al., 2004; Belarbi et al., 2012; Qin et al., 2015; Benzeguir et al., 2019; Mohamed et al., 2000). According to ACI 440.2R-17 (2017), enhancement of the shear resistance can be accomplished by placing FRP laminates on the surfaces of RC beams, as depicted in Figure 2.7. The FRP wrapping of the entire cross-section theoretically provides greater shear resistance than that provided by a partially wrapped cross-section (ACI 440.2R-17, 2017). However, a fully wrapped scheme is more suitable for application to RC columns since the implementation of the former scheme for RC T-beams can be unfeasible (ACI 440.2R-17, 2017). A recent study reported by Saribiyik et al. (2021) demonstrated the effectiveness of a full wrapping scheme with an experimental programme conducted on rectangular RC beams. It is important to stress that the implementation of the EB strengthening system strongly relies on the accessibility of the beam surfaces, and different configurations can therefore be considered as shown in Figure 2.11 (ACI 440.2R-17, 2017).

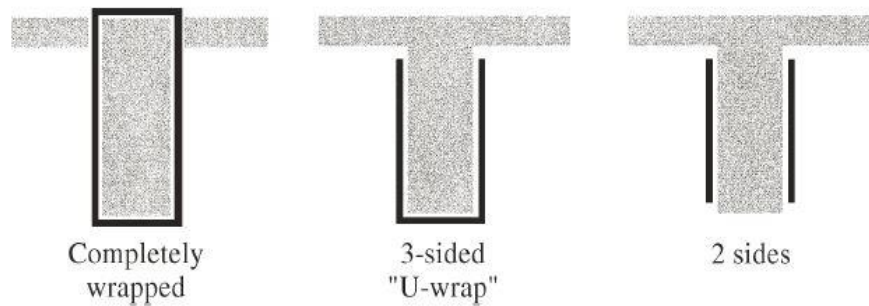


Figure 2.7. Various configurations of the EB FRP system (ACI 440.2R-17, 2017)

It is crucial to take into consideration the bond behaviour between concrete and FRP laminates, as it influences overall strengthened behaviour and determines the efficacy of EB FRP shear strengthening (Chaallal et al., 2011; Mofidi et al., 2012b; Caro et al., 2021). The EB systems can debond prematurely from concrete unless properly anchored (Dirar et al., 2013a; Sogut et al., 2019a; Sogut et al., 2021). Anchorage systems that allow for the better attachment of FRP shear reinforcement to concrete and provide the beam with a considerable shear strength increment can be used (Mofidi et al., 2012b). This increment in the shear strength through anchorage systems could be attributable to the fact that FRP shear reinforcement can reach higher strains (ACI 440.2R-17, 2017). According to Dirar et al. (2013a), anchored external FRP reinforcement may reach a 70-80% higher strength than that reached by an unanchored system. Recent improvements, namely externally bonded reinforcement on grooves (EBROG) and externally bonded reinforcement in grooves (EBRIG), have proved to provide RC beams with a remarkable increase in shear strength capacity (Mostofinejad and Tabatabaei Kashani, 2013; Mostofinejad et al., 2016). The increase in the contribution by FRP sheets to the shear resistance or the alteration of the failure mode from shear to flexure was achieved through the EBRIG or EBROG techniques (Mostofinejad and Tabatabaei Kashani, 2013; Mostofinejad et al., 2016).

2.4.2.2. Near-surface mounted (NSM) technique

The near-surface mounted technique has also been developed to offer an enhancement in the shear strength of existing shear-deficient RC beams (De Lorenzis and Nanni, 2001). This technique is principally applied to RC beams via the implementation of the steps described in the following sentences (De Lorenzis and Teg, 2007). The concrete surface is prepared by forming grooves. This is followed by filling the grooves with epoxy or cement grout. FRP bars are finally embedded into the grooves. Numerous researchers have verified the effectiveness of this technique by demonstrating a remarkable concomitant enhancement in shear strength (e.g., De Lorenzis and Nanni, 2001; Rizzo and De Lorenzis, 2009; Dias and Barros, 2008; Dias and Barros, 2012; Dias and Barros, 2013; Chaallal et al., 2011; Mofidi et al., 2016; Mostofinejad et al., 2019; Diab and Sayed, 2020). Similar to EB strengthening systems, this particular strengthening system also suffers from premature debonding unless properly anchored and has satisfactory concrete strength (Chaallal et al., 2011). Premature debonding mitigates the performance of the strengthening system by not allowing FRP shear reinforcement to attain higher strain values (Chaallal et al., 2011).

2.4.2.3. Deep Embedment (DE) technique

The deep embedment (DE), also referred to as embedded-trough section (ETS) in the literature, is a shear strengthening technique that has been demonstrated to noticeably enhance the shear strength capacity of RC beams (e.g., Valerio and Ibell, 2003; Valerio et al., 2009; Chaallal et al., 2011; Mofidi et al., 2012a; Breveglieri et al., 2015; Jemaa et al., 2015; Qin et al., 2015; Brindley, 2018; Raicic, 2019; Sogut et al., 2019(a); Sogut et al., 2019(b); Sogut et al. 2021). The implementation of this technique consists of simple steps, as described by Valerio et al. (2009). The first step is to drill vertical and/or inclined holes upwards from the bottom of the beam over the full depth. This step is followed by filling

existing holes with high viscosity epoxy. The final step is embedding FRP and/or steel bars into epoxy-filled holes. A typical DE strengthening system is depicted in Figure 2.8; such a system can be adopted without expending too much effort on surface preparation (Jemaa et al., 2015; Sogut et al., 2021).

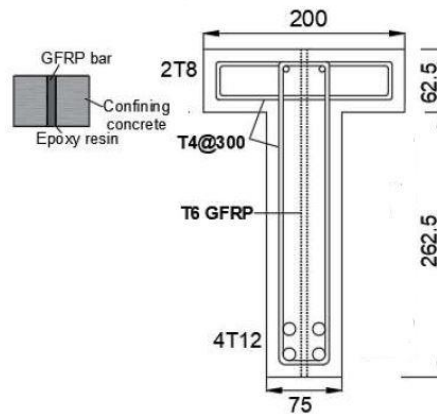


Figure 2.8. Configuration of an embedded FRP bar (Sogut et al., 2019a)

The DE technique is advantageous where the flange and/or web are inaccessible (Valerio and Ibell 2003; Sogut et al., 2022). Furthermore, in the case of T-beams, DE bars can be inserted along the full height of the cross-section, thereby connecting the compression chord to the tension chord and ensuring that truss action can be fully developed (Sogut et al., 2021; Sogut et al. 2022). However, the embedded length of DE bars may influence the effectiveness of this technique. It is therefore clear that further experimental study is required in this regard. It may also be difficult to drill holes in members with congested internal steel reinforcement. However, existing concrete members requiring shear strengthening usually include relatively low amounts of steel reinforcement. The locations of existing steel shear links or tension reinforcing bars can be determined from as-built drawings and/or by using cover metres.

Besides, core drilling machines with steel bar sensing function can be used to drill holes. Such drilling machines automatically shut off when they touch a steel bar, thereby ensuring integrity of the steel bars (Sogut et al., 2021).

2.5. Previous studies on DE shear strengthened RC beams

The experimental and numerical studies investigating the efficiency of the DE technique with a focus on the key parameters governing the strengthened behaviour have been conducted by numerous researchers during the last two decades, as shown in Table 2.1. The aim of this section is to discuss previous research studies on RC beams shear-strengthened with the DE technique. The important parameters influencing the effectiveness of the DE technique are also briefly given in this chapter. The effectiveness of the DE technique has also been investigated by conducting numerical studies, as given in Table 2.1 (Qapo et al., 2016; Caro, 2018; Bhanugoban et al., 2021). A three-dimensional FE model was developed by Qapo et al. (2016) and Caro (2018) using FE element software (DIANA) to conduct parametric studies on beams strengthened with the DE technique. Furthermore, Bhanugoban et al. (2021) developed a three-dimensional FE model using FE element software (MIDAS) to validate their experimental results as well as conduct a further parametric study to gain a better understanding of the influence of prestressed DE steel bars on the strengthened behaviour.

2.5.1. Existing unfilled holes

Experimental research conducted by Valerio and Ibell (2003) shed new light on the strengthening of shear-deficient concrete beams by proposing the DE technique. A total of 10 concrete beams without steel shear links were tested to failure. Two RC beams were

designed as a control beam and an unstrengthened beam with five vertical unfilled holes. The control beam and unstrengthened beam failed at shear force of 22.5 and 21 kN, respectively. This showed that existing holes in the shear span had an insignificant effect on shear strength. It is worth noting that the tests were conducted on rectangular RC beams. It is therefore clear that further experimental tests are required on RC T-beams in this regard.

2.5.2. DE bar type

Experimental and numerical research has been conducted by numerous researchers to attain a better understanding of the effect of embedded bar type on the strengthened behaviour, as given in Table 2.1. Valerio and Ibell (2003) tested a total of eight strengthened beams. The DE shear reinforcement involved either aramid FRP or conventional steel bars. The embedded FRP bars enhanced the shear strength by up to about 42.2% and altered the failure mode from brittle to ductile, while embedded steel bars only resulted in a flexural failure. It was also stated that the effectiveness of embedded steel bars was comparable to that of embedded AFRP bars. The further experimental results reported by Valerio et al. (2009) confirmed that that embedded CFRP and/or steel bars increased the shear resistance of both non-prestressed and prestressed beams. The experimental results showed that the shear resistance gain due to embedded CFRP bars and embedded steel bars for large-scale beams 14.6% and 18%, respectively. Breveglieri et al. (2015) performed an experimental study on beams strengthened with either embedded CFRP or steel bars to examine the impact of DE bar type on the strengthened behaviour. For strengthened beams with a shear reinforcement ratio of 0.1%, the shear resistance gain due to embedded CFRP bars varied from 53.1% to 120.9%, whereas the corresponding gain due to embedded steel bars varied from 68.1% to 108.5%. The experimental research was conducted by Mofidi et al. (2012a) to explore the differences between sand-coated and plain-surface CFRP bars. It was demonstrated that the

shear contribution of sand-coated CFRP bars was 6%, whereas the contribution of plain-surface CFRP bars was 14%. This was explained by the fact that better chemical bond behaviour developed when plain-surface CFRP bars were used (Mofidi et al. (2012a). However, it is important to note that both the ultimate stress and elastic modulus of plain-surface CFRP bars was higher than those of sand-coated CFRP bars.

An experimental programme involving ten RC continuous T-beams was conducted by Raicic et al. (2017). Until the current research was conducted, the effectiveness of the deep embedment technique had been investigated by considering an experimental programme conducted on simply supported beams. The aim of the study, therefore, was to examine the efficacy of the DE technique on RC continuous beams. The DE strengthening system consisted of embedded GFRP, CFRP, and steel bars. The test results showed that CFRP bars made a greater contribution to shear resistance than GFRP or steel bars in terms of strengthening continuous beams with the DE technique. For example, the contribution of embedded CFRP bars to the shear resistance varied from 70% to 81%, while the contributions of embedded GFRP and steel bars varied from 55% and 50% to 67% and 52%. These results were confirmed by the finite element parametric study conducted by Caro (2018). According to numerical results, embedded CFRP bars provided a greater shear resistance than embedded GFRP bars. Bui et al. (2020a) compared anchored DE GFRP bars to unanchored DE CFRP bars. The results showed that anchored vertical embedded GFRP bars provided more shear resistance than unanchored vertical embedded CFRP bars. However, the contribution of unanchored inclined embedded CFRP bars to the shear resistance was less than that of anchored inclined embedded GFRP bars (Bui et al., 2020a).

2.5.3. DE bar spacing, diameter, and inclination angle

The previous experimental and numerical studies clearly showed that the spacing, diameter and inclination angle of the embedded bars affected the strengthened behaviour (e.g., Valerio and Ibell, 2003; Valerio et al., 2009; Mofidi et al., 2012a; Breveglieri et al., 2015; Raicic et al., 2017). The experimental results reported by Valerio and Ibell (2003) demonstrated that the total shear force capacity decreased from 32 kN to 30 kN (about 7%) with a decrease in the number of DE AFRP bars in the shear span from two to one. The test results on small- and large-scale beams reported by Valerio et al. (2009) verified that the presence of two CFRP bars in the cross-section of the large-scale beam induced an increase in shear force capacity of 8.1% over that for one CFRP bar. Both a reduction in the spacing of embedded bars and the presence of shear links altered the failure mode of small-scale non-prestressed beams from shear to flexure. A reduction in embedded CFRP bar spacing from 105 mm to 75 mm instigated an additional increase in shear resistance of 17% for small-scale non-prestressed beams without shear links. Another experimental study was performed on strengthened RC beams with the DE/ETS shear strengthening technique (Mofidi et al., 2012a). The 12.7 mm diameter CFRP bars were placed at either 130 mm or 260 mm spacing in the shear span, whereas the 9.5 mm diameter CFRP bars were placed at 260 mm spacing. The effects of CFRP bar diameter and spacing were measured through these configurations. A reduction in FRP bar spacing from 260 mm to 130 mm instigated flexural failure. An increase in the diameter of FRP bars from 9.5 to 12.7 mm a higher shear resistance of 2%.

Embedded bars with an inclination angle of either 90° or 45° were used by Breveglieri et al. (2015) to examine the influence of inclination angle on the strengthened behaviour. The test results confirmed that embedded bars inclined at 45° had more shear resistance contribution compared to vertical embedded bars. For the strengthened beams with steel shear links, the

shear force gain obtained from 45° inclined embedded bars varied in the range of 56.1-120.9%, whereas vertical embedded bars enhanced the shear strength in the range of 4.8-68.1%. Further numerical results on the effects of DE bar inclination and diameter reported by Qapo (2016) and Caro (2018) were consistent with the previous experimental results. The inclination angle of embedded FRP bar was inversely proportional to the shear force gain whereas the diameter of embedded FRP bar was directly proportional to the shear force gain (Qapo et al., 2016; Caro, 2018). Similar to unanchored embedded FRP bars, a decrease in the inclination angle of anchored embedded GFRP bars from 90° to 45° resulted in an enhancement of shear strength (Bui et al., 2020a).

The test results on RC continuous T-beams strengthened with embedded bars reported by Raicic et al. (2017) were also comparable to the results reported in the literature for simply supported beams. The shear strength gain obtained from embedded steel bars remained almost constant with the decrease in spacing between embedded steel bars. The failure mode of strengthened beams was altered from shear to flexure with the reduction in spacing between embedded GFRP or CFRP bars. Moreover, the reduction in the inclination angle from 90° to 45° resulted in an additional increase of 11% in the shear force capacity of the beam strengthened with DE CFRP bars.

2.5.4. Steel shear link ratio

Previous research into the behaviour of RC beams strengthened with the DE technique clearly evidenced that the presence of existing steel shear links played a crucial role in shear strength gain due to embedded bars (Mofidi et al., 2012a; Breveglieri et al., 2015). Mofidi et al. (2012a) reported that increasing the shear reinforcement ratio instigated a reduction in the contribution of embedded CFRP bars to the shear strength. For instance, the contribution of embedded CFRP bars was measured to be 122% in the absence of steel shear links,

whereas the contribution of CFRP bars to shear resistance varied from 6% to 45% in the presence of steel shear links. Breveglieri et al. (2015) carried out another experimental research in which beams were initially reinforced in shear with either low or high amounts of steel shear links in order to measure the effect of the existing shear link ratio on the strengthened behaviour. According to the test results, decreasing the shear reinforcement ratio from 0.17% to 0.1% increased the contribution of embedded bars. For instance, the contribution of embedded steel bars to the shear resistance increased from 16.8% to 68.1% with a decrease in shear reinforcement ratio from 0.17% to 0.1%. Moreover, Qapo et al. (2016) and Caro (2018) proved the interaction between existing steel shear links and embedded FRP bars by conducting an associated numerical analysis. Their findings showed that the shear force gain due to embedded FRP bars decreased with an increase in the steel-to-FRP shear reinforcement ratio. The test results on RC beams strengthened with anchored GFRP bars were also consistent with the corresponding results for unanchored GFRP bars (Bui et al., 2020a). The main results indicated that the shear strength gain obtained from anchored embedded GFRP bars increased with a decrease in steel shear reinforcement ratio from 0.24% to 0.11%.

2.5.5. a/d ratio

The a/d ratio has a significant effect on the behaviour of RC beams, as mentioned in Section 2.2 (Kani, 1964; Kani, 1967). The influence of the a/d ratio on shear-strengthened RC T-beams with embedded GFRP bars was experimentally investigated by Dirar and Theofanous (2017). Two strengthened RC T-beams with an a/d ratio of either 1.9 or 3, together with their control beams, were included in the experimental programme, the details of which are depicted in Figure 2.9 (see Chapter 4 for further discussion). The experimental results proved the shear strength contribution of the GFRP bars embedded into the RC deep beam was less

than the corresponding contribution due to GFRP bars in the RC slender beam. The shear enhancement for deep and slender beams was by 33% and 96%, respectively. This was attributed to the arch action mechanism becoming dominant in deep beams. Thus, the shear resistance gain due to embedded GFRP bars remained limited. Moreover, the experimental results were compared to existing design models, which significantly underestimated the contribution of embedded GFRP bars to shear strength.

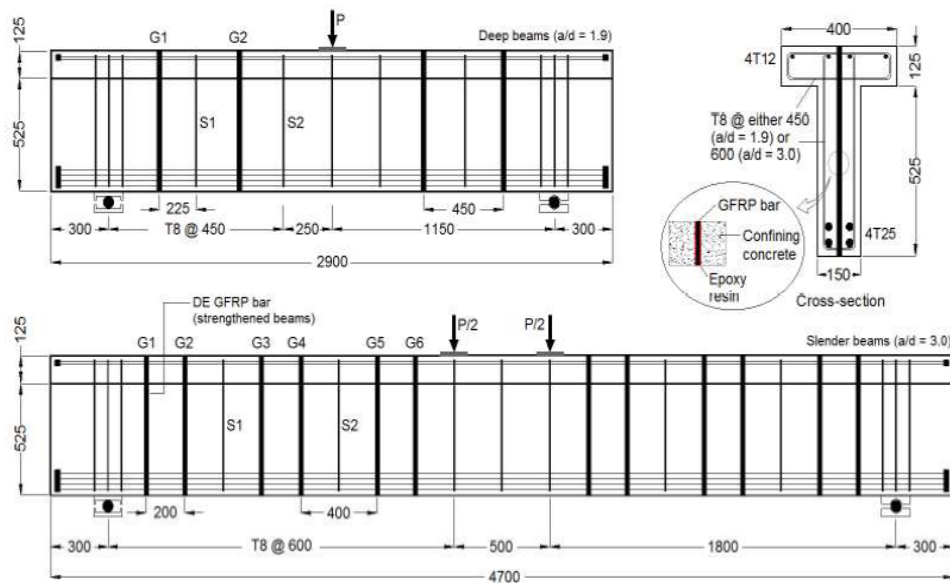


Figure 2.9. Tested beams (Dirar and Theofanous, 2017)

Caro (2018) carried out a FE parametric study to investigate the impact of a/d ratio on the strengthened behaviour. The modelled beams were identical to the tested beams described above. Both total shear force capacity and shear force gain due to embedded FRP bars decreased with an increase in the a/d ratio from 1.9 to 2.5. Moreover, Qapo et al. (2016) numerically investigated the effect of a/d ratio on slender RC beams strengthened with

embedded FRP bars. The results revealed that the shear strength gain due to embedded FRP bars decreased with the increase in a/d ratio from 2.6 to 4.1.

2.5.6. Size effect

Experimental research involving geometrically similar DE CFRP-strengthened RC beams was conducted by Brindley (2018). Two T-shaped cross sections with a scale factor of 1.33 were tested. The T-beams had web width of either 225 or 300 mm, flange width of either 570 or 760 mm, flange depth of either 120 or 160 mm, and effective depth of either 450 or 600 mm. Experimental results showed that the contribution of embedded CFRP bars to shear resistance was 50% for the medium-scale beam. The corresponding enhancement in the large-scale beam was found to be 28%. It was also stated that normalised shear stress at failure decreased with increasing beam size. Further numerical analysis was conducted by Qapo et al. (2016). It was also stated that either an increase or a decrease in beam size did not play a considerable role in gaining the shear strength. However, further experimental tests are required to fully understand the effect of beam size on the strengthened behaviour.

Jemaa et al. (2015) investigated the behaviour of a full-scale DE GFRP-strengthened RC beam. It is worth noting that the effect of beam size was not investigated in this research. The results revealed that the embedded GFRP bars increased the shear resistance by approximately 96%, validating the success of the deep embedment technique. The contributions of concrete, steel shear links, embedded FRP bars to the shear resistance were calculated based on the strain readings. Moreover, the higher contribution of FRP bars compared to those in the extant literature can be attributable to the higher effective depth of the beam, which provides better bond performance between embedded FRP bars and concrete (Sogut et al., 2019b). Further results are also discussed in Chapter 4.

2.5.7. Corroded shear links

Structurally deficient RC beams with existing uncorroded and corroded steel shear reinforcement were designed and strengthened with embedded CFRP bars in one part of the research conducted by Qin et al. (2015). The part of the experimental programme, corresponding to the DE technique, consisted of three unstrengthened and three DE FRP-strengthened beams. Thus, three sets of RC beams were targeted for investigation. The first set consisted of unstrengthened and DE CFRP-strengthened beams with uncorroded steel shear links (see Figure 2.10). The second and third sets involved unstrengthened and DE CFRP-strengthened beams reinforced in shear with corroded steel shear links. The corrosion levels of shear links in the second and third sets were 7 and 12%, respectively. Different concrete strength values obtained from test results encouraged the use of normalised shear stress values to make comparisons between tested beams. The normalised shear stress at failure decreased by 0.11 (14%) and 0.1 (12%) with the increase in the level of corrosion from 0 to 12% for the unstrengthened and strengthened beams, respectively. Moreover, normalised shear stress at failure remained almost constant with the increase in the level of corrosion from 0 to 7% for strengthened beams. Test results confirmed that DE CFRP bars increased the normalised shear stress regardless of corrosion level.

As stated above, Qin (2016) conducted tests on structurally deficient RC beams with existing uncorroded and corroded steel shear links (see above, Qin et al., 2015). All beams were designed to have a steel shear reinforcement ratio of 0.29%. The valuable findings in this PhD dissertation showed that the contribution of concrete to the shear resistance remained significant and the shear resistance gain due to embedded CFRP bars was relatively low. This can be attributable to the fact that a high steel shear reinforcement ratio provides better confinement. Further results are given in Chapter 6.

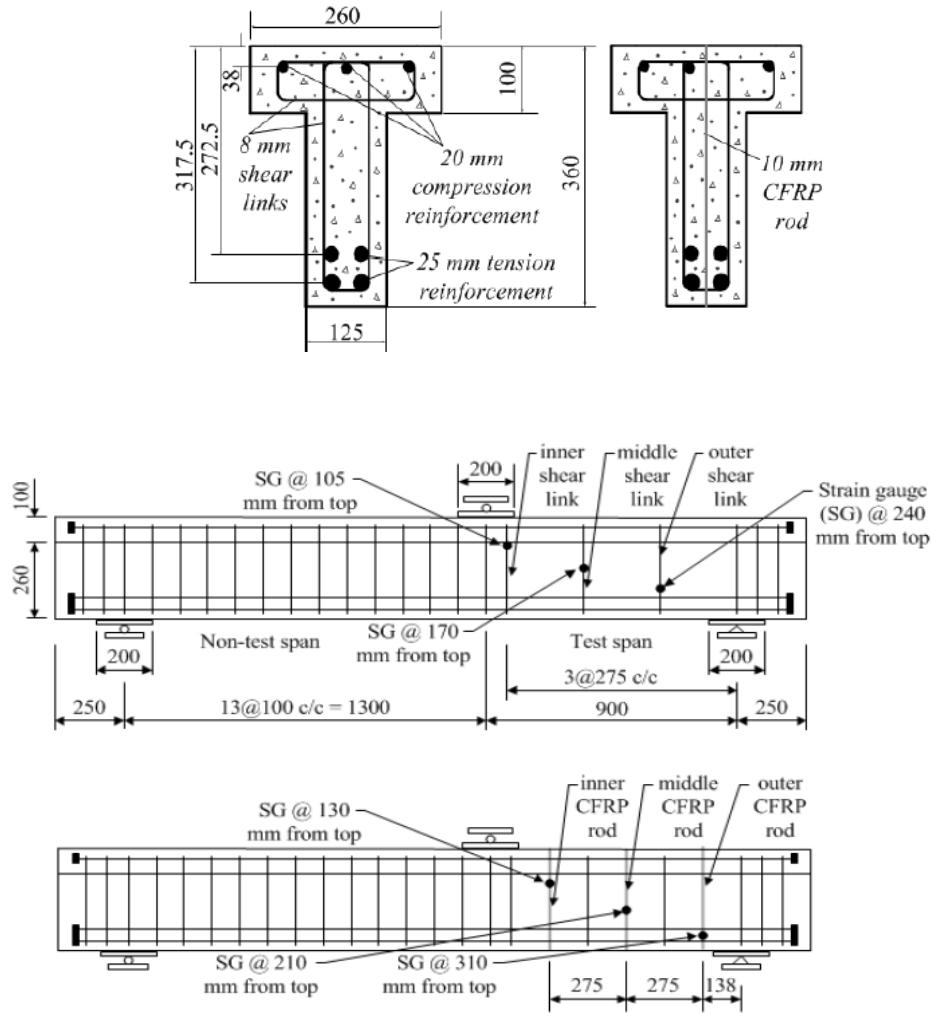


Figure 2.10. Test setup (Qin et al., 2015)

2.5.8. Anchorage system and Prestressed DE bar

Bui et al. (2020a) conducted experimental research on RC T-beams which had identical dimensions to the beams tested by Breveglieri et al. (2015). The effect of test parameters on the strengthened beams has already been discussed in previous subsections. The main contribution of this research to the current literature was to demonstrate the applicability of mechanically anchored embedded GFRP bars in the DE shear strengthening system. The FRP bars were fixed using nuts at their ends, as shown in Figure 2.11.

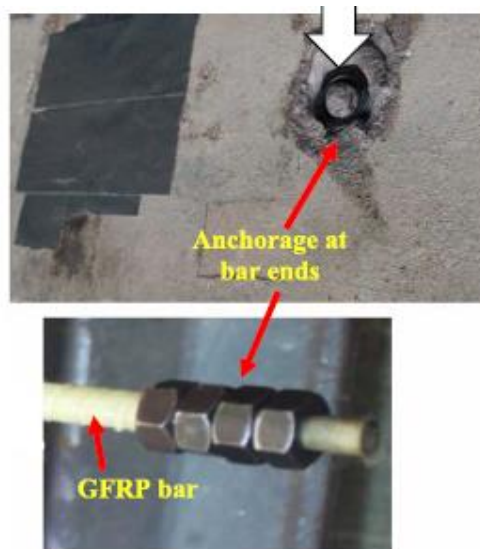


Figure 2.11. Mechanically anchored GFRP bar (Bui et al., 2020a)

Experimental and numerical research was conducted by Bhanugoban et al. (2021) to examine the applicability of prestressed DE steel bars for shear strengthening of RC beams. A total of five RC beams involving one unstrengthened (control), two beams strengthened with either normal or high-tensile DE steel bars and two beams strengthened with prestressed either normal or high-tensile DE steel bars were incorporated in the experimental programme. The prestress level was 40%. The normal and high-tensile DE steel bars provided a shear strength gain of 9.1 and 11.6%, respectively. The shear strength gains due to prestressed normal, and high-tensile DE steel bars were 34.9 and 30.3%, respectively. This indicated that an additional prestress instigated an enhancement of shear force capacity by 25.8 and 18.7% for the beams strengthened with prestressed normal and high-tensile DE steel bars, respectively. Both experimental and FE results showed that prestressed DE steel bars increased the shear force capacity to a greater extent than those without prestress.

Moreover, FE results revealed that the shear strength increased with increasing diameter of the DE steel bars. FE results also established that the shear strength decreased with an increase in the distance between the DE steel bars and the load. This study has valuable findings since the prestressed FRP bars can also be used to enhance the shear strength.

2.6. Summary and conclusions

This chapter overviews general shear mechanisms in uncracked and cracked RC beams as well as shear resistance models established in the literature to shed light on the identification of the behaviour of RC beams reinforced in shear with steel shear links. The general properties of FRP composites, external shear strengthening techniques with FRP composites, and the DE technique are also reflected. Moreover, previous research studies conducted on RC beams strengthened in shear with embedded FRP bars are incorporated in this chapter. Although valuable findings were obtained from numerical and experimental studies, there is still a potential lack of knowledge on the strengthened behaviour of RC beams. The current literature given in this chapter mainly addresses the influences of embedded bar diameter and spacing, shear link corrosion level, a/d ratio, moment-shear interaction, presence of internal steel shear reinforcement, beam size, concrete strength, and presence of anchored FRP bars. Moreover, a recent experimental study has been conducted to examine the efficacy of prestress embedded steel bars.

The effect of embedded bar type was mostly investigated by comparing embedded CFRP and steel bars. The results showed that the contributions of embedded CFRP and steel bars to the shear resistance were comparable. However, the comparison between embedded CFRP and GFRP bars has received less attention. For example, the contribution of DE CFRP

bars can be comparable to the contribution of DE GFRP bars if the GFRP shear reinforcement ratio is increased. Although previous research studies clearly showed that the presence of existing shear links decreased the effectiveness of the DE technique, there is still the need to research the interaction between embedded FRP bars and existing steel shear links. It may be useful to consider axial rigidity of FRP bars to design DE FRP shear strengthening system. The effect of tension reinforcement ratio on EB FRP-strengthened beams was reported (Dirar et al., 2012). However, the current literature does not cover the effect of tension reinforcement ratio on the DE FRP-strengthened behaviour. While the influence of existing holes on rectangular concrete beams was investigated by Valerio and Ibell (2003), the effect of existing holes on RC T-beams has not yet been identified. Similar to effects of tension reinforcement ratio and existing holes, the impact of the embedded length of DE bars on the strengthened behaviour has not yet been investigated. The beam size and a/d ratio are two main parameters governing the shear behaviour of RC beams, as previously mentioned in Section 2.2 (Kani, 1964; Kani, 1967; Bažant and Kim, 1984). The only and sole experimental study investigating the impact of a/d ratio on the DE FRP-strengthened behaviour was conducted by Dirar and Theofanous (2017). Further numerical research was carried out by Caro (2018). Therefore, a significant knowledge gap on the effect of a/d ratio on the DE FRP-strengthened behaviour still exists. Similar to the effect of a/d ratio, the only and sole experimental study was performed on geometrically similar RC T-beams by Brindley (2018). As can be seen in Table 2.1, most of the experimental study involved RC beams with an overall depth of less than 500 mm. It is crucial to investigate the effect of beam size on the behaviour of DE FRP-strengthened beams since an increase in the beams size instigates a reduction in shear strength and a transition from ductile to brittle behaviour (Kani, 1967; Bažant and Kim, 1984; Bažant, 1997). It was also demonstrated that the existing design models provide conservative predictions (Qapo et al., 2016; Dirar and

Theofanous, 2017). New design equations are therefore required. Thus, the test parameters described in Chapter 3 and Chapter 4 comprise steel-to-FRP shear reinforcement ratio, tension reinforcement ratio, presence of existing holes, embedded length of FRP bars, and a/d ratio. The influence of beam size on the DE FRP-strengthened behaviour is also incorporated in this study. Moreover, further numerical investigations, as well as new design equations for shear-strengthened RC beams with embedded FRP bars, are given in Chapter 6.

Table 2.1. Summary of previous studies on RC beams strengthened with the DE technique

Reference	Number of tested beams	Beam Geometry and Test Properties										Test Parameters												
		Rectangular	T-shaped	Slender ($a/d \geq 2.5$)	Deep ($a/d \leq 2.5$)	Depth \leq 500 mm	Depth \geq 500 mm	Simply supported	Continuous	RC beam	Prestressed Concrete beam	Unfilled holes	DE bar type	DE bar spacing	DE bar diameter	DE bar inclination angle	Steel shear link ratio	a/d ratio	Beam size	Corroded shear links	Concrete strength	Anchorage system	Prestressed DE bar	DE FRP surface coating
Valerio and Ibell (2003)	10																							
Valerio et al. (2009)	34																							
Mofidi et al. (2012a)	9																							
Qin et al. (2015)	6																							
Breveglieri et al. (2015)	19																							
Jemaa et al. (2015)	2																							
Qapo et al. (2016)	N/A*																							
Dirar and Theofanous (2017)	4																							
Raicic et al. (2017)	10																							
Brindley (2018)	4																							
Caro (2018)	N/A*																							
Bui et al. (2020a)	11																							
Bhanugoban et al. (2021) **	5																							

* Numerical analysis / ** Experimental and numerical research

CHAPTER 3: EXPERIMENTAL PROGRAMME

3.1. General

An experimental programme involving fifteen RC T-beams was set to meet the research objectives given in the first chapter. This chapter overviews the following;

- The experimental programme focussing on the geometrical details of the beams
- The fabrication process of the beams
- Explanation of shear strengthening process
- The properties of materials used in this experimental programme
- Description of experimental setup and instrumentation

The description, fabrication process, and DE shear strengthening scheme of the beams are reported in Section 3.2. Material properties of concrete, steel reinforcement, fibre reinforced polymer bars, and epoxy resin are covered in Section 3.3. The experimental setup and instrumentation are described in Section 3.4. Concluding remarks are reflected in Section 3.5.

3.2. Preparation of beams

A total of 15 RC T-beams were constructed and tested at the University of Birmingham Structural Engineering Laboratory. Section 2.6 clearly demonstrated that more research is needed to investigate the effects of the steel-to-FRP shear reinforcement ratio, tension reinforcement ratio, presence of existing holes, embedded length of FRP bars, a/d ratio, and beam size on the DE FRP-strengthened behaviour. As mentioned in Section 2.5, the large-scale unstrengthened and DE FRP-strengthened beams were tested by Dirar and Theofanous (2017) to investigate the effect of the a/d ratio on the DE FRP-strengthened behaviour. It is worth noting that the results of these beams were first reported by Jemaa et al. (2015). All dimensions of RC T-beams tested by Dirar and Theofanous (2017) were scaled down by multiplying 0.5 to produce the small-scale beams described in this chapter. To investigate the effect of beam size, all parameters (i.e., steel and FRP reinforcement ratios, a/d ratio, concrete strength) were kept constant. The beams had an a/d ratio of either 1.9 or 3, identical to those tested by Dirar and Theofanous (2017). The percentage of tension reinforcement was either 2.0 or 2.7% to explore the impact of tension reinforcement on the DE FRP-strengthened behaviour. The DE shear strengthening system consisted of different types of embedded FRP bars and different FRP shear reinforcement ratios to investigate steel-to-FRP shear reinforcement ratio. The effect of existing unfilled holes and embedded length of FRP bars on the unstrengthened and strengthened behaviour, respectively, was also examined. The embedded length of FRP bars was either 262.5 or 325 mm. The FRP bars with a length of 325 mm were inserted throughout the entire depth of the beam. This allows the investigation of the case where the truss action is fully developed. In some cases, it might be difficult to drill the holes throughout the entire depth of the RC T-beams. It is therefore that the FRP bars with a length of 262.5 mm were used to investigate the case where the tension

chord is not connected to the compression chord. Moreover, the maximum anchorage length for GFRP and CFRP bars recommended by TR55 (2012) was about 19 and 52 mm, respectively. The following subsections detail the geometrical dimensions, steel and FRP reinforcement details, manufacturing process, and DE shear strengthening scheme.

3.2.1. Description of beams

The experimental programme involved three unstrengthened (control) RC T-beams, two unstrengthened RC T-beams with existing unfilled holes, and ten DE FRP-strengthened RC T-beams. The unstrengthened beams had a three-part designation, whereas the DE FRP-strengthened beams and unstrengthened beams with unfilled holes had a four-part designation. The first part indicates that a beam was either an unstrengthened (U) or a strengthened (S) specimen. The second part denotes that a beam was either a slender (S) or a deep (D) specimen. The slender specimens had a shear span-to-effective depth ratio (a/d) of 3 whereas deep specimens had an a/d ratio of 1.9. The third part refers to the percentage of tension reinforcement (either 2.0 or 2.7) in the maximum moment zone. The percentage of tension reinforcement is defined as follows;

$$\rho_l = \frac{A_s}{b_w \cdot d} * 100 (\%) \quad (3.1)$$

where A_s is the area of tension reinforcement, b_w is the web width of the beam and d is the effective depth of the beam.

The fourth part refers to either the number of unfilled holes (either H3 for 3 holes or H6 for 6 holes) in the tested shear span with a hole length of 325 mm, or the type (either glass (G) or carbon (C)), number (2, 3, or 6), and embedded length (either 262.5 or 325 mm) of DE FRP bars installed in the tested shear span. Hence, the designation S/S/2.7/C3-325 refers to

a strengthened slender beam with a tension reinforcement ratio of 2.7% and 3 CFRP bars with an embedded length of 325 mm. Table 3.1 contains details on the tested beams. It is worth noting that the test performed on S/S/2.7/G3-325 was repeated to measure the accuracy of the experimental results. The repeated beam was referred to S/S/2.7/G3-325*.

Table 3.1. Details of tested beams

Specimen Reference	ρ_t (%)	FRP Material Type	Number of FRP bars	Number of Unfilled Holes	Embedded FRP Bar or Hole Length (mm)	a/d
U/S/2.0	2.0	-	-	-	-	3
U/S/2.7	2.7	-	-	-	-	3
U/D/2.7	2.7	-	-	-	-	1.9
U/S/2.7/H3-325	2.7	-	-	3	325	3
U/S/2.0/H6-325	2.0	-	-	6	325	3
S/S/2.0/G3-325	2.0	Glass	3	-	325	3
S/S/2.7/G3-325	2.7	Glass	3	-	325	3
S/S/2.7/G3-325*	2.7	Glass	3	-	325	3
S/S/2.0/G6-325	2.0	Glass	6	-	325	3
S/S/2.7/G6-262.5	2.7	Glass	6	-	262.5	3
S/S/2.7/G6-325	2.7	Glass	6	-	325	3
S/S/2.7/C3-262.5	2.7	Carbon	3	-	262.5	3
S/S/2.7/C3-325	2.7	Carbon	3	-	325	3
S/D/2.7/G2-325	2.7	Glass	2	-	325	1.9
S/D/2.7/C2-325	2.7	Carbon	2	-	325	1.9

➤ *Slender beams;*

The slender RC T-beams had a flange width of 200 mm, flange depth of about 63 mm, web width of 75 mm and overall height of 325 mm. As shown in Figure 3.1, the slender beams with an effective depth of about 300 mm and an a/d ratio of 3 were tested in a three-point bending configuration. This setup allowed two tests to be conducted on one beam by testing one beam end zone while keeping the other end unstressed and vice versa. The beams were longitudinally reinforced in compression with one layer of two 8 mm diameter steel bars. The tension reinforcement comprised either four 12 mm diameter steel bars or four 12 mm and two 10 mm diameter steel bars (see Figure 3.1 (a)), resulting in a tension reinforcement ratio in the maximum moment zone of either 2.0 or 2.7%, respectively. The steel shear reinforcement of the tested shear span consisted of 4 mm diameter steel shear links spaced at 300 mm centre-to-centre (c/c), indicating a steel shear reinforcement ratio of 0.11%. The percentage of steel shear reinforcement ratio is determined as follows;

$$\rho_s = \frac{A_{sw}}{b_w \cdot s} * 100 (\%) \quad (3.2)$$

where A_{sw} is the area of steel shear reinforcement, b_w is the web width of the beam and s is the spacing of steel shear reinforcement.

This steel shear link configuration is representative of earlier design practice in the UK (Concrete Society, 2009, Qin et al., 2015, Sogut et al., 2021). The non-test span was reinforced in shear with 4 mm diameter steel shear links spaced at 150 mm (c/c). This configuration provided the non-test span with a shear resistance higher than that of the test span. The DE shear strengthening system involved 6 mm sand-coated FRP bars spaced as

depicted in Figure 3.1 (c). The beams with 3 DE bars had an FRP shear reinforcement ratio of 0.125% whereas the beams with 6 DE bars had an FRP shear reinforcement ratio of 0.25%. The FRP shear reinforcement ratio was determined according to Eq. 3.3. The position and spacing of unfilled holes in the tested shear spans of the beams are also shown in Figure 3.1 (c).

$$\rho_f = \frac{A_f}{b_w \cdot s_f} * 100 (\%) \quad (3.3)$$

where A_f is the area of FRP shear reinforcement and s_f is the spacing of FRP shear reinforcement.

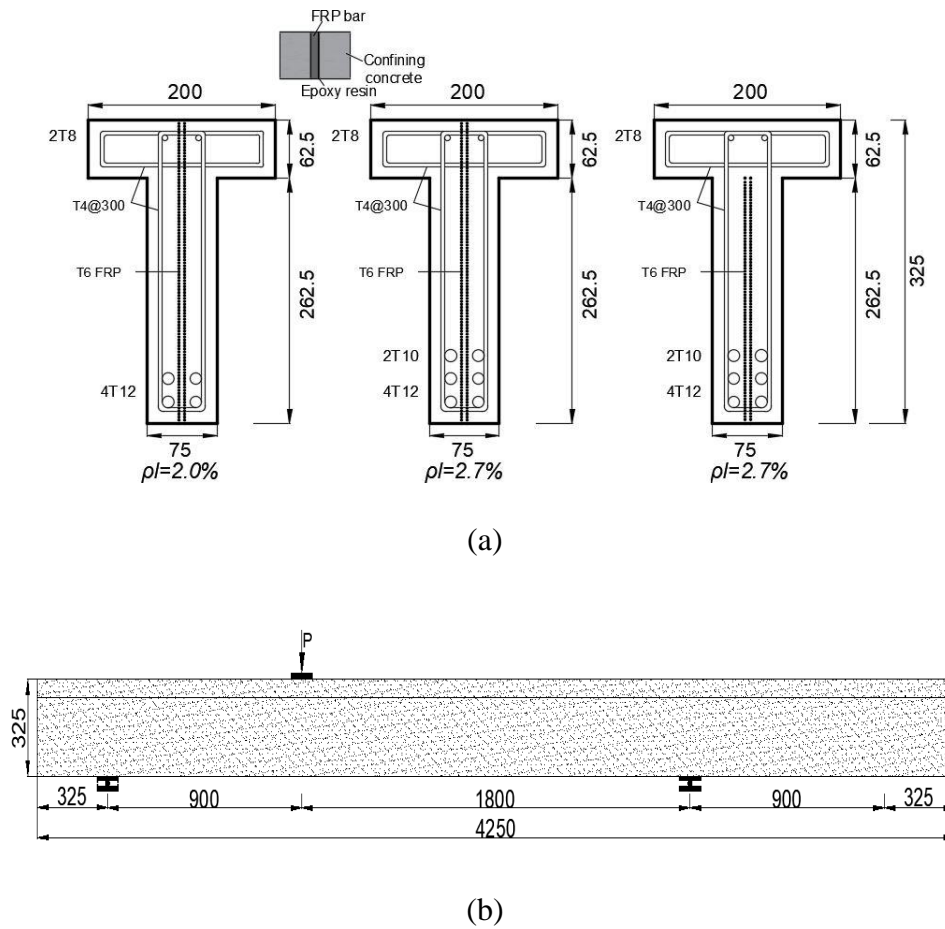
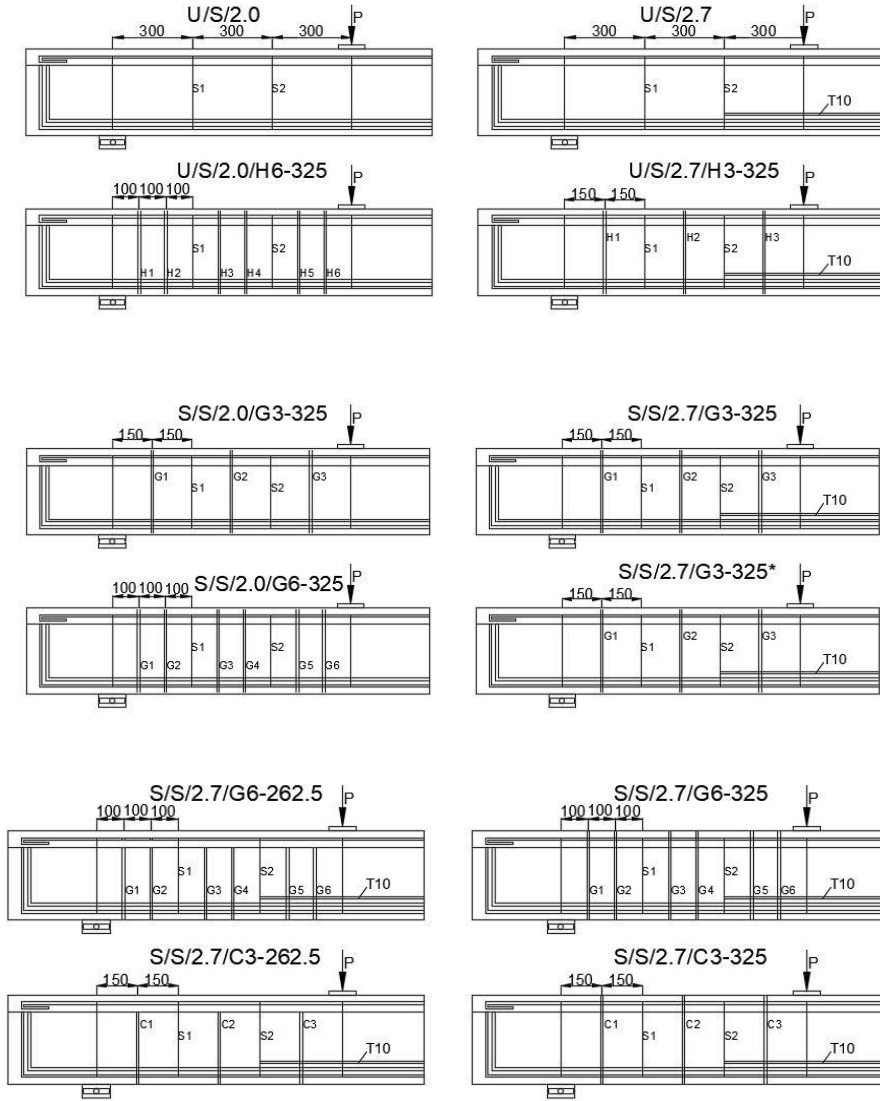


Figure 3.1. Continued



(c)

Figure 3.1. Details of slender beams; (a) cross-section of beams (b) elevation of beams (c) FRP and steel reinforcement details (units in millimetres)

➤ *Deep beams;*

Three RC deep beams were also tested in a three-point bending setup. The deep beams had a tension reinforcement ratio and overall length of 2.7% and 2125 mm, respectively, as demonstrated in Figure 3.2. Similar to the slender beams, the effective depth, total height, width, flange depth, and flange width of the deep beams were 300 mm, 325 mm, 75 mm, 63 mm, and 200 mm, respectively. All deep beams had an a/d ratio of 1.9. As shown in Figure

3.2 (a), the beams were reinforced in compression with two 8 mm diameter steel bars. The tension reinforcement consisted of four 12 mm and two 10 mm diameter steel bars, resulting in a tension reinforcement ratio of 2.7%. The steel shear reinforcement comprised 4 mm diameter shear links spaced at 225 mm (c/c), resulting in a steel shear reinforcement ratio of 0.15%. To provide a non-test span with a shear resistance higher than that of the corresponding test span, the spacing of steel shear links was reduced in the non-test span as demonstrated in Figure 3.2. The DE FRP shear reinforcement consisted of 6 mm sand-coated FRP bars spaced at a distance of 225 mm (c/c). The DE FRP shear reinforcement ratio was 0.17% for strengthened deep beams.

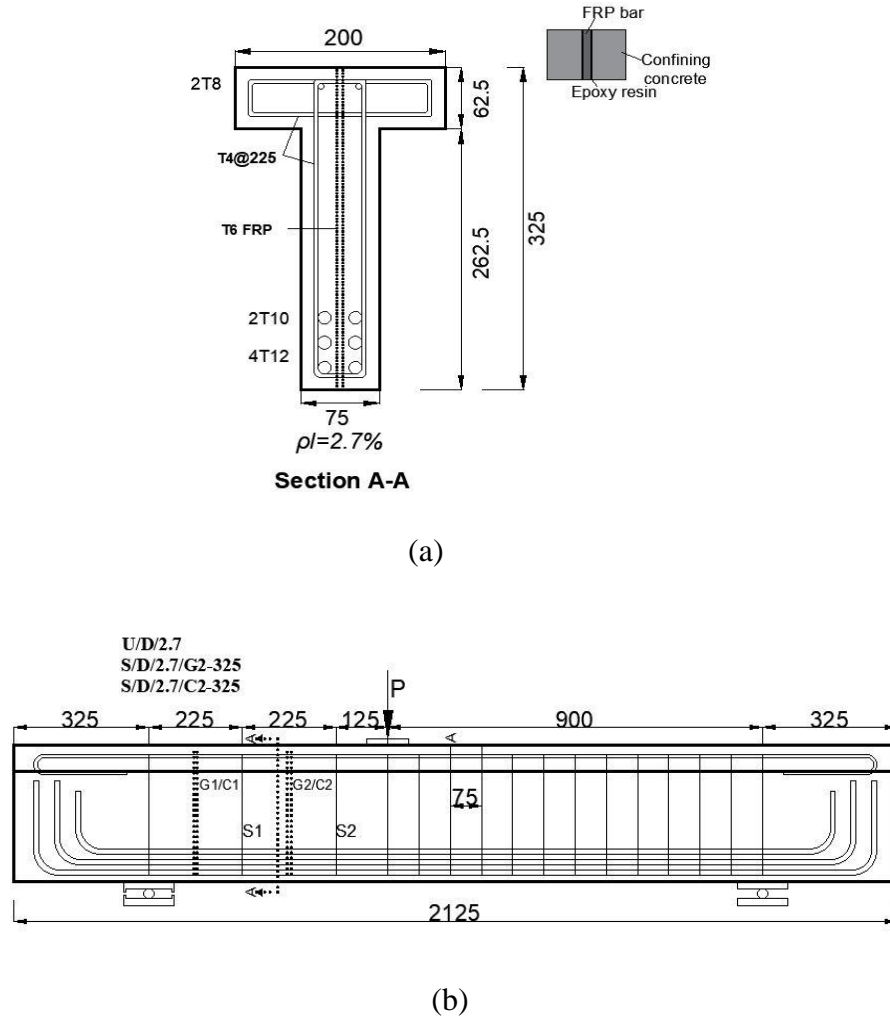
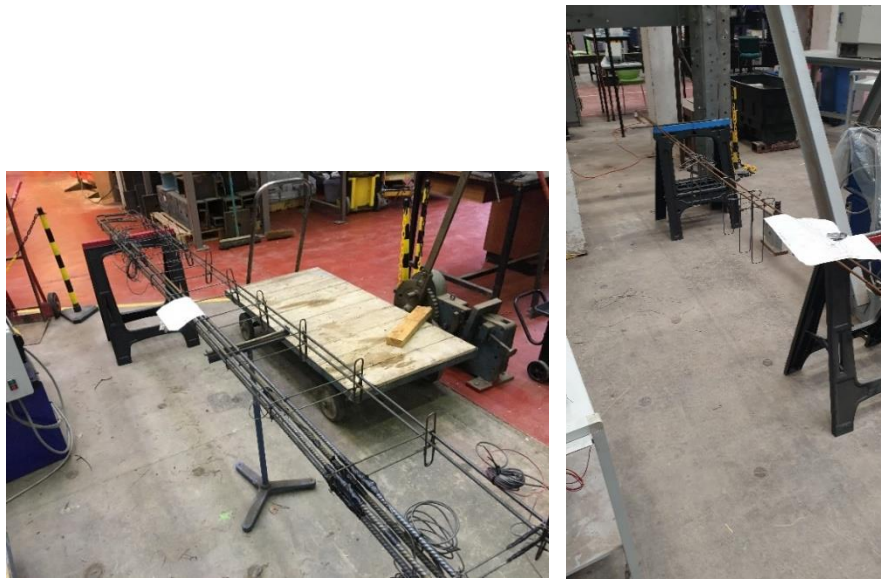


Figure 3.2. Details of deep beams; (a) cross-section of beams (b) elevation of beams (units in millimetres)

3.2.2. Fabrication of specimens

All beams were fabricated at the University of Birmingham Structural Engineering Laboratory. The steel reinforcement cages of the specimens were built, as demonstrated in Figure 3.3 (a). The longitudinal steel reinforcement bars were bended and delivered by the supplier, whereas 4 mm steel reinforcement bars were bended at the laboratory to produce steel shear links. The details of attaching strain gauges are discussed in Section 3.4. A reusable plywood (wood-based material) mould was manufactured for the beams (see Figure 3.3 (b)). As shown in Figure 3.3 (c), each beam was cast from grade C40 concrete. The material properties of the concrete are given in detail in Section 3.3.



(a)

Figure 3.3. Continued



(b)



(c)

Figure 3.3. Fabrication of specimens; (a) steel reinforcement cage (b) wood formwork (c) casting concrete

3.2.3. Strengthening process

In order to embed the FRP bars, vertical holes (hole diameter equals to 1.5 times FRP bar diameter) were formed in the shear spans of the beams, through the centreline of the cross-sections, at the FRP bar locations shown in Figure 3.1 and 3.2. The vertical holes were

created by installing PVC rods at the required positions within the steel reinforcement cage before casting the concrete as shown in Figure 3.4 (a). The PVC rods were removed from the concrete 24 hours after casting. A 10 mm diameter drill bit was then used to enlarge the cast-in-place holes in the beams. Prior to installing the FRP bars, the drilled holes were roughened by a wire brush and cleaned with compressed air. The lower ends of the holes were sealed, and epoxy resin was used to fill two-thirds of the holes. The FRP bars were covered with a thin layer of the adhesive and inserted into the holes (see Figure 3.4 (b)). Any excess epoxy was removed. It has already been demonstrated that it is possible to install FRP bars without using cast-in-place holes (Valerio and Ibell 2003, Chaallal et al. 2011, Breveglieri et al. 2015). The procedure explained above for embedding the FRP bars was used for simplicity. It should be noted that the explained process above was also used in the case of S/S/2.7/G6-262.5 and S/S/2.7/C3-262.5. The only difference was that the beam flange was filled with high strength grout after the process described above. The material properties of FRP bars and used adhesive are given in the following section.

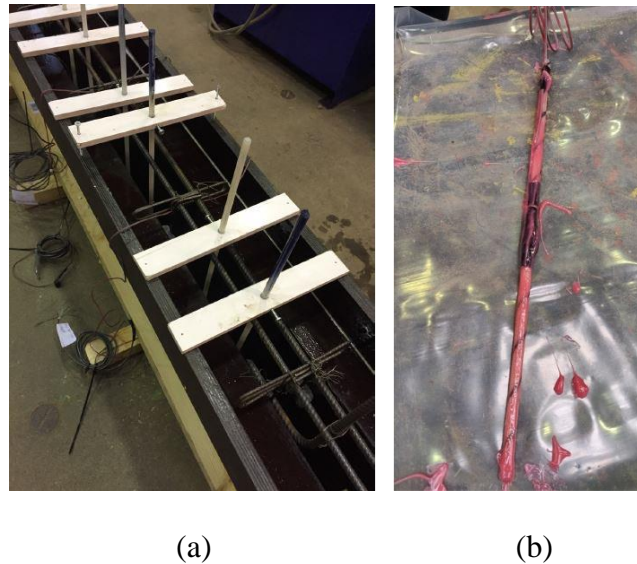


Figure 3.4. Continued



(c)

Figure 3.4. Embedding FRP bars; (a) PVC rods (b) a thin layer adhesive on an FRP bar (c)

Embedded FRP bars

3.3. Material properties

The properties of the concrete, steel reinforcement bars, FRP bars, and epoxy resin used in the experimental research are summarised in the subsequent subsections. The proportions of coarse and fine aggregate, cement, water and superplasticiser are detailed in the first subsection. The mechanical properties of steel reinforcement bars, FRP bars and epoxy resin declared by their manufacturers are incorporated in the remaining subsections.

3.3.1. Concrete

Each RC T-beam was cast from a single batch of ready-mixed concrete with a maximum aggregate size of 10 mm and a target concrete cylinder and cube compressive strength of 40 and 50 MPa, respectively. The targeted concrete compressive strength was preferred as it allowed a relatively high flexural-to-shear strength ratio. The concrete pre-mixed

proportions were cement: sand: coarse aggregate = 1: 1.30: 2.65 and the water-to-cement ratio was 0.42. A superplasticiser (Alphaflow 420) dosage of 0.75% by weight of cement was added to ensure adequate workability of the concrete mix. The concrete mixture proportions are summarised in Table 3.2.

Table 3.2. Concrete mixture

Coarse Aggregate (kg/m³)	Fine Aggregate (kg/m³)	Cement (kg/m³)	Water (kg/m³)	Superplasticiser (kg/m³)
1165	572	440	186	3.3

Each concrete batch was used to cast one RC T-beam, four cubes (100x100x100 mm) and four cylinders (100x200 mm). Each RC beam, together with corresponding concrete cube and cylinder samples, was cured under laboratory air conditions. Standard compression tests conforming to BS EN 12390-3 (2009, 2019) were conducted on the day of beam testing on cubes and cylinder specimens. The results obtained from at least two cube and two-cylinder samples on the day of beam testing showed that the concrete had average cylinder and cube compressive strength values of 41.3 and 50.5 MPa, and standard deviation values of 2.3 and 1.6 MPa, respectively. The average concrete compression test results on the day of beam testing for each RC T-beam are given in Table 3.3. Except for U/S/2.0 and S/S/2.0/G6-325, all beams were tested between 10 and 28 days after casting. U/S/2.0 and S/S/2.0/G6-325 were tested immediately after 28 days after casting. The concrete compressive tests conducted on cylinder samples at 28 days showed that the average concrete strength was 46 MPa.

Table 3.3. Average concrete compression test result for each specimen

Specimen Reference	Average Cube compressive strength (MPa)	Average Cylinder compressive strength (MPa)
U/S/2.0	45.7	50.4
U/S/2.7	42.7	48.8
U/D/2.7	39.6	52.3
U/S/2.7/H3-325	40.3	49.5
U/S/2.0/H6-325	38.6	50.2
S/S/2.0/G3-325	38.6	50.2
S/S/2.7/G3-325	39.2	50.1
S/S/2.7/G3-325*	40.6	49.9
S/S/2.0/G6-325	45.7	50.4
S/S/2.7/G6-262.5	40.6	49.9
S/S/2.7/G6-325	40.3	49.5
S/S/2.7/C3-262.5	39.2	50.1
S/S/2.7/C3-325	42.7	48.8
S/D/2.7/G2-325	42	54.7
S/D/2.7/C2-325	41.2	53.1

3.3.2. Steel reinforcement

Ribbed steel reinforcement bars with four different diameters (4 mm, 8 mm, 10 mm, or 12 mm) were used in this experimental programme. The grade of the reinforcement bars was B500B according to BS 4449 (2005). The yield strengths (f_y), ultimate strength (f_u) and elastic moduli (E_s) of the longitudinal and transverse reinforcement bars, as declared by the manufacturers, are reported in Table 3.4.

Table 3.4. Material properties of steel reinforcement bars

Property	4 mm Steel bars	8, 10 and 12 mm Steel bars
Elastic modulus (E_s) (MPa)	200000	200000
Yield strength (f_y) (MPa)	540	580
Ultimate Strength (f_u) (MPa)	680	680

3.3.3. Fibre reinforced polymer and epoxy resin

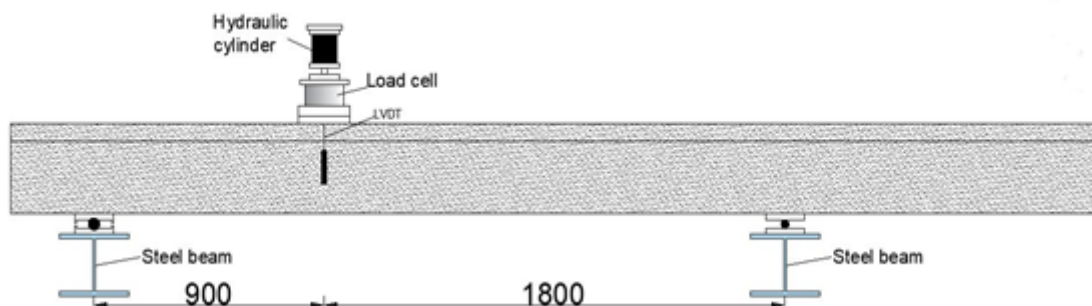
For the purpose of strengthening the RC T-beams, either sand-coated glass or carbon FRP bars with a diameter of 6 mm were employed. The mechanical characteristics of the FRP bars were declared by the manufacturer. The sand-coated 6 mm diameter GFRP and CFRP bars had tensile strengths of 900 and 2300 MPa, elastic moduli of 46 and 130 GPa, and ultimate strains of 1.9 and 1.7%, respectively. A commercially available high viscosity epoxy resin (Hilti RE 500) was used to bond the FRP bars to the concrete. This epoxy resin was chosen due to its excellent bond performance (Valerio et al., 2009). The bond strength, compressive strength, compressive modulus, tensile strength, and elongation at failure of the

epoxy resin were 12.4 MPa, 82.7 MPa, 1493 MPa, 43.5 MPa and 2%, respectively, as certified by the manufacturer.

3.4. Test setup and instrumentation

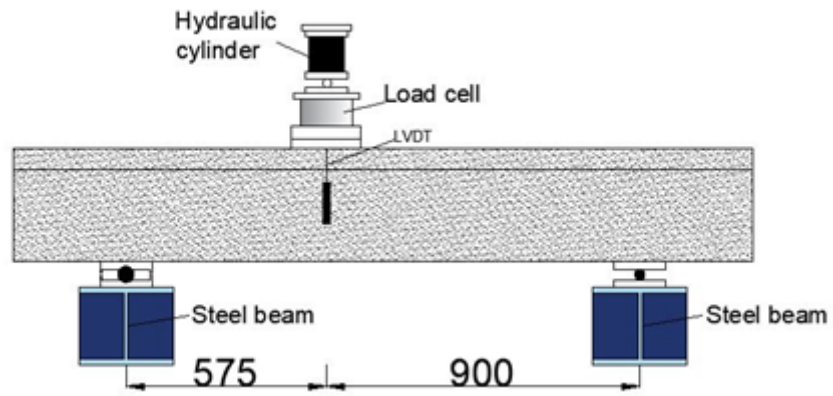
The RC T-beams were tested in a three-point bending configuration as shown in Figure 3.5. As mentioned in Section 3.2.1, this loading configuration allowed two slender beam tests to be performed on one beam specimen by testing one beam end zone while keeping the other end unstressed and vice versa. The load was applied using a 1000 kN hydraulic cylinder. The beams were whitewashed before testing. This process facilitated the observation of crack development and thus helped tracing of crack patterns up to beam failure. The cracks were traced at a load increment of 10 kN.

The experimental setup of slender and deep beams is depicted in Figure 3.5. The supporting steel plates had a width of 100 mm, length of 200 mm and thickness of 10 mm. The centre-to-centre lengths of the test spans were 575 mm and 900 mm for the deep and slender beams, respectively. The length between the loading point and the farthest support was 900 mm and 1800 mm for the deep and slender beams, respectively. A steel loading plate with a width of 140 mm, a length of 255 mm, and a thickness of 25 mm was used.



(a)

Figure 3.5. Continued



(b)



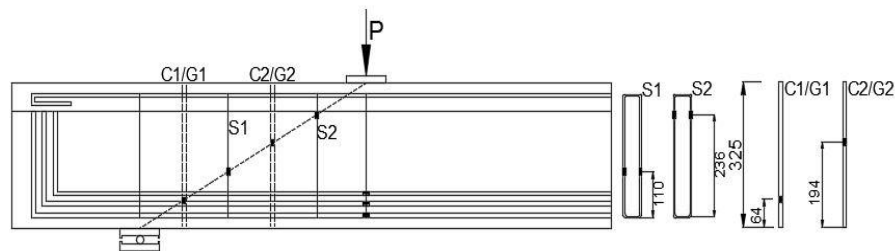
(c)



(d)

Figure 3.5. Experimental setup of slender and deep beams (a) schematic view of slender beams (b) schematic view of deep beams (c) slender beam before testing (d) deep beam before testing (units in millimetres)

The load was measured by a 1000 kN load cell placed between the hydraulic cylinder and the RC T-beam, as shown in Figure 3.5. The vertical deflection under applied load was measured by displacement transducers, which were attached to each side of the steel loading plate. The tension reinforcement at the position of the maximum bending moment was instrumented with 6 mm-120 Ω strain gauges to measure strain. The strain in the steel and FRP shear reinforcement was measured using 3 mm-120 Ω strain gauges positioned along the line joining the support and loading point, which was a trajectory of expected shear cracks. The locations of the strain gauges are detailed in Figure 3.6 for deep and slender beams. A protective coating was spread on each strain gauge to avoid damaging strain gauges during contact with the fresh concrete and epoxy resin (see Figure 3.7). The readings of the 1000 kN load cell, displacement transducers, and strain gauges were obtained using a data logger connected to a personal computer.



(a)

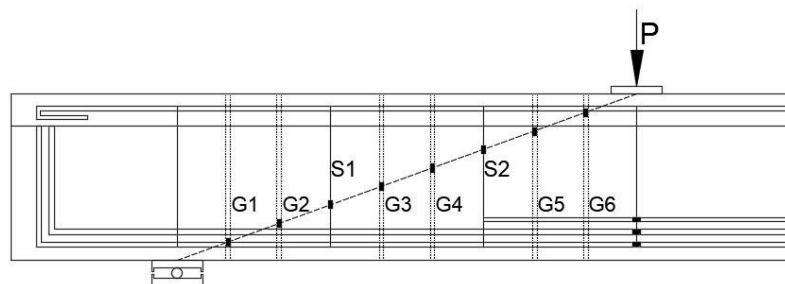
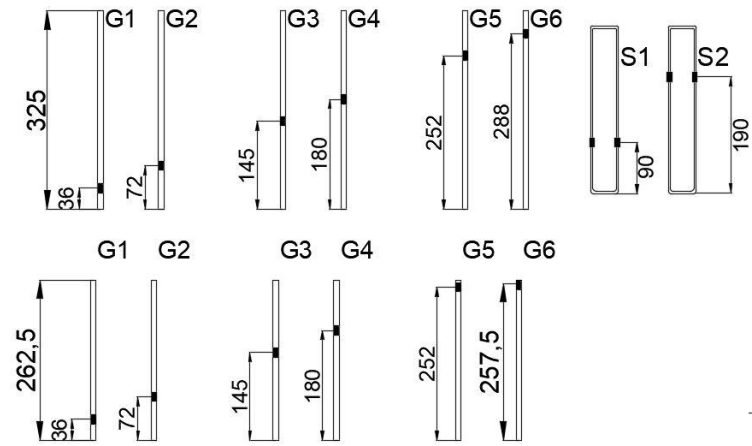
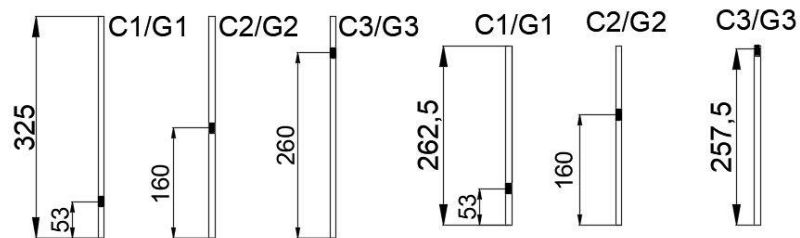
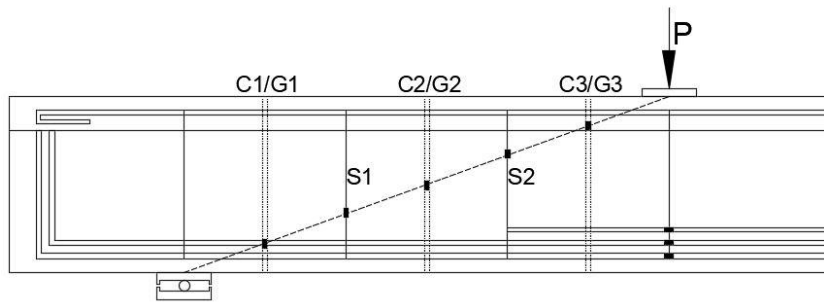


Figure 3.6. Continued



(b)



(c)

Figure 3.6. Positions of strain gauges (a) Deep beams (b) Slender beams with 6 FRP bars
(c) Slender beams with 3 FRP bars (units in millimetres)

The below steps, which were also successfully implemented by Qin (2016) for attaching strain gauges to the steel and FRP reinforcement, were followed;

- A flat file was used to remove the ribs of the steel reinforcement and then a sand paper was used to obtain a smooth surface. It should be noted that a sand paper was only used on the surface of the FRP bars. This prevented inflicting damage on the FRP bars.
- Alcohol was then used to clean the surface of the steel reinforcement whereas clean water was used for cleaning the surface of the FRP bars.
- Transparent tape was used to position strain gauges on the surface of steel and/or FRP bars. This process was followed by using a super glue to stick strain gauges.
- The final step comprised spreading protective coating on each strain gauge to avoid damaging strain gauges during contact with fresh concrete and epoxy resin. Some of details of the process described above are demonstrated in Figure 3.7.

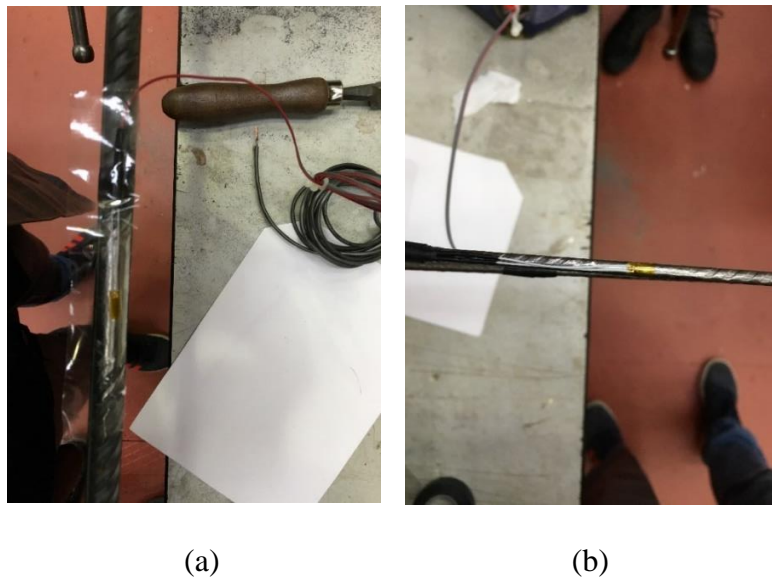


Figure 3.7. Continued

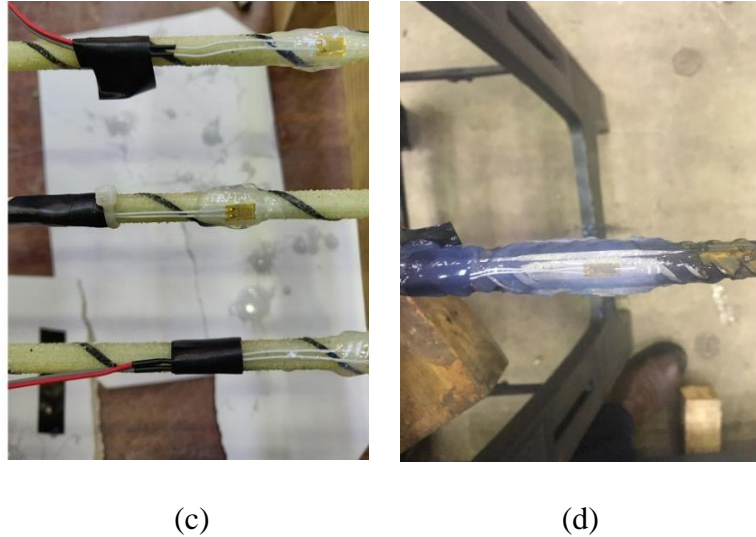


Figure 3.7. Strain gauges (a) on tension reinforcement (b) on 4 mm diameter steel shear link (c) on GFRP bar with protective coating (d) on tension reinforcement with protective coating

3.5. Summary and conclusions

Fifteen RC T-beams, which comprised the experimental programme described in this chapter, were designed, fabricated and tested at the University of Birmingham Structural Engineering Laboratory. The details of the steel reinforcement configurations, FRP shear strengthening schemes, materials, testing procedure and instrumentation were given. All beams had the same cross-section and were tested under three-point bending setup. The beams had an a/d of either 1.9 or 3. The results on the day of beam testing showed that the concrete had average cylinder and cube compressive strength values of 41.3 and 50.5 MPa, and standard deviation values of 2.3 and 1.6 MPa, respectively. The mechanical properties of the steel reinforcement and FRP bars were declared by the manufacturers. The tension reinforcement, steel shear links, and FRP bars were equipped with strain gauges to measure variation in strain during physical testing. The applied load was measured using a 1000 kN load cell. The vertical deflection of the beams was measured using two displacement

transducers, one at each side of the loading point. The readings of the load cell, displacement transducers and strain gauges were obtained using a data logger connected to a personal computer.

CHAPTER 4: EXPERIMENTAL RESULTS AND DISCUSSION

4.1. General

The experimental results of the unstrengthened and DE FRP-strengthened RC beams are presented in this chapter. The experimental programme was conducted to explore the effectiveness of embedded FRP bars for strengthening of shear-deficient RC beams. Fifteen RC T-beams, comprising five unstrengthened beams and ten beams strengthened in shear with embedded FRP bars, were tested to failure. The test parameters included steel-to-FRP shear reinforcement ratio, tension reinforcement ratio, presence of existing holes, embedded length of FRP bars and a/d ratio.

Section 4.2 presents the experimental observations and measurements. The experimental results are presented in terms of cracking, failure modes, shear force-deflection response and strain in both steel shear links and embedded FRP bars. The discussion of the experimental results is presented in Section 4.3. The discussion section provides a summary of the experimental results; the components of shear resistance; and the effect of steel-to-FRP shear reinforcement ratio, size, a/d ratio, FRP bar depth and presence of holes on the DE FRP strengthened behaviour. The valuable findings obtained from the experimental results are summarised in Section 4.4.

4.2. Experimental observations and measurements

4.2.1. Unstrengthened beams

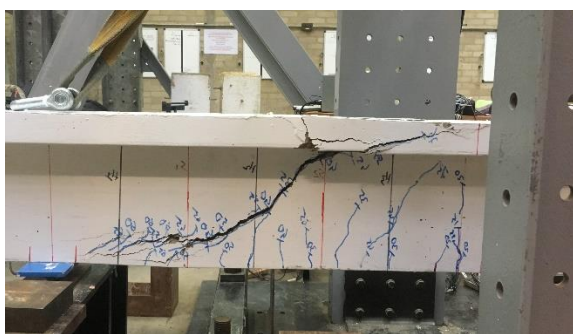
The unstrengthened slender beams (U/S/2.0, U/S/2.7, U/S/2.7/H3-325, and U/S/2.0/H6-325) failed in shear due to a diagonal shear crack as demonstrated in Figure 4.1. The formation of flexural cracks at the soffit of the beams under the load started at a shear force of about 10 kN. With increased loading, the flexural cracks extended into the shear span. The outermost flexural cracks turned into inclined cracks at a shear force of about 25 kN. Upon further loading, more inclined cracks occurred in the shear span and, a diagonal tension failure was observed finally.



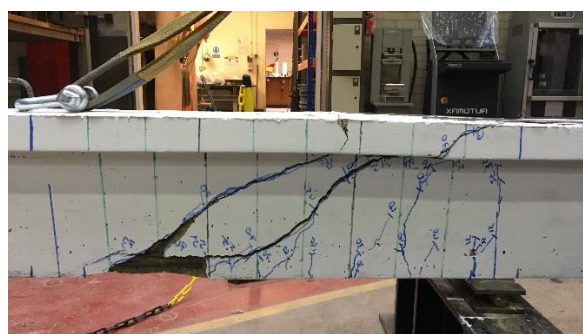
U/S/2.0



U/S/2.7



U/S/2.7/H3-325



U/S/2.0/H6-325

Figure 4.1. Crack patterns of the unstrengthened slender beams at failure

The unstrengthened deep beam (U/D/2.7) also failed in shear as demonstrated in Figure 4.2. The formation of flexural cracks in the maximum moment zone of the beam initiated at a shear force of 12 kN. Upon further loading, the flexural cracks propagated into the shear span. The outermost flexural cracks in the shear span of the beam turned into inclined cracks at a shear force of about 30 kN. With increased loading, inclined cracks extended between the loading and support plates. The flange of the beam representing the compression zone was penetrated by inclined cracks and a shear-compression failure was eventually observed. The crushed concrete in the compression zone as well as next to the support clearly characterised the shear-compression failure. Of note is that the impact of a/d ratio on the failure mode of unstrengthened beams was clearly observed. Slender beams failed due to diagonal tension whereas the unstrengthened deep beam exhibited a shear-compression failure. This can be attributable to arch action in deep beams where the acting load is transferred to the support by direct compression.



Figure 4.2. Crack pattern of the unstrengthened deep beam at failure

Figure 4.3 illustrates the shear force-deflection curves for the unstrengthened beams. A quasi-linear relationship between shear force and deflection was observed for all beams before reaching peak shear force. This was followed by an observation of a sudden drop in load, which demonstrated shear failure. U/D/2.7 had the highest cracked stiffness compared to the remaining unstrengthened slender beams. This can be attributable to the fact that the slender beams were longer and subjected to higher bending moments. Thus, more cracks appeared in the shear spans of slender beams, and this instigated a reduction in the stiffness of slender beams. It can also be seen that an increase in the tension reinforcement ratio from 2.0 to 2.7% caused up to a 22% increase in the cracked stiffness of U/S/2.7 compared with that of U/S/2.0. 3 and 6 holes in the shear span caused a reduction in the stiffness of U/S/2.7/H3-325 and U/S/2.0/H6-325, respectively, compared with that of U/S/2.7 and U/S/2.0, respectively.

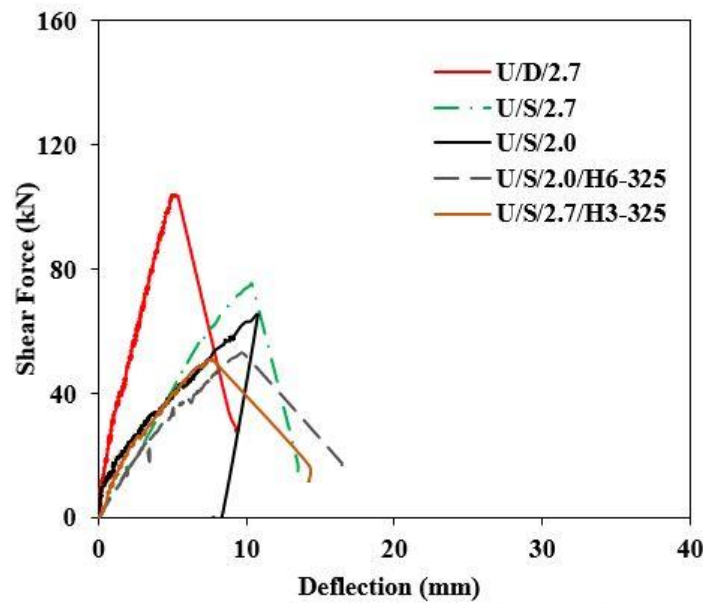


Figure 4.3. Shear force vs deflection for the unstrengthened beams

Figure 4.4 shows the shear force-strain curves for the steel shear links in the unstrengthened beams. The positions of the strain gauges attached to the first and second steel shear links (S1 and S2) are depicted in Figure 3.6. The steel shear links in U/S/2.0, U/S/2.7, U/S/2.7/H3-325, U/S/2.0/H6-325 were inactive up to the formation of inclined cracks at a shear force of 20-35 kN. Upon further loading, these shear links started to develop strain, showing their contribution to the shear resistance of the beams. The steel shear links in U/D/2.7 became active at a shear force of 30-35 kN. With increased loading, the steel shear links continued to develop strain. In the final stage, all shear links exceeded the yield strain of 0.0027.

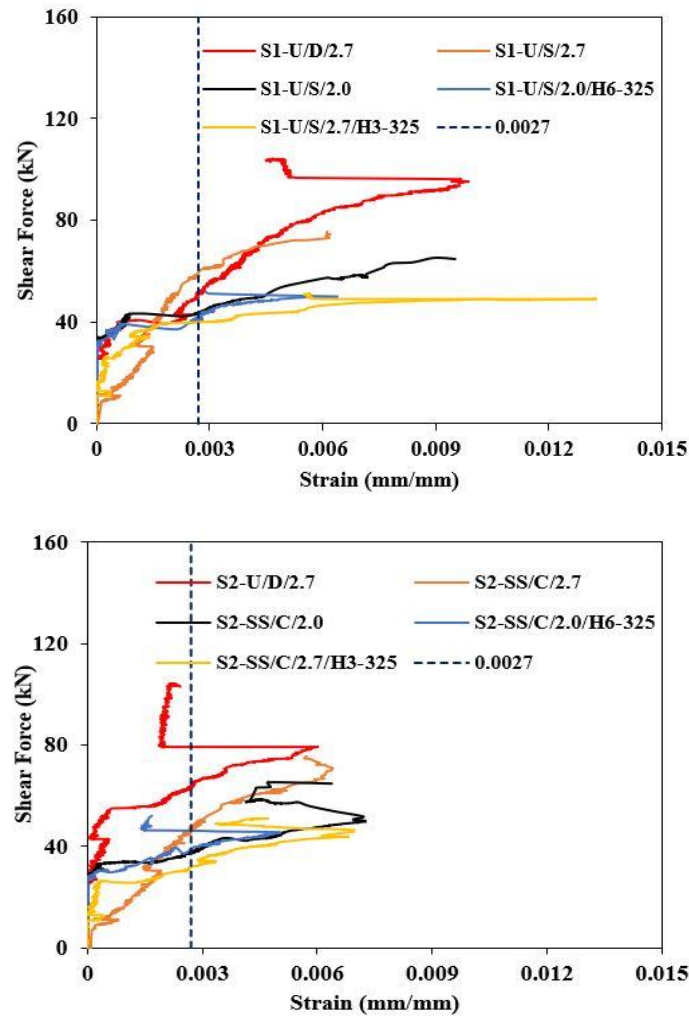


Figure 4.4. Shear force vs strain in the steel shear links of the unstrengthened beams

4.2.2. Strengthened beams

The strengthened beams were categorised into three groups. The first group consisted of the strengthened slender beams with 3 FRP bars. The second group comprised the strengthened slender beams with 6 FRP bars. The strengthened deep beams with 2 FRP bars were included in the third group.

4.2.2.1. First group of strengthened beams

The first group of strengthened beams; which consisted of S/S/2.0/G3-325, S/S/2.7/G3-325, S/S/2.7/G3-325*, S/S/2.7/C3-262.5 and S/S/2.7/C3-325; failed in shear with a diagonal tensile fracture. Figure 4.5 demonstrates the crack patterns of the beams at failure. Similar to the corresponding control beams, formation of flexural cracks initiated at a shear force of about 10 kN. The first shear crack emerged once the shear force reached about 25 kN. More inclined cracks induced by increased loading propagated into the shear spans and, eventually, a diagonal tension failure occurred. Of note is that the inclination of shear cracks at failure, compared to those in the corresponding control beams, increased due to the presence of the DE FRP bars. Besides, S/S/2.7/C3-325 had less inclined cracks than S/S/2.0/G3-325, S/S/2.7/G3-325, and S/S/2.7/G3-325*, although these four beams were strengthened with three FRP bars. This can be explained by the higher elastic modulus of the CFRP bars. S/S/2.7/G3-325 and S/S/2.7/G3-325* had comparable crack patterns at failure. Comparable crack patterns were also observed for S/S/2.7/C3-262.5 and S/S/2.7/C3-325.



S/S/2.0/G3-325



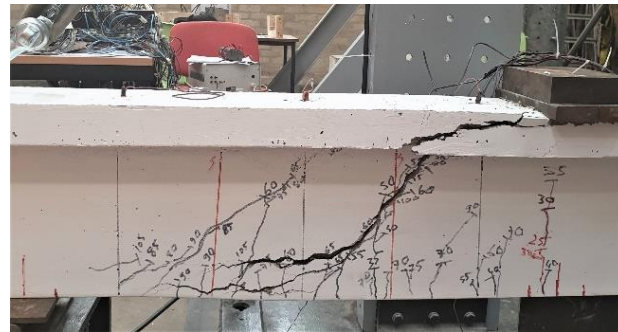
S/S/2.7/G3-325



S/S/2.7/G3-325*



S/S/2.7/C3-262.5



S/S/2.7/C3-325

Figure 4.5. Crack patterns at failure (slender beams strengthened with 3 FRP bars)

The shear force vs deflection curves of the first group of strengthened beams are depicted in Figure 4.6. All five beams had a quasi-linear shear force-deflection response until failure. All beams had comparable uncracked stiffness. The cracked stiffness of the beams was also comparable up to the formation of inclined cracks. SS/S/2.7/C3-325 had a stiffer response after the formation of inclined cracks. This can be explained by the higher elastic modulus

of the CFRP bars. The CFRP bars are therefore more effective in resisting inclined crack opening and controlling deflection. The shear force-deflection curves of S/S/2.0/G3-325, S/S/2.7/G3-325, and S/S/2.7/G3-325* had almost the same trend up to failure. SS/S/2.7/C3-262.5 had the lowest post-cracking stiffness, which shows that decreasing the embedded length of FRP bars negatively impacts the stiffness of DE shear-strengthened beams.

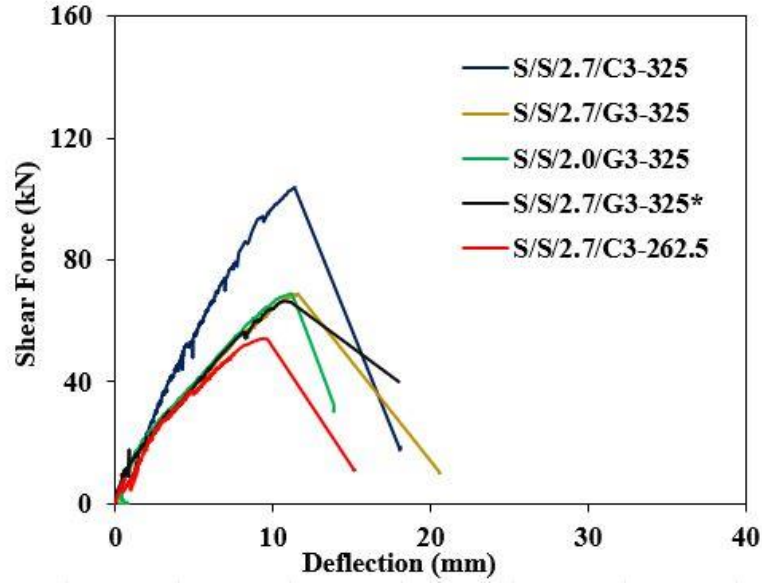


Figure 4.6. Shear force vs deflection for the strengthened slender beams with 3 FRP bars

Figure 4.7 presents the shear force-strain curves for the steel shear links in the first group of strengthened beams. The designation of the first and second steel shear links (S1 and S2) is given in Figure 3.6. The steel shear links did not contribute to the shear force resistance until the first inclined crack appeared in the shear span of the beams. Upon further loading, all shear links started to develop strain but unfortunately the strain gauges attached to the first shear links of SS/S/2.7/G3-325* and SS/S/2.7/C3-262.5 were damaged. As shown in Figure 4.7, all shear links, apart from S1 in SS/S/2.7/G3-325* and SS/S/2.7/C3-262.5, exceeded the yield strain of 0.0027.

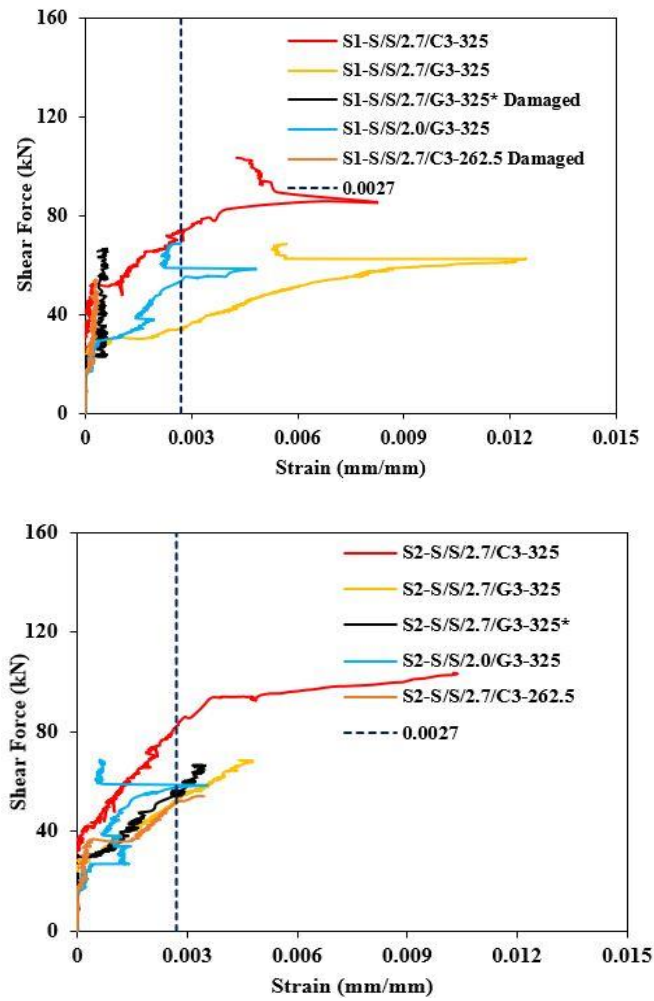


Figure 4.7. Shear force vs strain in steel shear links of the strengthened slender beams with 3 FRP bars

Figure 4.8 illustrates the shear force-strain curves for the FRP bars (see Figure 3.6 for FRP bar designation and positions of strain gauges). Similar to the steel shear links, the DE FRP bars were inactive up to the formation of inclined cracks. Upon further loading, the DE FRP bars started to develop strain but the CFRP bars developed strain at a slower rate compared to the GFRP bars. This can be attributable to the higher elastic modulus of the CFRP bars.

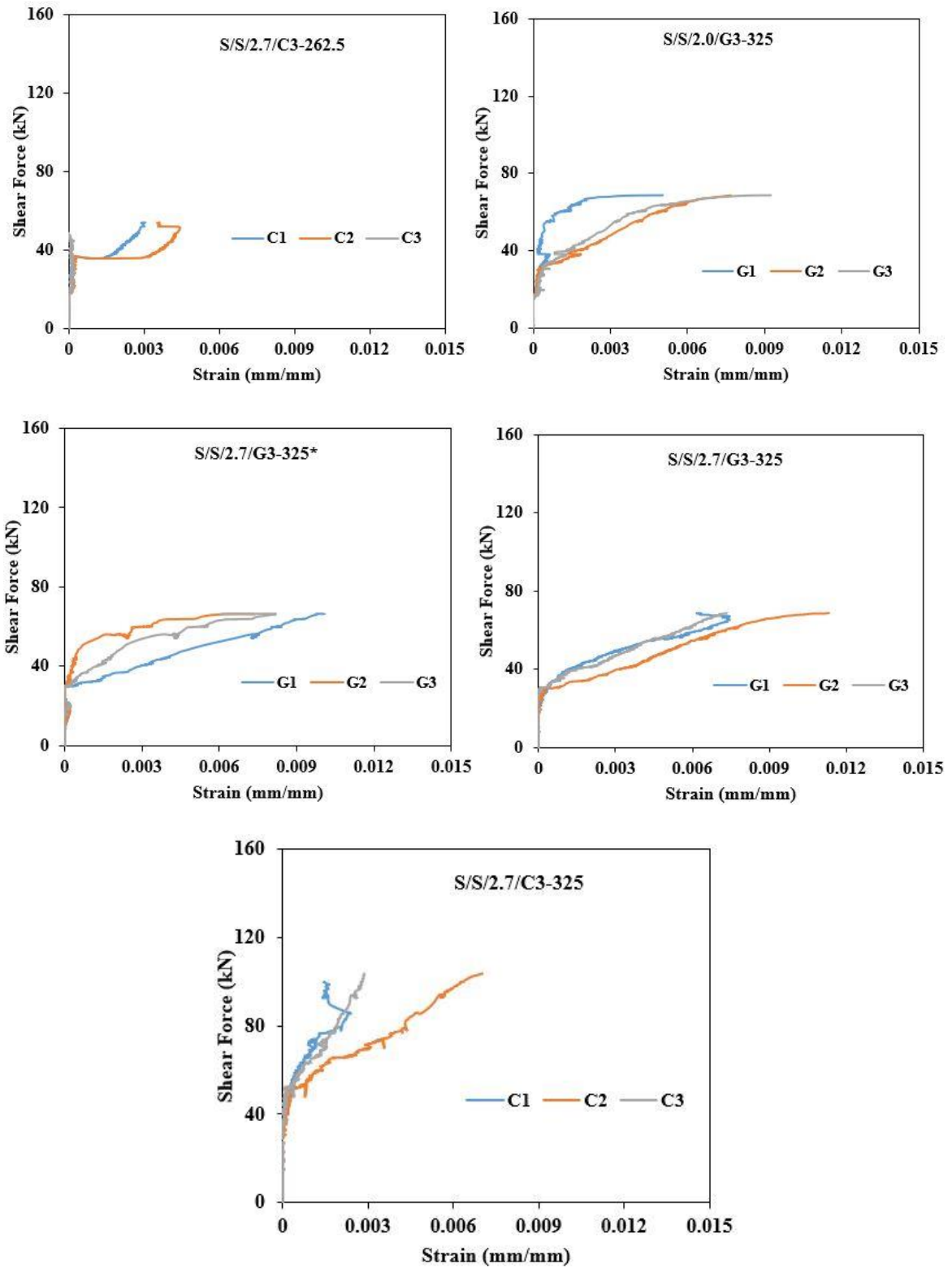
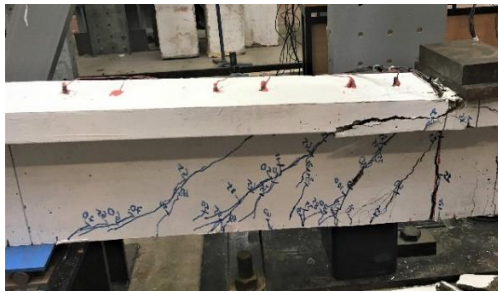


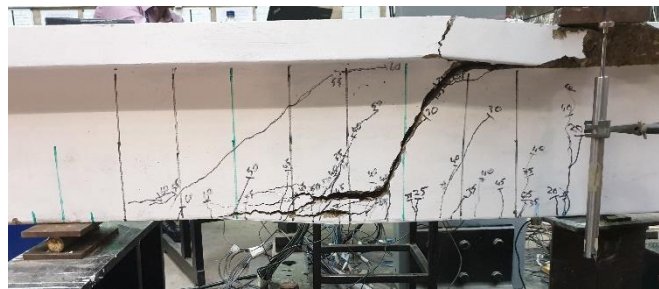
Figure 4.8. Shear force vs strain in the FRP bars of the strengthened slender beams with 3 FRP bars

4.2.2.2. Second group of strengthened beams

The second group of strengthened beams consisted of S/S/2.0/G6-325, S/S/2.7/G6-262.5 and S/S/2.7/G6-325. S/S/2.0/G6-325 failed in flexure, whereas the remaining two beams failed in shear. The crack patterns of the three beams at failure are depicted in Figure 4.9. The formation of flexural cracks at the maximum moment zone started at a shear force of about 10 kN. The first inclined crack occurred in the shear spans of the beams at a shear force of about 25 kN. Upon further loading, further inclined cracks were traced in the shear spans of the beams. Finally, an inclined crack caused a diagonal tension failure.



S/S/2.0/G6-325



S/S/2.7/G6-262.5



S/S/2.7/G6-325

Figure 4.9. Crack patterns at failure (strengthened slender beams with 6 FRP bars)

Figure 4.10 illustrates the shear force-deflection curves of the second group of strengthened beams. Except for S/S/2.0/G6-325, the beams had a quasi-linear shear-force deflection response up to failure. S/S/2.0/G6-325 had a ductile failure featuring an approximately 60 mm plateau. All three beams had comparable uncracked stiffness but S/S/2.7/G6-325 featured a stiffer response after the formation of inclined cracks.

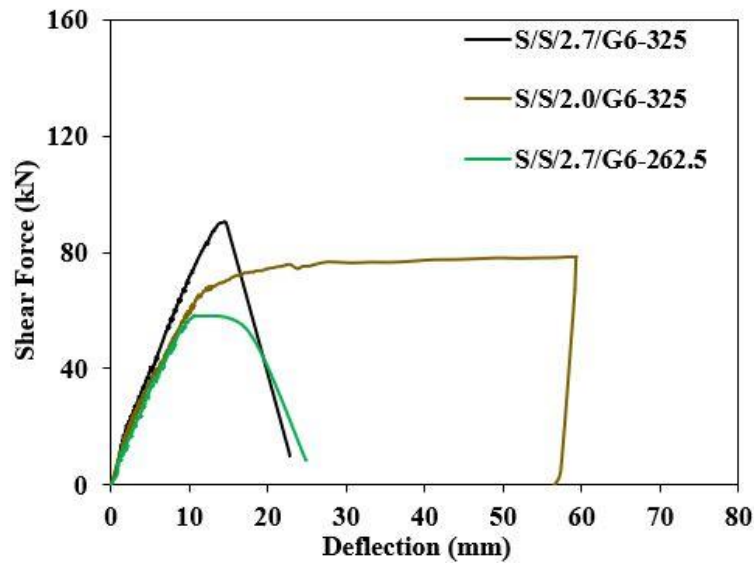


Figure 4.10. Shear force vs deflection for the strengthened slender beams with 6 FRP bars

The relationship between the shear force and strain measured in the steel shear links is shown in Figure 4.11 for the second group of strengthened beams. The designations of the first and second steel shear links (S1 and S2) are depicted in Figure 3.6. All shear links did not contribute to the shear force resistance until the first diagonal crack formed. Upon increased loading, the strain values in the steel shear links started to increase. As shown in Figure 4.11, the steel shear links attained or exceeded the yield strain of 0.0027.

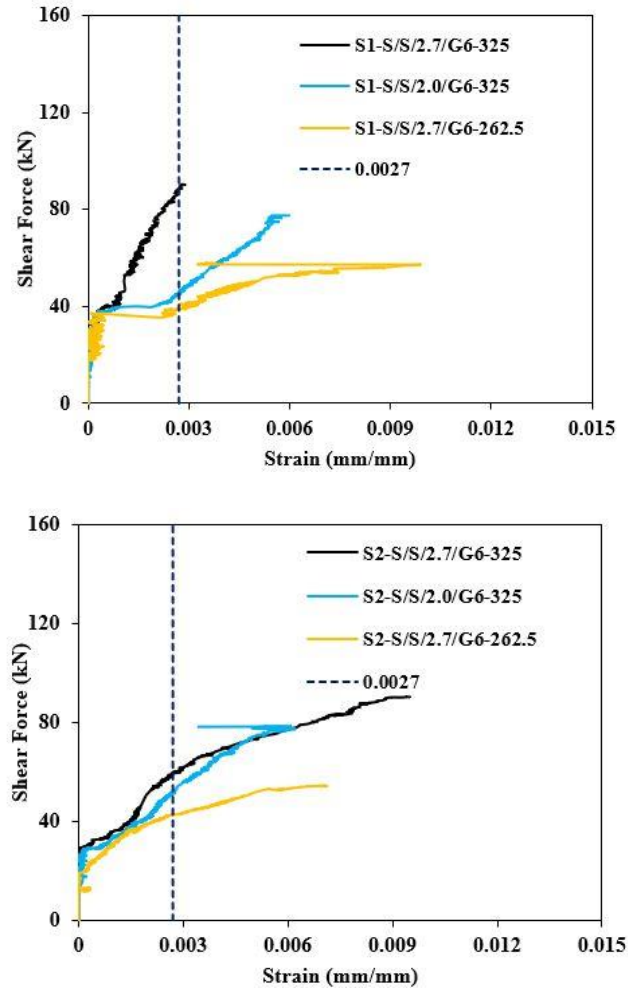


Figure 4.11. Shear force vs strain in the steel shear links of the strengthened slender beams with 6 FRP bars

It is worth noting that the longitudinal steel bars of S/S/2.0/G6-325 exceeded the yield strain of 0.0029. Figure 4.12 shows the relationship between shear force and strain values developed in the longitudinal steel reinforcement (see Figure 3.6 for positions of strain gauges). As can be seen in Figure 4.12, a quasi-linear relationship existed between shear force and strain values up to the yield strain. This was followed by a long plateau.

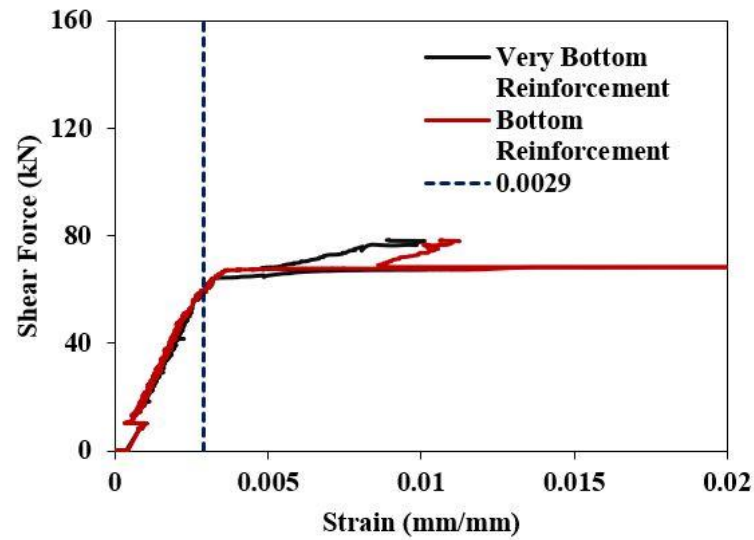


Figure 4.12. Shear force vs strain in the longitudinal reinforcement of S/S/2.0/G6-325

The variations between shear force and strain values developed in the FRP bars are exhibited in Figure 4.13. (see Figure 3.6 for FRP bar designation and positions of strain gauges). The crack patterns of the beams are also given in Figure 4.9. Similar to shear force-strain variations shown in Figure 4.11 for the steel shear links, the FRP bars were inactive until the formation of inclined cracks. Upon further loading, the FRP bars started to contribute to the shear force resistance. The FRP strain values measured in S/S/2.0/G6-325 were lower than those in S/S/2.7/G6-325. This can be explained by the fact that S/S/2.0/G6-325 failed in flexure before reaching its ultimate shear force capacity.

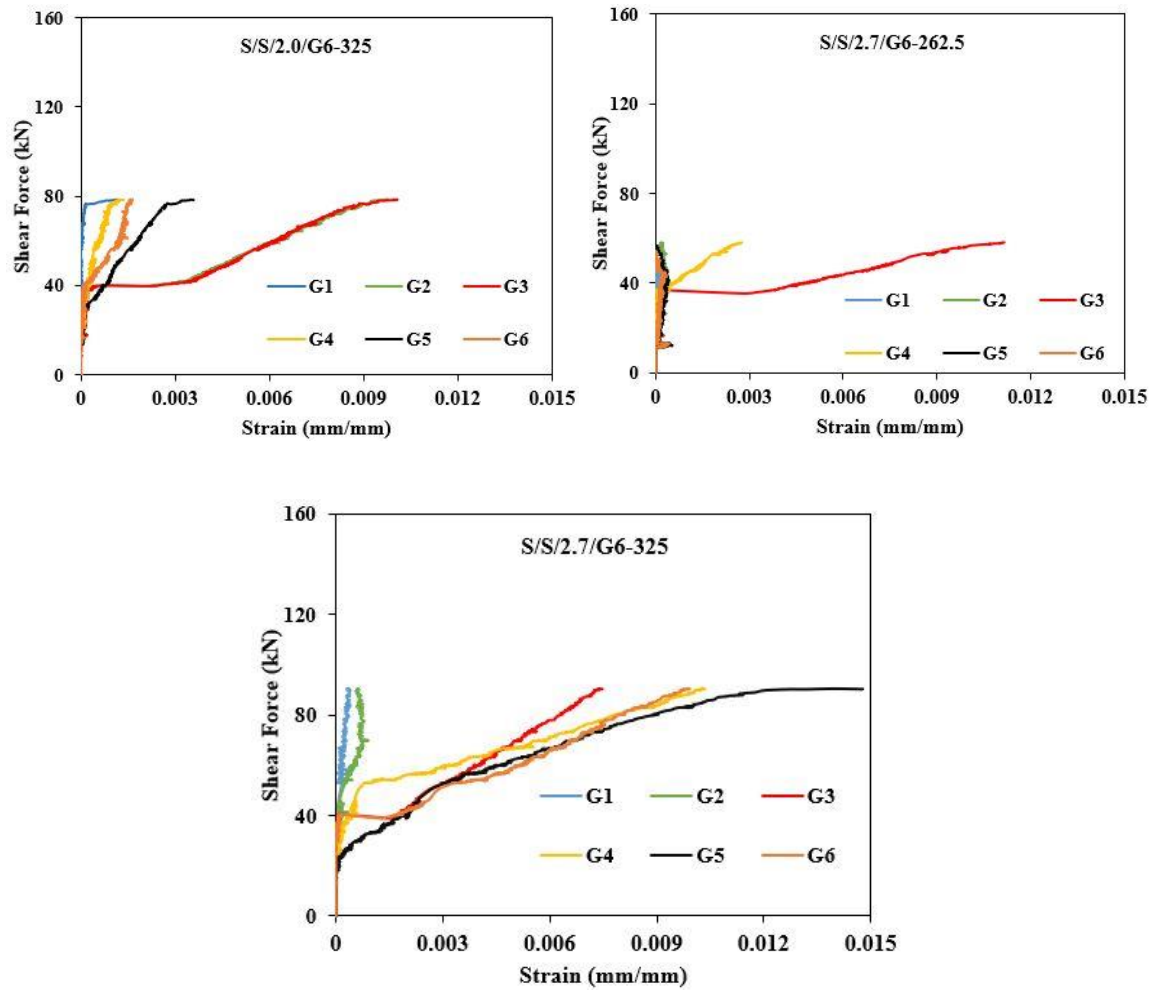


Figure 4.13. Shear force vs strain in the FRP bars of the strengthened slender beams with 6 FRP bars

4.2.2.3. Third group of strengthened beams

The third group of strengthened beams consisted of deep beams strengthened with 2 FRP bars (S/D/2.7/G2-325 and S/D/2.7/C2-325). The crack patterns of the beams at failure are demonstrated in Figure 4.14. Similar to the unstrengthened deep beam, the formation of flexural cracks in the maximum moment zone were observed at a shear force of 12 kN. An increase in loading instigated the propagation of flexural cracks into the shear span and an inclined crack was observed at a shear force of about 30 kN. Upon further loading, the flange

of the beam representing the compression zone was penetrated by inclined cracks and shear-compression failure was eventually observed. The crack pattern of both strengthened deep beams was comparable to that of corresponding control deep beam (see Figure 4.2).



S/D/2.7/G2-325

S/D/2.7/C2-325

Figure 4.14. Crack patterns at failure (strengthened deep beams with 2 FRP bars)

Figure 4.15 illustrates the shear force-deflection curves of the third group of strengthened beams. S/D/2.7/G2-325 had a quasi-linear shear-force deflection response until failure whereas S/D/2.7/C2-325 had a nonlinear response. The pre-cracking stiffness was comparable for both beams. Due to the higher elastic modulus of the CFRP bars, S/D/2.7/C2-325 had a slightly higher stiffness than S/D/2.7/G2-325 after the formation of inclined cracks. Of note is that the shear force capacity of S/D/2.7/C2-325 at failure was 134.7 kN and the corresponding deflection value at failure was 11.3 mm. But the penultimate readings obtained from the data logger were 134 kN and 6.9 mm, respectively. The readings obtained from the data logger just after failure were 27.3 kN and 13.5 mm, respectively. This can be explained by the brittle failure mode, which instigated a sudden jump in displacement transducers (see Figure 4.15).

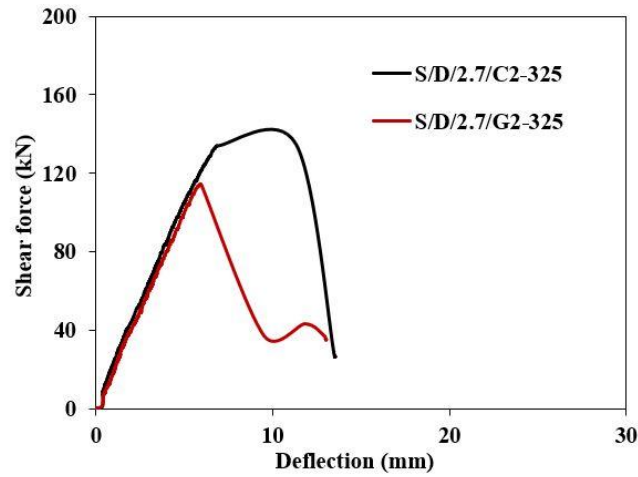


Figure 4.15. Shear force vs deflection for the strengthened deep beams with 2 FRP bars

Figure 4.16 presents the variation between shear force and strain measured in the steel shear links of the third group of strengthened beams. The designations of the first and second steel shear links (S1 and S2) are shown in Figure 3.6. The steel shear links became active after the development of an inclined crack. Except for S2 in S/D/2.7/G2-325, all shear links attained or exceeded the yield strain of 0.0027. S2-S/D/2.7/G2-325 reached a maximum strain of 0.0025.

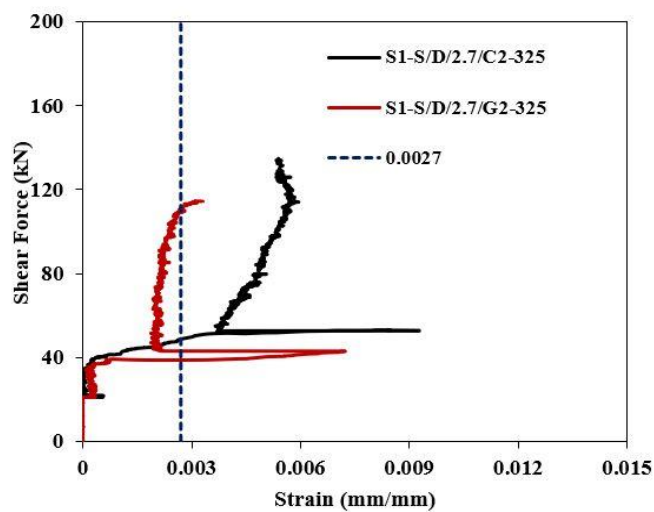


Figure 4.16. Continued

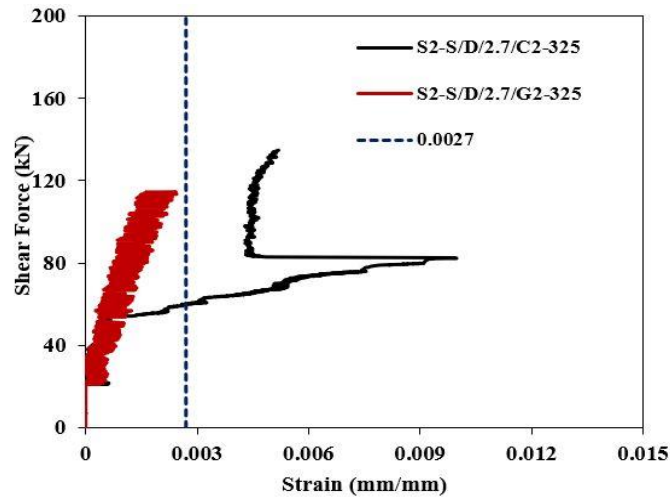


Figure 4.16. Shear force vs strain in the steel shear links of the strengthened deep beams with 2 FRP bars

Strain gauge readings obtained for the FRP bars in the deep beams are given Figure 4.17 (see Figure 3.6 for the FRP bar designation and positions of strain gauges). Similar to the corresponding steel shear links, the FRP bars remained inactive before the formation of the first inclined crack. The CFRP bars developed strain at a slower rate compared to the corresponding GFRP bars. As previously mentioned, this can be explained by the higher elastic modulus of the CFRP bars.

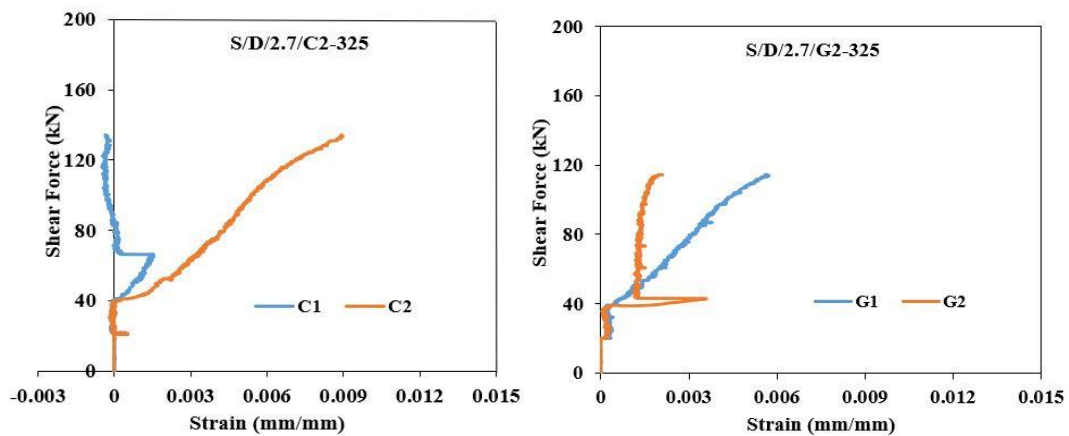


Figure 4.17. Shear force vs strain in the FRP bars of the strengthened deep beams with 2 FRP bars

4.3. Discussion

4.3.1. Shear strength

The unstrengthened shear force capacity, shear force at failure, gain in shear resistance due to the DE FRP bars, maximum deflection at failure and failure mode of each beam are detailed in Table 4.1. The control beams (U/S/2.0, U/S/2.7 and U/D/2.7) failed at a shear force of about 65.5, 75.5 and 103.9 kN, respectively. The higher shear force capacity of U/S/2.7 compared to that of U/S/2.0 is attributable to the higher tension reinforcement ratio, which enhanced dowel action. The shear strength increased from 75.5 to 103.9 kN with decreasing the a/d ratio from 3 to 1.9. This increase can be attributable to arch action which provides a higher shear strength compared to beam action.

Existing holes decreased the shear strength of U/S/2.7/H3-325 and U/S/2.0/H6-325 compared with the corresponding control beams. The reduction in the shear strength of U/S/2.7/H3-325 was about 32.4% (from 75.5 to 51 kN) and the corresponding reduction for U/S/2.0/H6-325 was about 19% (from 65.5 to 53 kN). Although Valerio and Ibell (2003) stated that the decrease in the shear resistance instigated by the presence of existing holes was insignificant for rectangular concrete beams, the shear resistance of RC T-beams can be provided by both the flange and the web instead of the web only (Kotsovos et al. 1987). This explains the shear resistance reduction in the tested T-beams due to the presence of holes. This most unfavourable situation can be still avoided by drilling and filling holes one by one. S/S/2.0/G6-325 and S/S/2.7/G6-325 failed in flexure and shear, respectively, with a strength gain of 13 and 15 kN, respectively. This demonstrated that an increase in tension reinforcement ratio from 2.0 to 2.7 changed the failure mode and had an insignificant effect on the gain due to DE GFRP bars. The strength gains due to 3 GFRP bars in S/S/2.0/G3-325, S/S/2.7/G3-325 and S/S/2.7/G3-325* were negligible. The ineffectiveness of 3 GFRP

bars can be explained by the fact that the axial rigidity (i.e., the elastic modulus multiplied by the cross-sectional area of the FRP bars) of the 3 GFRP bars is lower than that of the existing steel shear links. The axial rigidity of the FRP and steel bars is given in Table 4.2. As a result, the steel shear links attracted higher forces than the DE GFRP bars. A high FRP axial rigidity and/or low FRP spacing can therefore enhance the effectiveness of the DE GFRP bars. A shear strength enhancement of 37.2% (28.1 kN) was achieved by 3 CFRP bars embedded into S/S/2.7/C3-325. This result confirms that DE shear strengthening is effective when the axial rigidity of the FRP bars is higher than that of the steel bars (see Table 4.2).

The experimental results also suggest that the embedded length of FRP bars had a considerable impact on the shear resistance enhancement. A decrease in the embedded length of GFRP bars from 325 mm to 262.5 mm instigated a reduction in shear resistance by about 35.7% (from 90.5 kN to 58.2 kN). The corresponding reduction for CFRP bars with decreasing the embedded length was by about 47.7% (from 103.6 kN to 54.2 kN). This can be attributed to the fact that FRP bars with lower embedded length can no longer effectively join the tension and compression chords, and therefore truss action does not fully develop.

S/D/2.7/G2-325 failed at a shear force of 114.4 kN, attaining 10.5 kN (10.1%) increase in shear force capacity. The deep beam strengthened with CFRP bars had also higher shear resistance than that of strengthened with GFRP bars. S/D/2.7/C2-325 failed at a shear force of 134.7 kN and the DE CFRP bars increased the shear resistance by 29.6% (30.8 kN). The shear strength gain in S/D/2.7/C2-325 also verified that, for the same number of FRP bars, the higher elastic modulus of CFRP bars provides RC beams with higher shear resistance. As previously mentioned, the CFRP bars played a vital role in resisting inclined crack opening.

Table 4.1. Experimental results

Specimen Reference	Unstrengthened shear force capacity (kN)	Shear force capacity at failure (kN)	Gain due to DE FRP bars (kN)	Gain due to DE FRP bars (%)	Deflection at failure (mm)	Failure mode
U/S/2.0	65.5	65.5	-	-	10.7	Diagonal Tension
U/S/2.7	75.5	75.5	-	-	10.1	Diagonal Tension
U/D/2.7	103.9	103.9	-	-	5.1	Shear-Compression
U/S/2.7/H3-325	51	51	-	-	7.7	Diagonal Tension
U/S/2.0/H6-325	53	53	-	-	9.8	Diagonal Tension
S/S/2.0/G3-325	65.5	68.7	3.2	4.8	11.2	Diagonal Tension
S/S/2.7/G3-325	75.5	68.7	0	0	11.6	Diagonal Tension
S/S/2.7/G3-325*	75.5	66.5	0	0	10.7	Diagonal Tension
SS/S/2.0/G6-325	65.5	78.5	13	19.8	>50*	Flexure
S/S/2.7/G6-262.5	75.5	58.2	0	0	10.7	Diagonal Tension
S/S/2.7/G6-325	75.5	90.5	15	19.8	14.7	Diagonal Tension
S/S/2.7/C3-262.5	75.5	54.2	0	0	9.5	Diagonal Tension
S/S/2.7/C3-325	75.5	103.6	28.1	37.2	11.3	Diagonal Tension
S/D/2.7/G2-325	103.9	114.4	10.5	10.1	5.9	Shear-Compression
S/D/2.7/C2-325	103.9	134.7	30.8	29.6	11.3	Shear-Compression

Table 4.2. Axial rigidity of the FRP bars and steel shear links

Specimen	S1 (kN)	S2 (kN)	G1/C1 (kN)	G2/C2 (kN)	G3/C3 (kN)	G4 (kN)	G5 (kN)	G6 (kN)	Total axial rigidity of shear links (kN)	Total axial rigidity of FRP bars (kN)
U/S/2.0	5027	5027	-	-	-	-	-	-	10053	-
U/S/2.7	5027	5027	-	-	-	-	-	-	10053	-
U/D/2.7	5027	5027	-	-	-	-	-	-	10053	-
U/S/2.7/H3-325	5027	5027	-	-	-	-	-	-	10053	-
U/S/2.0/H6-325	5027	5027	-	-	-	-	-	-	10053	-
S/S/2.0/G3-325	5027	5027	1300	1300	1300	-	-	-	10053	3900
S/S/2.7/G3-325	5027	5027	1300	1300	1300				10053	3900
S/S/2.7/G3-325*	5027	5027	1300	1300	1300				10053	3900
SS/S/2.0/G6-325	5027	5027	1300	1300	1300	1300	1300	1300	10053	7800
S/S/2.7/G6-262.5	5027	5027	1300	1300	1300	1300	1300	1300	10053	7800
S/S/2.7/G6-325	5027	5027	1300	1300	1300	1300	1300	1300	10053	7800
S/S/2.7/C3-262.5	5027	5027	3675	3675	3675				10053	11025
S/S/2.7/C3-325	5027	5027	3675	3675	3675				10053	11025
S/D/2.7/G2-325	5027	5027	1300	1300					10053	2600
S/D/2.7/C2-325	5027	5027	3675	3675					10053	7350

4.3.2. Components of Shear Resistance

Strain values developed by the steel shear links and DE FRP bars were used to calculate the shear resistance components of the slender and deep beams.

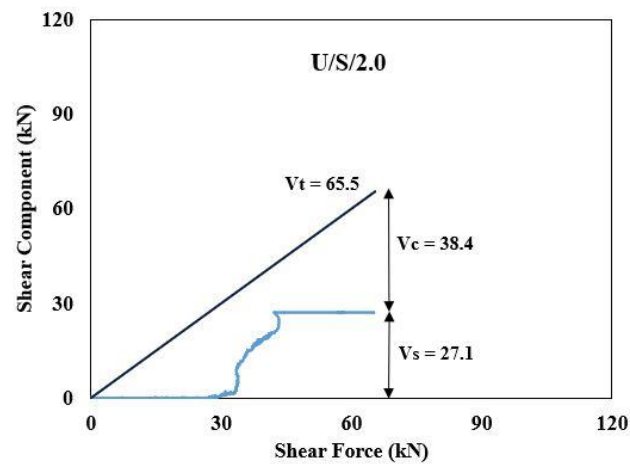
4.3.2.1. Unstrengthened beams

The strain gauge readings depicted in Figure 4.4 were used to calculate the contributions of the steel shear reinforcement to the shear force capacity. As previously stated, all steel shear links attained or exceeded the yield strain of 0.0027. All steel shear links were also intersected by the main shear crack that caused either a diagonal tension or shear-compression failure (see Figure 4.1 and 4.2); hence the steel contribution (V_s) to the shear resistance of the unstrengthened beams was computed as the yield strength of the steel shear links (540 MPa) multiplied by the total cross-sectional area of two shear links (50.2 mm²). The total shear force capacity (V_t) of the unstrengthened beams can be stated as the sum of the concrete contribution (V_c) and the steel contribution (V_s), as given in Equation 4.1.

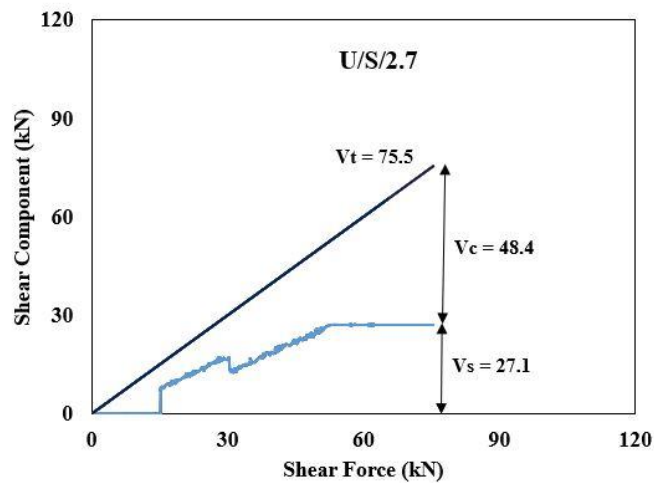
$$V_t = V_c + V_s \quad (4.1)$$

Hence, the concrete contribution in each unstrengthened beam was calculated as the total shear force capacity minus V_s . Figure 4.18 depicts the components of shear resistance vs. shear force for the unstrengthened beams (U/S/2.0, U/S/2.7, U/S/2.7/H3-325, U/S/2.0/H6-325 and U/D/2.7). The steel shear links contribution to the shear resistance of each beam was 27.1 kN, based on the calculation described in the preceding paragraph. The concrete contribution to the shear resistance increased from 38.4 to 48.4 kN with increasing the

tension reinforcement ratio from 2.0 to 2.7%. This 10 kN difference can be attributable to the enhanced dowel action provided by the additional tension reinforcement. The existing three and six holes in U/S/2.7/H3-325 and U/S/2.0/H6-325 reduced the concrete contribution by 24.5 and 12.5 kN, respectively. The concrete contribution to the shear resistance also increased from 48.4 to 76.8 kN with decreasing a/d ratio from 3 to 1.9. As previously mentioned, this can be attributable to arch action, which provides a higher shear strength.

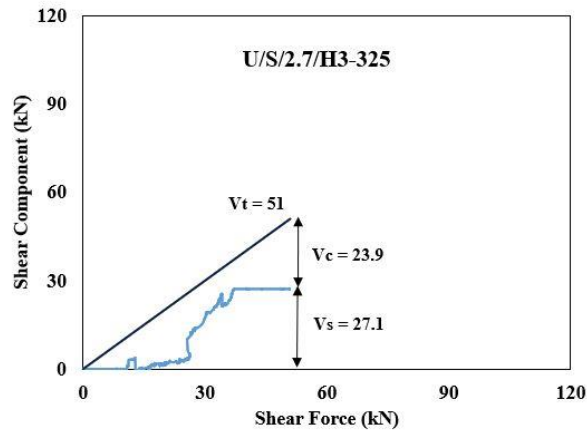


(a)

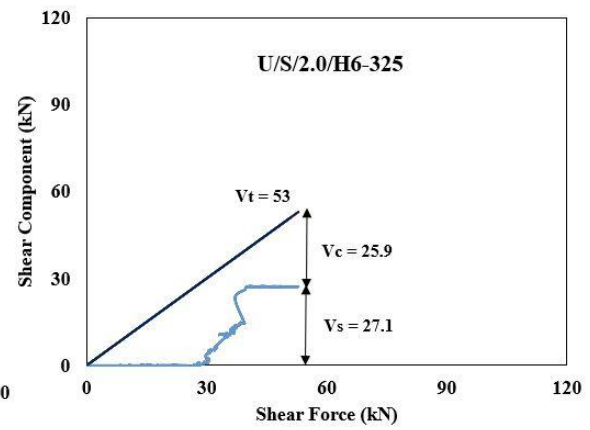


(b)

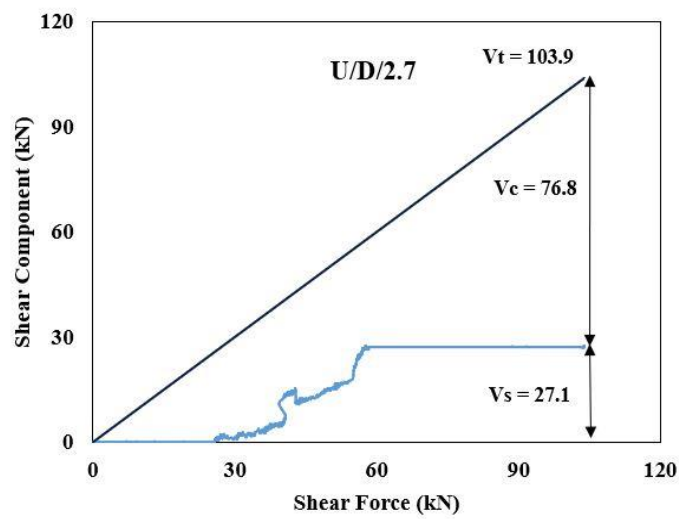
Figure 4.18. Continued



(c)



(d)



(e)

Figure 4.18. Components of shear resistance (a) U/S/2.0 (b) U/S/2.7 (c) U/S/2.7/H3-325, (d) U/S/2.0/H6-325 (e) U/D/2.7

4.3.2.2. Strengthened beams

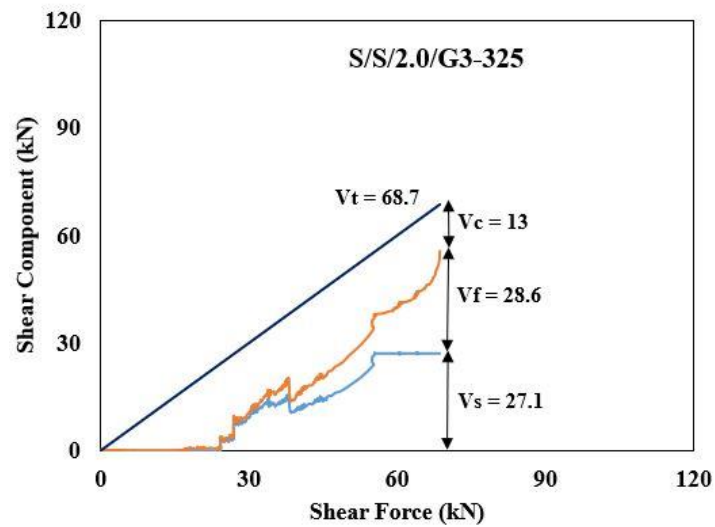
The strain gauge readings illustrated in Figure 4.7, 4.8, 4.11, 4.13, 4.16 and 4.17 were used to calculate the contributions of the steel and FRP shear reinforcement to the shear resistance of the strengthened beams. Similar to the unstrengthened beams, the shear cracks that instigated failure intersected the steel shear links (see Figure 4.5, 4.9 and 4.14). The contribution of the steel shear links to the shear resistance of each strengthened beams was also calculated as the yield strength of the shear links multiplied by the cross-sectional area of the two steel shear links. The FRP contribution (V_f) to the shear resistance was based on the strain in the DE FRP bars intersected by the main shear crack that caused failure (see Figure 4.5, 4.9 and 4.14). The strain in these bars was multiplied by the axial rigidity (see Table 4.2) of the FRP bars. For example, V_f in S/S/2.7/G6-325 was calculated based on the strain in the DE GFRP bars G3, G4, G5 and G6 whereas the strain in G1 and G2 was ignored since these two bars were not intersected by the main shear crack.

The total shear force capacity of the strengthened beams can be expressed as given in Equation 4.2.

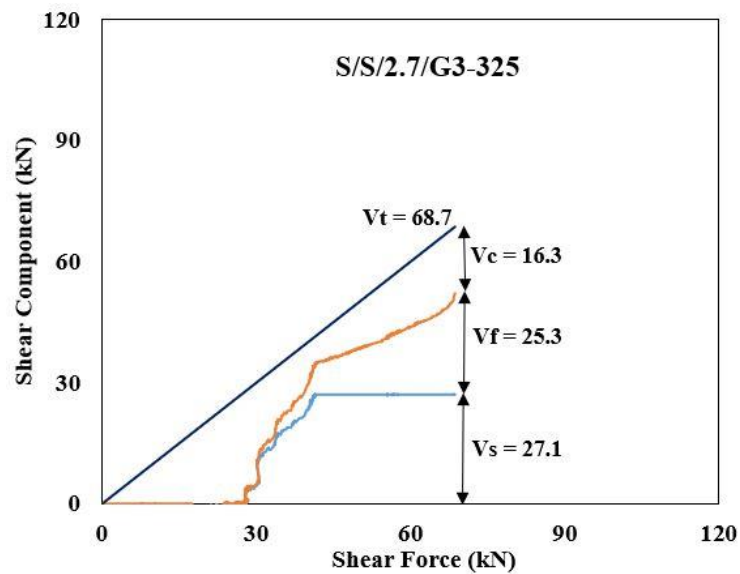
$$V_t = V_c + V_s + V_f \quad (4.2)$$

V_c was calculated by subtracting the sum of V_s and V_f from the total shear force capacity. Figure 4.19 shows the shear resistance components vs shear force for the strengthened beams that failed in shear. Similar to the unstrengthened beams, the contribution of the steel shear links for the strengthened beams was 27.1 kN. However, the contribution of steel shear links to the shear resistance of S/D/2.7/G2-325 was 26.1 kN since S2 in S/D/2.7/G2-325 reached a maximum strain of 0.0025, as previously mentioned. Moreover, V_s values for SS/S/2.7/G3-

325* and SS/S/2.7/C3-262.5 were unable to be calculated since the strain gauges attached to the first shear links were damaged as previously mentioned. However, V_f values for SS/S/2.7/G3-325* and SS/S/2.7/C3-262.5 were 20 and 16.2 kN, respectively.

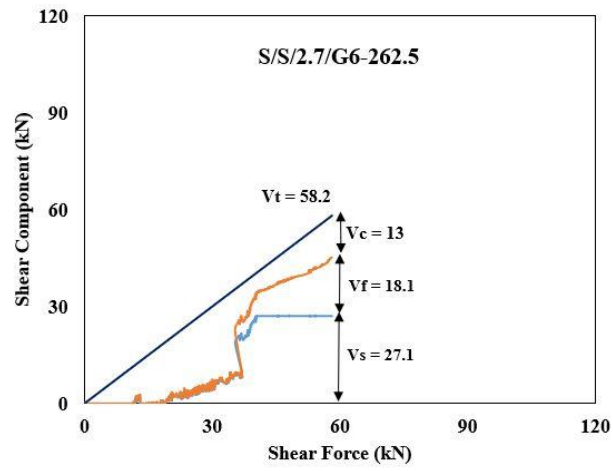


(a)

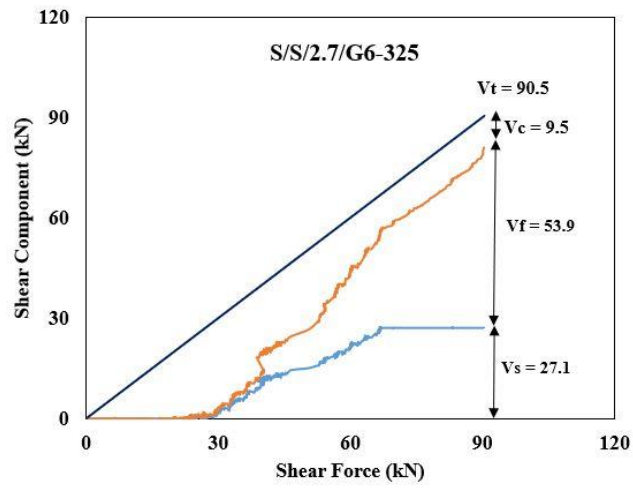


(b)

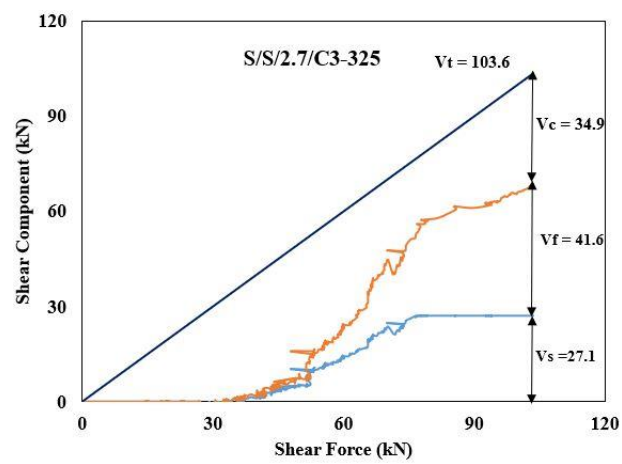
Figure 4.19. Continued



(c)

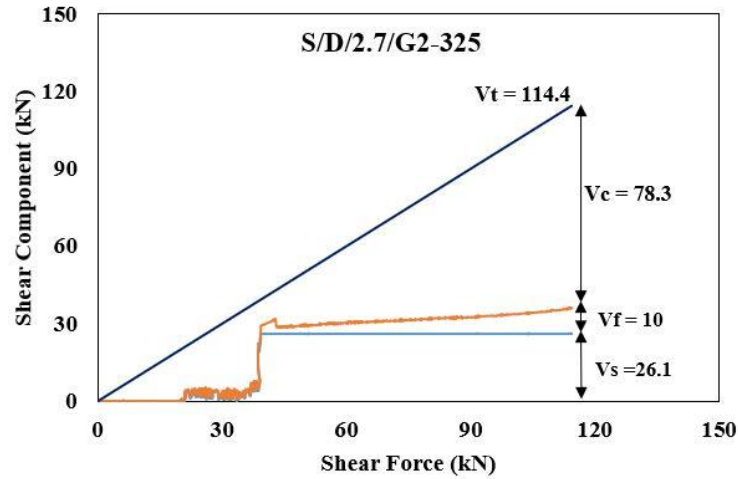


(d)

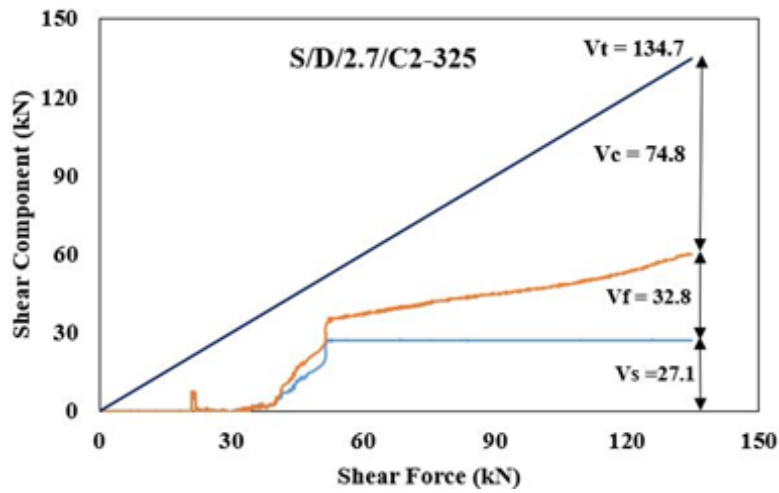


(e)

Figure 4.19. Continued



(f)



(g)

Figure 4.19. Components of shear resistance (a) S/S/2.0/G3-325, (b) S/S/2.7/G3-325, (c) S/S/2.7/G6-262.5, (d) S/S/2.7/G6-325, (e) S/S/2.7/C3-325, (f) S/D/2.7/G2-325, (g) S/D/2.7/C2-325

An important implication of the results shown in Figure 4.19 is that the subtraction of the unstrengthened shear force capacity from the strengthened shear force capacity does not always give a correct estimate of V_f . For example, the overall shear strength gain for

S/S/2.0/G3-325, S/S/2.7/G3-325* and S/S/2.7/G3-325 was negligible (see Table 4.1). Yet, the strain-based V_f values for these three beams were 28.6, 20 and 25.3 kN, respectively. Similarly, the overall shear strength gain for S/S/2.7/G6-325 and S/S/2.7/C3-325 was 15 and 28.1 kN, respectively, whereas the strain-based V_f values were 53.9 and 41.6 kN, respectively. This discrepancy occurs because V_c in the strengthened beams reduces with increased loading. The shear strength gain reported in Table 4.1 is therefore the difference between the strain-based V_f values and the reduction in V_c values (compared with the corresponding control beam). For example, the shear strength gain for S/S/2.0/G3-325 is $28.6 \text{ kN} - (38.4 \text{ kN} - 13.0 \text{ kN}) = 3.2 \text{ kN}$.

In contrast to slender beams, the overall shear strength gain for S/D/2.7/G2-325 and S/D/2.7/C2-325 reported in Table 4.1 was comparable to strain-based V_f values shown in Figure 4.19. For example, strain-based V_f values for S/D/2.7/G2-325 and S/D/2.7/C2-325 were 10 and 32.8 kN, respectively, and the corresponding values calculated based on the subtraction of the unstrengthened shear force capacity from the strengthened shear force capacity were 10.5 and 30.8 kN, respectively. This result also further explains that a significant percentage of the shear force is carried by a concrete arch, and truss action becomes less effective in deep beams compared with slender beams. Thus, the concrete contribution to the shear resistance of deep beams strengthened with DE FRP bars remained significant.

4.3.3. Effect of steel-to-FRP shear reinforcement ratio

Figure 4.20 (a) and 4.20 (b) show the experimental variations of V_c and V_f , respectively, with steel-to-FRP shear reinforcement ratio. The steel-to-FRP shear reinforcement ratio was defined as $(E_s A_s / b_w s) / (E_f A_f / b_w s_f)$. The steel-to-FRP shear reinforcement ratios for S/S/2.0/G3-325, S/S/2.7/G3-325, S/S/2.7/G6-325 and S/S/2.7/C3-325 were 3.82, 3.82, 1.91

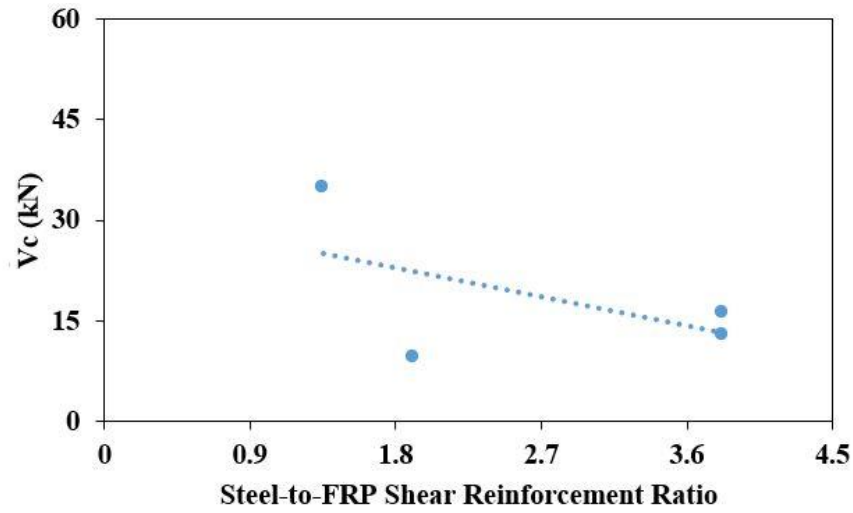
and 1.35, respectively. The total shear force capacity increased from 68.7 to 103.6 kN with decreasing the steel-to-FRP shear reinforcement ratio from 3.82 to 1.35.

The concrete contribution increased from 13 to 34.9 kN with decreasing the steel-to-FRP shear reinforcement ratio from 3.82 to 1.35. The relatively higher axial rigidity of the CFRP bars (3675 kN per bar) in S/S/2.7/C3-325 controlled crack opening and resulted in a relatively high V_c value (34.9 kN). On the other hand, the GFRP bars in the remaining 3 beams that failed in shear were much less effective in controlling crack width and maintaining aggregate interlock. As a result, the GFRP-strengthened beams had relatively low V_c values that varied from 9.5 to 16.3 kN. However, further experimental tests are required to confirm these results.

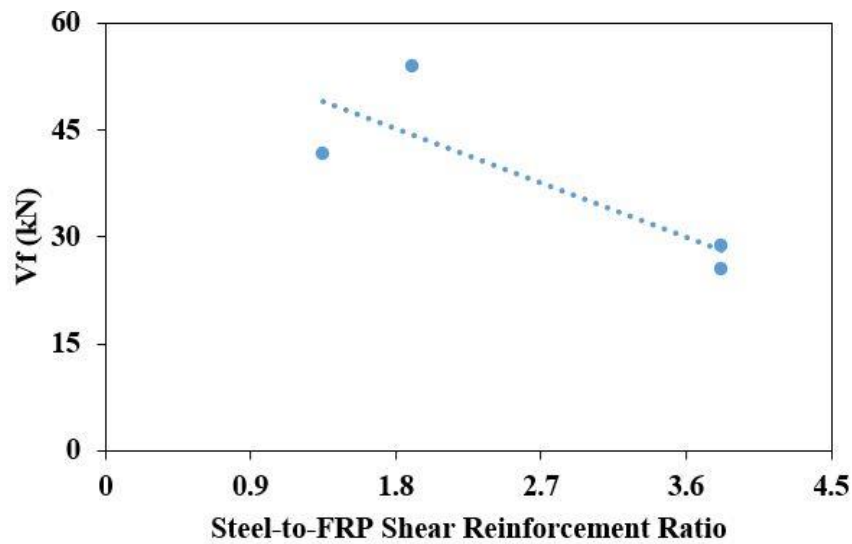
The FRP contributions for S/S/2.7/C3-325 and S/S/2.7/G6-325 were 41.6 and 53.9 kN, respectively. These values are significantly higher than the corresponding values of 25.3 and 28.6 kN obtained for S/S/2.7/G3-325 and S/S/2.0/G3-325, respectively. This result shows that the FRP contribution also increases with decreasing steel-to-FRP shear reinforcement ratio. As explained earlier, this is due to the higher elastic modulus of steel, which resulted in the steel shear links attracting higher forces than the DE FRP bars.

The total shear force capacity and FRP contribution to the shear resistance also increased with decreasing steel-to-FRP shear reinforcement ratio in DE FRP strengthened deep beams. S/D/2.7/C2-325 and S/D/2.7/G2-325 had a steel-to-FRP shear reinforcement ratio of 1.37 and 3.86, respectively. The total shear force capacity increased from 114.4 to 134.7 kN with decreasing the steel-to-FRP shear reinforcement ratio from 3.86 to 1.37. A decrease in steel-to-FRP shear reinforcement ratio also instigated an increase in the FRP contribution to the shear resistance from 10 to 32.8 kN. The concrete contribution to the shear resistance of S/D/2.7/C2-325 and S/D/2.7/G2-325 was 74.8 and 78.3 kN, respectively. This indicated that the concrete contribution remained almost constant with the increasing steel-to-FRP

reinforcement ratio. It should be noted that the concrete contribution to the corresponding control beam was 76.8 kN. As previously stated, truss action is less effective in deep beams compared to slender beams. Thus, the concrete contribution remained significant even with the presence of additional DE FRP bars.



(a)



(b)

Figure 4.20. Experimental variations of V_c and V_f , vs. steel-to-FRP shear reinforcement ratio: (a) V_c , (b) V_f ,

4.3.4. Size effect

As previously explained in Chapter 2, size effect in shear-deficient RC beams instigates a decrease in shear stress at failure with increasing beam size (Bazant, 1997). The large-scale deep and slender beams tested by Dirar and Theofanous (2017) are incorporated in this chapter. It is worth noting that the results of large-scale slender beams were first published by Jemaa et al. (2015). The experimental details of these beams were given in Chapter 2. As mentioned in Chapter 3, all dimensions of the large-scale beams reported by Dirar and Theofanous (2017) were scaled down to fabricate the small-scale beams tested in this research. Moreover, all parameters (i.e., concrete strength, DE FRP and steel reinforcement ratios) were kept constant.

Figure 4.21 presents the effect of beam size on shear strength for slender beams with the a/d ratio of 3. The shear stress (S) at failure was calculated as the shear force (V_t) at failure divided by the resultant of the beam web width (b_w) times effective depth (d), as given in Equation 4.3. U/S/2.7 and U/3 had a shear stress of 3.4 and 1.7 MPa, respectively, at failure. The corresponding stress at failure for S/S/2.7/G6-325 and S/3 was 4.0 and 3.3 MPa, respectively.

$$S = \frac{V_t}{b_w d} \left(\frac{N}{mm^2} \right) \quad (4.3)$$

Figure 4.21 clearly indicates a shear-strength loss with the increase in d from 300 to 600 mm for both unstrengthened and strengthened beams. The stress loss at failure was 50% for the unstrengthened beams (U/S/2.7 and U/3). The corresponding loss for the strengthened beams

(S/S/2.7/G6-325 and S/3) was 18%. This result confirmed that the size effect was significantly mitigated by DE GFRP bars.

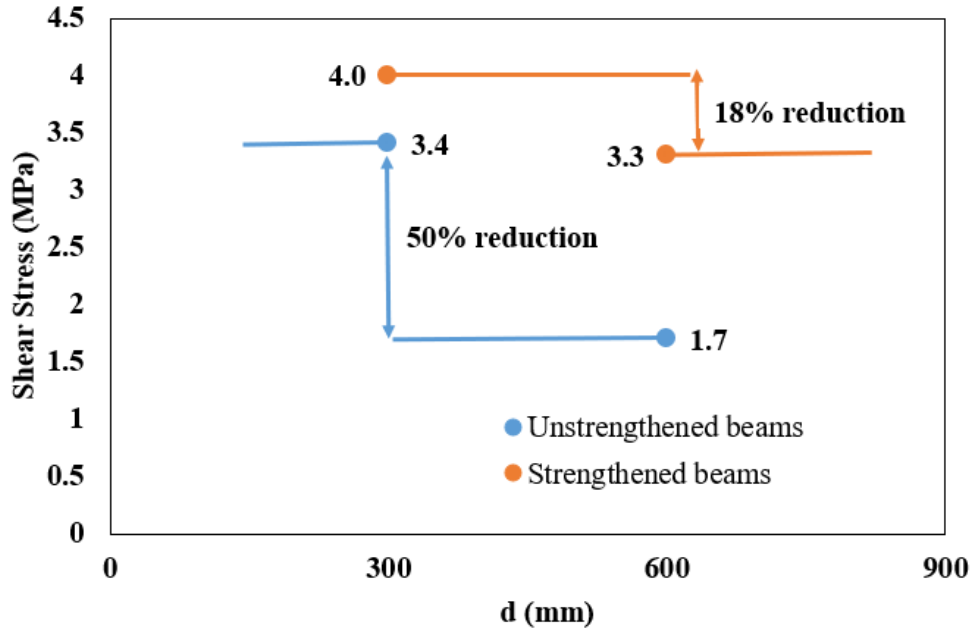


Figure 4.21. Effect of size on shear strength for slender beams

The shear resistance components of U/3 and S/3 were given by Jemaa et al. (2015). The contribution of steel shear links to the shear resistance was 108 kN for both unstrengthened and strengthened beams. The concrete contribution was 41.5 and 57.6 kN for unstrengthened and strengthened beams, respectively. The contribution of DE FRP reinforcement to the shear resistance was 127.4 kN. The shear resistance components of the beams were used to calculate the shear stress components based on Equation 4.3. The shear stress components of U/3 and S/3 together with the shear stress components of U/S/2.7 and S/S/2.7/G6-325 are given in Figure 4.22. The shear links contribution (S_s) to the shear stress was 1.2 MPa for all beams. With the increase in d from 300 to 600 mm, the concrete contribution (S_c) significantly reduced from 2.2 to 0.5 MPa for the unstrengthened beams. However, S_c

remained comparable for the strengthened beams. The contribution of the DE GFRP bars (S_f) to the shear stress also decreased from 2.4 to 1.4 MPa with the increase in beam size.

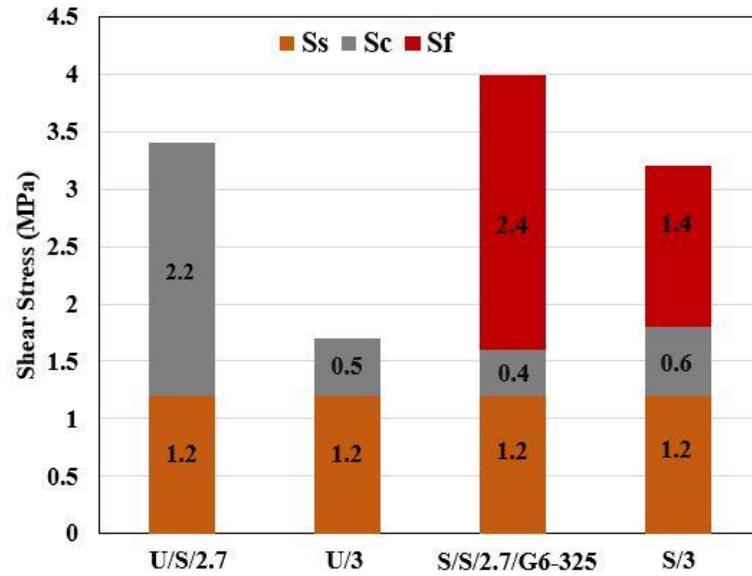


Figure 4.22. Components of shear stress for slender beams at failure

The increase in effective depth from 300 to 600 mm improved the effectiveness of the DE FRP shear strengthening system. As previously stated, the provision of 6 GFRP bars in the small-scale slender beams enhanced the shear strength by 19.8%. The corresponding shear strength enhancement for the large-scale beams was 96%. The higher percentage enhancement in the shear strength of S/3 is attributable to the higher effective depth, which provides better bond performance between the DE GFRP bars and the concrete.

Figure 4.23 shows the effect of beam size on shear strength for the unstrengthened and DE FRP strengthened deep beams with an a/d ratio of 1.9. The small-scale deep beams (U/D/2.7, S/D/2.7/G2-325 and S/D/2.7/C2-325) had a shear stress of 4.6, 5.1 and 6.0 MPa, respectively, at failure whereas corresponding shear stress at failure for the large-scale deep

beams (U/1.9, S/1.9 and SC/1.9) were 3.4, 4.6 and 5.4 MPa, respectively. It is important to note that the shear force capacity result of SC/1.9 can be found elsewhere (Caro, 2018; Caro et al., 2021). The shear strength loss for the unstrengthened deep beams with the increase in effective depth from 300 to 600 mm was 26%. The corresponding shear strength loss in the DE GFRP- and CFRP-strengthened beams was 10%. This result demonstrates that embedded FRP bars can also mitigate size effect in deep beams.

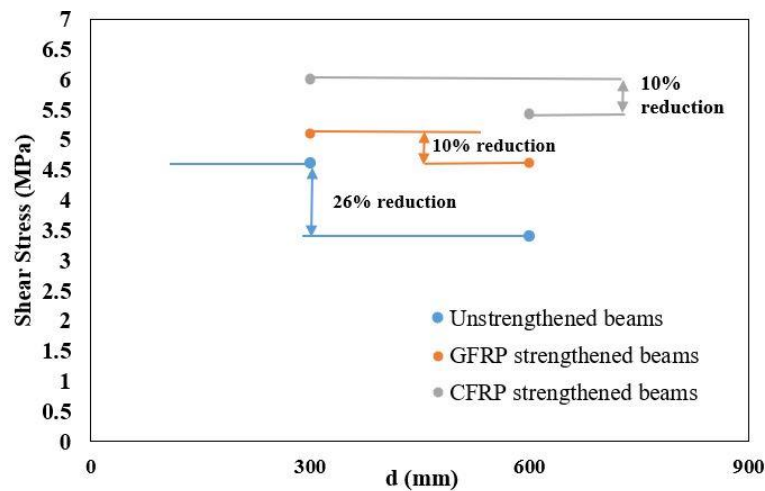
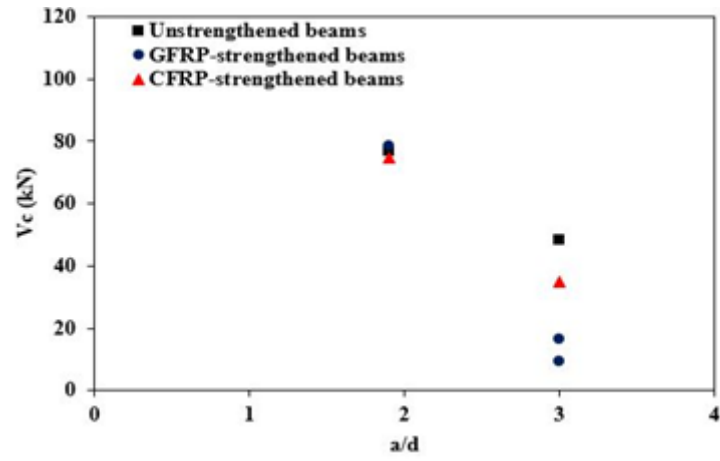


Figure 4.23. Effect of size on shear strength for deep beams

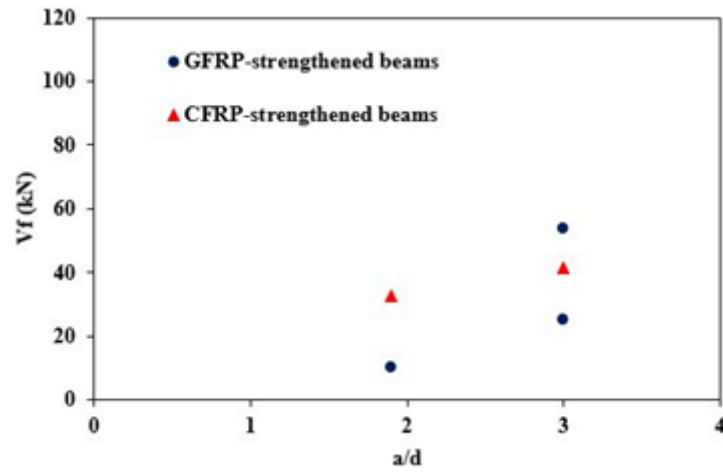
The effectiveness of the DE FRP shear strengthening system in deep beams also increased with increasing the effective depth from 300 to 600 mm. The DE GFRP and CFRP bars in the small-scale beams increased the shear strength by 10.1 and 29.6%, respectively. The corresponding shear strength enhancements in the large-scale beams were 33.2 and 57.6%. This can also be explained by the better bond performance between the DE FRP bars and the concrete as a result of the increased bonded length in the large-scale deep beams.

4.3.5. Effect of shear span-to-effective depth ratio (a/d)

As previously mentioned, the shear force transfer mechanism in RC beams with a/d ratios less than 2.5 is governed by arch action, and thus beam action is no longer applicable. The acting load on the beam can be directly transferred to the support. Therefore, a/d ratio is a key parameter governing the DE FRP-strengthened behaviour. Figure 4.24 (a) and 4.24 (b) show the experimental variations of V_c and V_f , respectively, with a/d ratio. As also mentioned in section 4.3.3, the concrete contribution remained almost constant for deep beams with a/d ratio of 1.9 whereas the concrete contribution reduced with presence of FRP bars for slender beams with a/d ratio of 3. As explained earlier, this can be attributable to truss action which is less effective in deep beams. The contribution of DE CFRP bars decreased from 41.6 to 32.8 kN (about 21%) with decreasing a/d ratio from 3 to 1.9. Similar to DE CFRP bars, the contribution of DE GFRP bars reduced with decreasing a/d ratio from 3 to 1.9. The corresponding reductions for DE GFRP-strengthened beams were from 53.9 to 10 kN (about 81%) and from 25.3 to 10 kN (about 60%). All these results show that the FRP contribution decreases with decreasing a/d ratio. Dirar and Theofanous (2017) also stated that the percentage shear force gain due to DE FRP bars decreased with decreasing the a/d ratio from 3.0 to 1.9. The percentage shear force gains due to GFRP bars were 96 and 33.2% for the a/d ratios of 3.0 and 1.9, respectively.



(a)



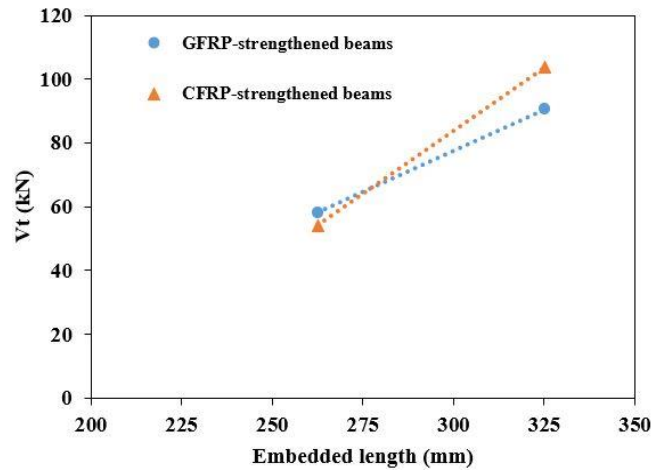
(b)

Figure 4.24. Experimental variations of V_c and V_f , vs. a/d ratio: (a) V_c , (b) V_f .

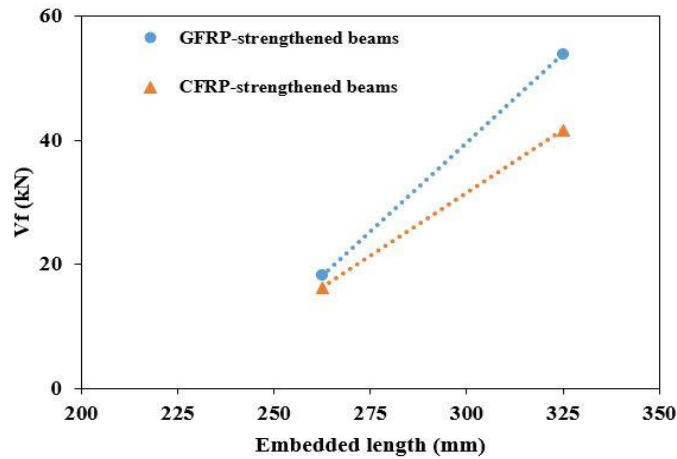
4.3.6. Effect of FRP bar depth

Figure 4.25 (a) and 4.25 (b) illustrate the experimental variations in V_t and V_f , respectively, with embedded length of FRP bars. As can be seen in Figure 4.25, an increase in the embedded length of GFRP bars from 262.5 to 325 mm caused an increase in V_t and V_f by 32.3 and 35.8 kN (55.5 and 197.8%), respectively. The corresponding enhancements in V_t

and V_f for CFRP bars were by 49.4 and 25.4 kN (91.1 and 156.8%), respectively. These results are important since the effectiveness of DE FRP bars is significantly governed by the embedded length of FRP bars. The strengthened depth of shear deficient RC beams should be equal to the full height of the cross-section. This allows truss action to be fully developed by effectively connecting the compression chord to the tension chord in slender beams.



(a)



(b)

Figure 4.25. Effect of FRP bar depth on (a) V_t (b) V_f

4.3.7. Effect of holes

As previously stated, existing holes instigated premature shear failure in U/S/2.7/H3-325 and U/S/2.0/H6-325. A previous investigation on rectangular RC beams demonstrated that existing holes had an insignificant effect on the shear resistance (Valerio and Ibell 2003). However, the existing holes in the tested T-shaped RC beams reduced the shear strength in comparison with the corresponding control beams. This can be explained by the effect of cross-section of RC beams since the flange can carry significant shear force in RC T-beams. But this most unfavourable situation can still be avoided by drilling and filling holes one by one.

Figure 4.26 presents the shear stress at failure versus A_n / A_t (i.e. net cross-sectional area / total cross-sectional area) for U/S/2.0, U/S/2.7, U/S/2.7/H3-325 and U/S/2.0/H6-325. The shear stress was calculated based on Equation 4.3. U/S/2.0, U/S/2.7, U/S/2.7/H3-325 and U/S/2.0/H6-325 had shear stress of 2.91, 3.36, 2.62 and 2.72 MPa, respectively. The existing 6 holes reduced the shear stress at failure from 2.91 to 2.72 MPa, a reduction of about 7%. The corresponding shear stress loss at failure for the 3 holes was from 3.36 to 2.62 MPa, a decrease of about 22%. Further experimental studies are required to confirm these results.

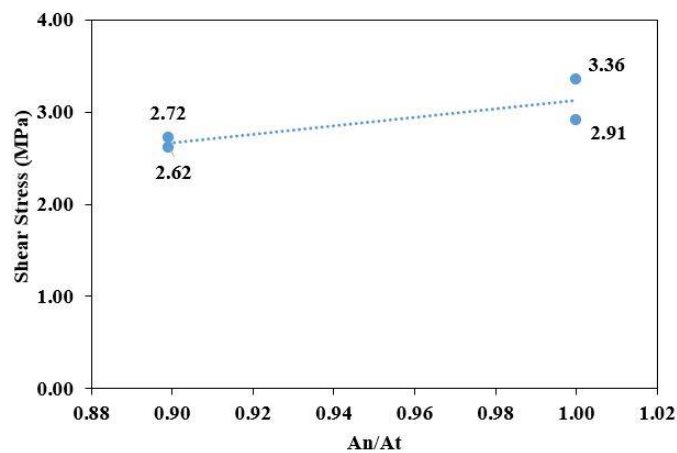


Figure 4.26. Shear stress at failure vs. A_n / A_t

4.4. Summary and conclusions

This chapter presents the results of an experimental investigation on the structural behaviour of RC T-beams strengthened in shear with embedded FRP bars. It provides insights into the influence of the steel-to-FRP shear reinforcement ratio, beam size, a/d ratio, tension reinforcement ratio, presence of existing holes and embedded length of FRP bars on the structural behaviour of DE FRP-strengthened beams. Based on the experimental results, the following conclusions are drawn:

- The total shear force capacity as well as the DE FRP and concrete contributions to the shear strength decreased with increasing steel-to-FRP shear reinforcement ratio. Thus, calculating the DE FRP shear resistance as the difference between the strengthened and unstrengthened shear force capacities can lead to erroneous results.
- The tension reinforcement ratio had a clear effect on failure mode. The tested strengthened beams with a tension reinforcement ratio equal to 2.0% failed in flexure whereas the tested strengthened beams with 2.7% tension reinforcement ratio failed in shear. However, the tension reinforcement ratio did not influence the gain due to FRP bars.
- The control and GFRP-strengthened beams had comparable cracked stiffness whereas the CFRP-strengthened beams had higher cracked stiffness, demonstrating the effectiveness of CFRP bars in controlling crack opening.
- The experimental results showed that the embedded FRP bars significantly mitigated size effect in DE FRP-strengthened RC T-beams. The reduction in shear stress at failure of the unstrengthened and strengthened slender beams was 50 and 18%, respectively. The corresponding values for deep beams were 26 and 10%, respectively.

- The experimental results confirmed that a/d ratio plays a vital role in governing DE FRP-strengthened behaviour. The concrete contribution to the shear resistance and total shear force capacity increased with decreasing a/d ratio, whereas the contribution of DE FRP bars decreased with decreasing a/d ratio. The contribution of DE CFRP bars decreased by about 21% with decreasing a/d ratio from 3 to 1.9. The corresponding reduction for DE GFRP bars was about either 81% or 60%
- In contrast to test results on rectangular shaped RC beams reported in the published literature, existing holes instigated premature shear failure in RC T-beams before reaching their nominal shear force capacity. The shear strength reduction due to existing holes ranged from 7 to 22%.
- The embedded length of FRP bars had a clear effect on shear resistance. Both the FRP contribution and the total shear resistance increased with increasing embedded length from 262.5 to 325 mm. The embedded length of FRP bars is therefore one of the main parameters influencing the strengthened behaviour.

CHAPTER 5: FINITE ELEMENT MODELLING

5.1. General

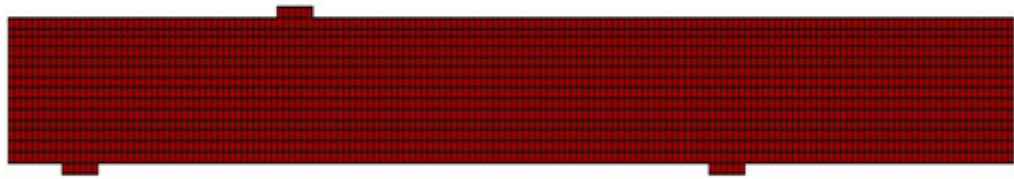
This chapter aims to present a nonlinear finite element (FE) predictive tool that accurately simulates the structural behaviour of the tested beams as well as beams reported in the literature. A two-dimensional nonlinear FE model was developed using VecTor2 software package and validated against test results. As mentioned in Chapter 2, VecTor2 utilizes the theoretical background of the Disturbed Stress Field Model (DSFM) (Vecchio, 2000), a developed version of the Modified Compression Field Theory (MCFT) (Vecchio and Collins, 1986). Crack shear slip deformations play a crucial role in characterising this development (Vector2 & Formworks User`s Manual, 2013). VecTor2 utilizes a smeared-crack approach to predict the structural behaviour of RC membrane elements. Moreover, VecTor2 is also user-friendly software and offers a wide range of constitutive models for concrete (Vector2 & Formworks User`s Manual, 2013).

The geometrical details including element types and mesh density together with constitutive material models and solution algorithm are briefly explained in Section 5.2. The validation of the nonlinear FE model against the experimental results is addressed in Section 5.3. The experimental results are also compared to the FE predictions in Section 5.3. This comparison comprises shear force-deflection curves as well as crack patterns at failure. Section 5.4

further validates the proposed FE model against test results reported in the literature. Section 5.5 concludes the chapter with focussing on key findings.

5.2. FE model

A two-dimensional FE model was developed to numerically simulate the structural behaviour of tested beams described in Chapter 3. The same FE model was used for all beams throughout this study unless otherwise stated. Figure 5.1 shows typical FE models for the tested slender and deep beams.



(a)



(b)

Figure 5.1. FE model (a) slender beam (b) deep beam

5.2.1. Geometric modelling, element, and mesh details

As shown in Figure 5.2, two-dimensional four-node rectangular plane stress elements with two degrees of freedom at each node were used for the concrete. Nodes of i, j, m, and n, respectively, in an anti-clockwise direction, were used to create the element. Any size for the width and height can be used for rectangular plane stress elements however the aspect ratio should not exceed 1.5 (Vector2 & Formworks User`s Manual, 2013). The mesh sensitivity was investigated by considering one unstrengthened and two DE FRP-strengthened beams as shown in Figure 5.3. The investigated average mesh sizes were 15, 25, 35 and 45 mm. The finest mesh size caused a significant reduction in the shear strength. The average mesh size of 25 mm resulted in a better crack pattern compared to coarser mesh sizes. The average mesh size of concrete in each direction was therefore taken between $2.5d_a$ (where d_a is the maximum aggregate size (10 mm)). This is broadly consistent with the recommendation of Bažant and Oh (1983) to use a concrete mesh size of $3d_a$. Moreover, Dirar et al. (2013b) successfully used a mesh size of $2.5d_a$ to model FRP shear-strengthened RC T-beams. For convenience, the loading and support steel plates had the same element type and size as the concrete.

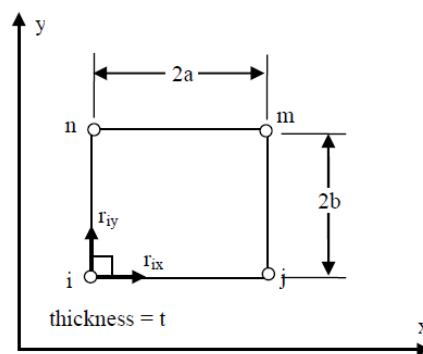


Figure 5.2. Rectangular plane stress element (Vector2 & Formworks User`s Manual, 2013)

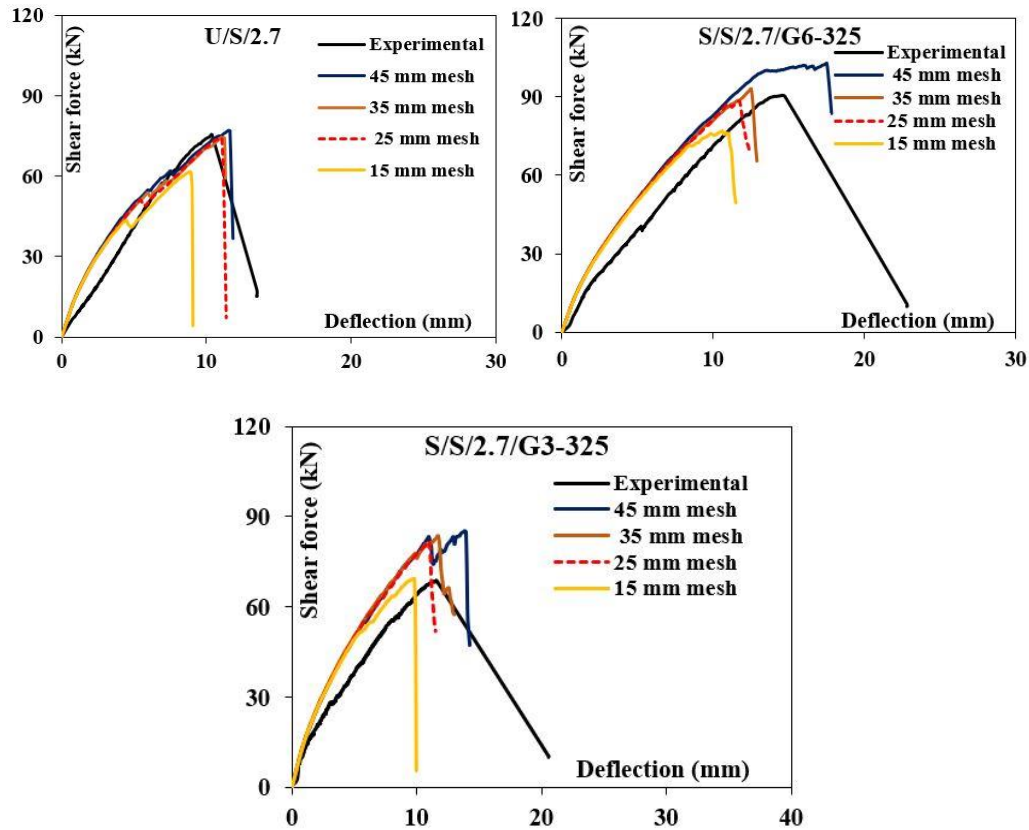


Figure 5.3. Comparison of different mesh sizes

The steel and FRP bars can be modelled as either smeared or discrete reinforcement in VecTor2 software. The steel bars were modelled as discrete reinforcement using two-node truss elements with two degrees of freedom at each node, as demonstrated in Figure 5.4. The truss elements can be modelled with any angle (α) between x- and y-axes.

Bond failure between the concrete and the steel bars was not the governing failure mode of the tested beams. Perfect bond was therefore assumed between the concrete and the steel reinforcement. A similar approach was successfully used by Qapo et al. (2016) to model RC T-beams strengthened in shear with DE FRP bars. There is still the potential for localized slip between the reinforcement and surrounding concrete in the tested beams. However, this

does not affect the overall predicted behaviour as demonstrated by the comparison between the experimental and numerical results (see Section 5.3).

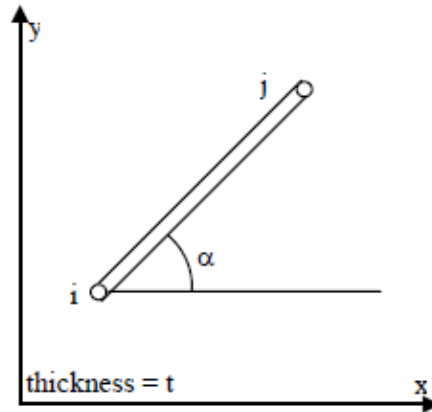


Figure 5.4. Truss element (Vector2 & Formworks User`s Manual, 2013)

The embedded FRP bars were also modelled as discrete reinforcement using two-node truss elements. The embedded FRP bars were assumed to be perfectly bonded to concrete since the failure mode of tested beams was not governed by the bond failure (see Chapter 4). This approach is consistent with the results stated by Qapo et al. (2016), Qapo (2016), and Bui et al. (2020b). It was indicated that there was an insignificant difference between predictions of perfect bond assumption and predictions of bond-slip model for the ultimate shear force capacity and deflection at failure. This can be explained by the fact that failure due to debonding can be avoided by using the DE/ETS shear strengthening technique for shear-deficient RC beams. Godat et al. (2013) also successfully modelled DE FRP-strengthened beams with an assumption of perfect bond since debonding of embedded FRP bars was not observed up to the failure of the beams (Godat et al., 2013).

5.2.2. Material modelling

The material properties of concrete, steel, and FRP reinforcement given in Chapter 3 were utilised to develop the FE model. The constitutive models adopted for the concrete, steel, and FRP reinforcement are briefly described in the below subsections.

5.2.2.1. Concrete

As previously mentioned, the DSFM formulations for crack shear slip deformation are built in VecTor2. Walraven's model (Walraven and Reinhardt 1981), the default model in VecTor2 for crack slip calculation, was used. It should be noted that analysis proceeds according to the MCFT if the crack slip calculation is not considered (Vector2 & Formworks User's Manual, 2013). The crack width check may be designated as quarter or half of the aggregate size, based on the recommendation of VecTor2 User's Manual (2013). The crack width limit was taken as the default value of aggregate size/2.5 throughout this study.

A wide range of constitutive models for concrete in compression is incorporated in VecTor2 software. More information can be found in Vector2 & Formworks User's Manual (2013). The concrete in compression was modelled by Thorenfeldt's et al. (1987) stress-strain curve, which is given by Equation 5.1.

$$f_{ci} = - \left(\frac{\varepsilon_{ci}}{\varepsilon_p} \right) f_p \frac{n}{n - 1 + \left(\frac{\varepsilon_{ci}}{\varepsilon_p} \right)^{nk}} \quad (5.1)$$

where f_{ci} (MPa) represents the concrete compressive stress at a given strain ε_{ci} (mm/mm); f_p (MPa) is the concrete cylinder compressive strength and ε_p (mm/mm) is the corresponding

strain; n is a parameter equal to $0.8 + (f_p/17)$; and k , a parameter with regard to the descending branch of the curve, is calculated as follows;

$$k = \begin{cases} 1 & \text{for } \varepsilon_p < \varepsilon_{ci} < 0 \\ 0.67 + \frac{f_p}{62} \geq 1 & \text{for } \varepsilon_{ci} < \varepsilon_p < 0 \end{cases} \quad (5.2)$$

The softening of concrete in compression caused by lateral cracking was incorporated by adopting the model developed by Vecchio and Collins (1993) as follows (Vector2 & Formworks User`s Manual (2013);

$$\beta_d = \frac{1}{1 + C_s C_d} \leq 1 \quad (5.3)$$

$$C_d = 0.27 \left(\frac{\varepsilon_{c1}}{\varepsilon_0} - 0.37 \right) \quad 0 \leq C_d \leq 50 \quad (5.4)$$

$$C_s = \begin{cases} 1 & \text{if shear slip not considered} \\ 0.55 & \text{if shear slip considered} \end{cases} \quad (5.5)$$

$$f_{pk} = \beta_d f_c \text{ and } \varepsilon_{pk} = \varepsilon_0 \quad (5.6)$$

where β_d is the reduction factor for the concrete compressive strength, ε_{c1} is the principal tensile strain, f_c is the compressive strength of concrete, ε_0 is the corresponding strain, f_{pk} is the peak concrete compressive strength, ε_{pk} is the corresponding strain, C_d is the factor given in Equation 5.4, and C_s is the factor governing the effect of shear slip.

Of note is that β_d is only used to reduce f_c to calculate f_{pk} for strength-only softened models as shown in Equation in 5.6. More details on the models can be found elsewhere (VecTor2 & Formworks User`s Manual 2013). Moreover, Poisson`s ratio of concrete was taken as 0.15 based on the recommendation of CEB-FIP Model Code (1990).

The concrete behaviour in tension was assumed as linear-elastic prior to concrete cracking. A bilinear tension softening model adapted from CEB-FIP Model Code (1990) by VecTor2 was used to model the post-cracking behaviour of concrete. The fracture energy (G_F) of concrete was calculated according to Equation 5.7, also given by CEB-FIP Model Code (1990).

$$G_F = G_{Fo} \left(\frac{f_{cm}}{f_{cmo}} \right)^{0.7} (N/mm) \quad (5.7)$$

where G_{Fo} is the base value of fracture energy (taken as 0.0263 N/mm for a maximum aggregate size of 10 mm) and f_{cmo} is taken as 10 MPa. f_{cm} is the mean compressive strength of concrete and can be calculated as $f_{ck} + 8$ MPa (where f_{ck} is the characteristic strength value). Tension stiffening of the concrete was simulated using the model developed by Bentz (2005). The concrete tensile strength (f_t) was defined in accordance with JSCE (2002), as given by Equation 5.8.

$$f_t = 0.44 (f_c)^{0.5} \quad (5.8)$$

The elastic modulus of concrete (E_c) was defined in accordance with Equation 5.9 proposed by Wang et al. (1978). Dirar et al. (2013b), Qapo (2016), and Qapo et al. (2016) successfully implemented the below equation for numerical simulation of EB and DE FRP-strengthened RC beams.

$$E_c = 271 f_c + 978 \text{ (in Ksi)} \quad (5.9)$$

5.2.2.2. Steel and FRP reinforcement

The stress-strain model for the steel reinforcement as well as the loading and support plates had an initial linear-elastic response followed by a yield plateau and a nonlinear strain-hardening phase up to rupture. An elastic plastic model for the relationship between the dowel force and the relative displacement of cracks was considered. Tassios model reported in VecTor2 & Formworks User`s Manual (2013) was used for the dowel action. He and Kwan (2001) demonstrated the possibility of modelling the reinforcement as a beam supported by an elastic concrete foundation (VecTor2 & Formworks User`s Manual 2013). The dowel force (V_d) can be calculated according to the below equation (VecTor2 & Formworks User`s Manual 2013).

$$V_d = E_s I_z \lambda^3 \delta_s \leq V_{du} \quad (5.10)$$

$$I_z = \frac{\pi d_b^4}{64} \quad (5.11)$$

$$\lambda = \sqrt[4]{\frac{k_c d_b}{4E_s I_z}} \quad (5.12)$$

$$k_c = \frac{127c\sqrt{f_c}}{(d_b)^{2/3}} \quad c = 0.8 \quad (5.13)$$

$$V_{du} = 1.27 d_b^2 \sqrt{f_c f_y} \quad (5.14)$$

where δ_s is the shear slip throughout, d_b is the reinforcement diameter, E_s is the elastic modulus of the reinforcement, f_y is the yield strength of the reinforcement, f_c is the concrete strength, I_z is the second moment of area of the reinforcement bar, λ , a parameter, is responsible for the comparison between the concrete and the reinforcement stiffness, k_c is the notional elastic concrete foundation stiffness, c is a coefficient representing bar spacing (taken as 0.8) and V_{du} is the ultimate dowel force. The default option of Tassios crack slip model was used for all beams in this study. A linear-brittle stress-strain model, based on the ultimate strength values reported in Chapter 3, was used for the embedded FRP bars. The constitutive models for the FE model and main input parameters are summarised in Table

5.1. It is worth noting that most of the material models used to develop the FE model were default models recommended by VecTor2 software.

Table 5.1. Summary of FE model

Concrete Models		Reinforcement Models					
Concrete Pre- and Post-Peak	Popovics (HSC) Base Curve	Hysteretic Response*		Bauschinger Effect (Seckin)			
Compression Softening	Vecchio 1992-B (e1-e0-Form)	Dowel Action*		Tassios (crack slip)			
Tension Stiffening*	Modified Bentz 2003	Buckling*		Akkaya 2012 (Modified Dhakal-Maekawa)			
Tension Softening*	Bilinear	Main Input Parameters					
Confined Strength*	Kupfer/Richart	f _c (MPa)	f _t (MPa)	G _F (N/mm)	E _c (MPa)	Max. Agg. Size	Poisson's ratio
Dilation*	Variable-Isotropic	41	2.82	0.08	17850	10	0.15
Cracking Criterion*	Mohr-Coulomb (Stress)	Analysis Models					
Crack Stress Calculation*	Basic (DSFM/MCFT)	Strain History*		Previous Loading Considered			
Crack Width Check*	Agg. / 2.5	Cracking Spacing*		CEB-FIP 1978-Deformed			
Crack Slip Calculation*	Walraven	Max. No. of Iterations		100			
Creep and Relaxation*	Not Considered	Convergence Limit*		1.00001			
Hysteretic Response*	Nonlinear/w-Plastic Offsets	Structural Damping*		Not Considered			
Bond	Perfect Bond	Geometric Nonlinearity*		Considered			
* Default models		Convergence Criteria*		Displacements-Weighted Average			

5.2.3. Solution algorithm

VecTor2 utilizes an incremental-iterative algorithm to solve the nonlinear equations. A displacement control approach was used where the load was applied in increments of 0.1

mm. For each increment, the secant stiffness was used to iteratively search for equilibrium. Convergence was successfully achieved at the end of each increment using this procedure.

5.3. Validation

A two-dimensional FE model was developed using VecTor2 software, as explained in the previous section. The FE model was validated against the test results reported in Chapter 4. The comparative study results between tested and modelled beams are presented and discussed with regard to shear force capacity, deflection and crack patterns at failure. The verified FE model was also utilised to conduct the parametric studies reported in Chapter 6.

5.3.1. Overall response

The FE predictions in terms of shear force at failure and deflection at peak load together with the corresponding experimental results are presented in Table 5.2. The predicted and experimental initial stiffness values are also given in Table 5.2. The FE results were in good agreement with the experimental results in terms of predicting ultimate shear force capacity. The mean value of the predicted-to-experimental shear force at failure is 1.03 with a standard deviation of 0.1, demonstrating the accuracy of the FE model in terms of predicting ultimate shear force capacity. The corresponding values for the deflection at peak shear force, excluding SS/S/2.0/G6-325 which failed in flexure, were 0.87 and 0.23, respectively. The mean error of the predicted-to-experimental shear force at failure is calculated to be 7.5% whereas the corresponding mean error for the deflection at peak shear force, excluding SS/S/2.0/G6-325, is 18.7%. As can also be seen in Table 5.2, the mean value for the predicted-to-experimental initial stiffness is 1.35 with a standard deviation of 0.34. The mean error for the predicted-to-experimental initial stiffness is 34.5%.

Table 5.2. Comparison between experimental results and FE predictions

Beam	Shear force at failure (kN)			Deflection at peak shear force (mm)			Initial stiffness (kN/mm)		
	Experimental	FE Prediction	FE/Exp.	Experimental	FE Prediction	FE/Exp.	Experimental	FE Prediction	FE/Exp.
U/S/2.0	65.5	73.6	1.12	10.7	11.7	1.09	13.6	13.9	1.02
U/S/2.7	75.5	74.4	0.99	10.1	11	1.09	10.4	14.3	1.38
U/D/2.7	103.9	103.3	0.99	5.1	3.9	0.76	50	62.5	1.25
S/S/2.0/G3-325	68.7	76.8	1.12	11.2	11.2	1.00	13.2	13.9	1.05
S/S/2.7/G3-325	68.7	81.8	1.19	11.6	10.9	0.94	11.9	14.3	1.2
S/S/2.0/G6-325	78.5	85.3	1.09	>50.0*	>22*	-*	10.4	13.9	1.34
S/S/2.7/G6-325	90.5	88.2	0.97	14.7	11.7	0.80	11.4	14.3	1.25
S/S/2.7/C3-325	103.6	89.8	0.87	11.3	12.1	1.07	13.2	14.3	1.08
S/D/2.7/G2-325	114.4	113.5	0.99	5.9	4.0	0.68	29.4	62.5	2.13
S/D/2.7/C2-325	134.7	129.4	0.96	11.3	4.8	0.42	35.7	62.5	1.75
Mean			1.03			0.87			1.35
Mean error			7.5%			18.3%			34.5%
Standard deviation			0.1			0.23			0.34
*Flexural failure									

5.3.2. Unstrengthened beams

As demonstrated in Figure 5.5, the shear force-deflection curves of the unstrengthened beams obtained from experimental results were compared to those obtained from numerical analysis. The predicted shear force-deflection curves were quasilinear prior to cracking. Subsequently, the shear force-deflection curves turned nonlinear due to stiffness deterioration instigated by cracking. Upon further loading, the post-cracked stiffness continued to deteriorate up to failure. The brittle failure of the three beams, characterised by a sudden drop in load, was accurately predicted.

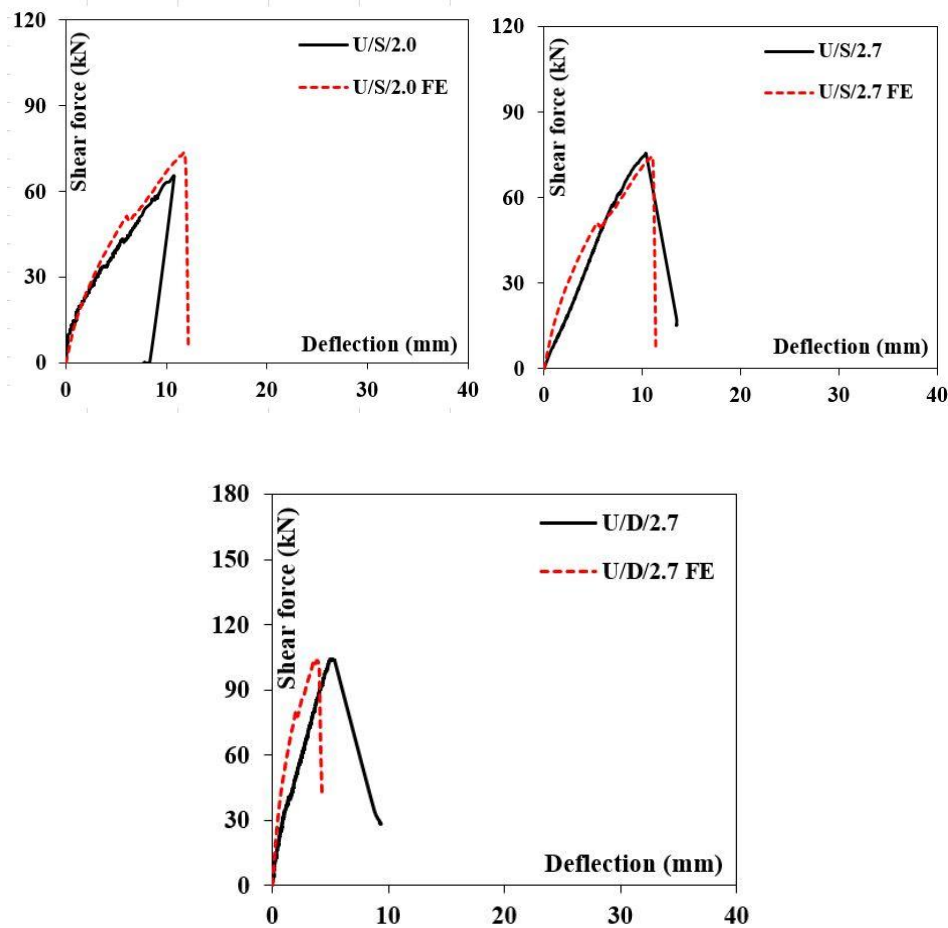
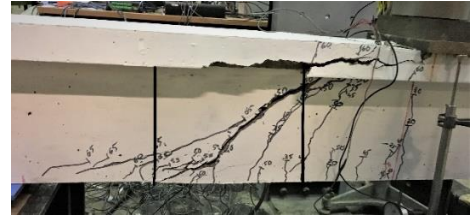
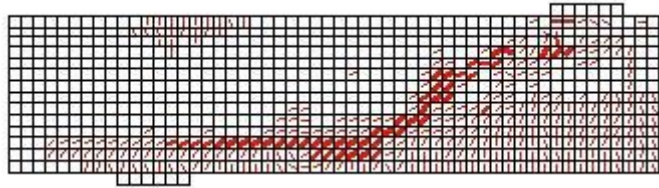
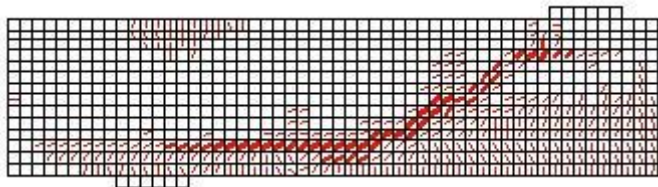


Figure 5.5. Experimental and FE-predicted shear force-deflection curves for the unstrengthened beams

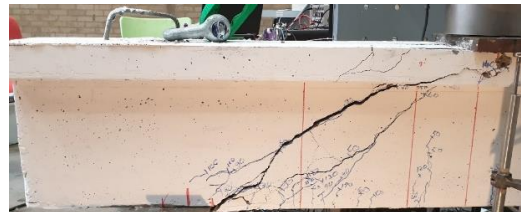
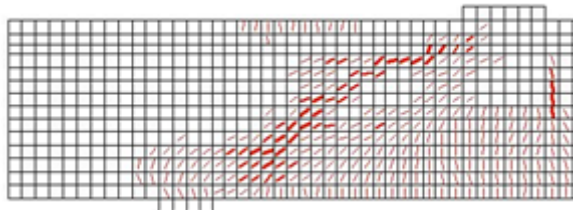
Figure 5.6 demonstrates that the cracks at failure for the unstrengthened beams were accurately predicted. Similar to experimental observations, a diagonal tension failure and a shear-compression failure instigated by an inclined crack occurred in the unstrengthened slender and deep beams, respectively.



U/S/2.0



U/S/2.7



U/D/2.7

Figure 5.6. Experimental and FE-predicted crack patterns at failure for the unstrengthened beams

5.3.3. Strengthened beams

Figure 5.7 compares the experimental shear force-deflection curves with the numerical shear-force deflection curves for the strengthened beams. The comparisons clearly show that the pre-cracking stiffness compared to post-cracking stiffness was more accurately predicted. This might be attributable to the perfect bond assumption. With increasing loading, the stiffness deterioration instigated by cracking resulted in the shear force-deflection curves becoming nonlinear. Upon further loading, the post-cracked stiffness continued to deteriorate up to failure. S/S/2.0/G6-325 failed in flexure whereas remaining strengthened beams failed in shear.

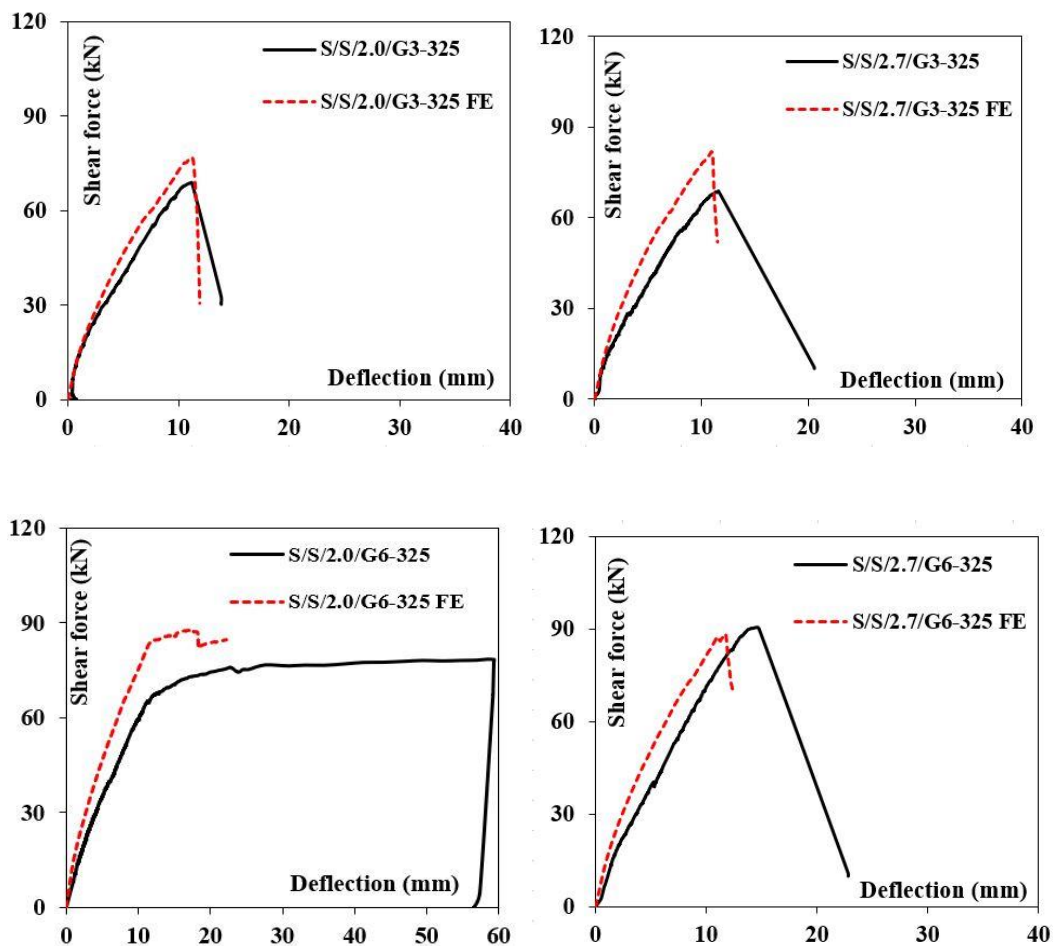


Figure 5.7. Continued

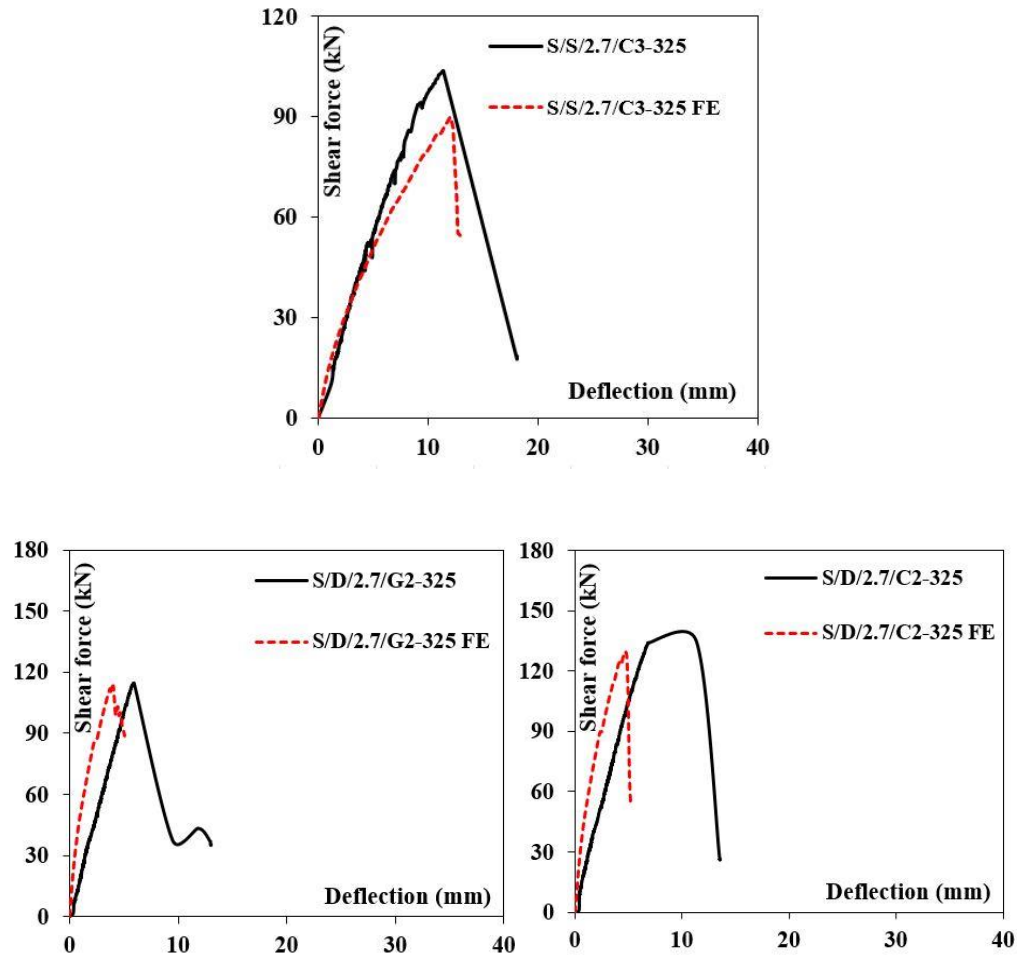
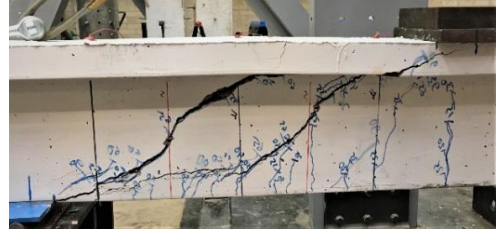
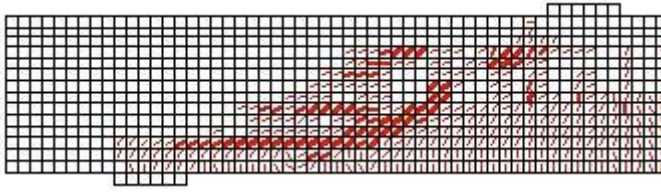
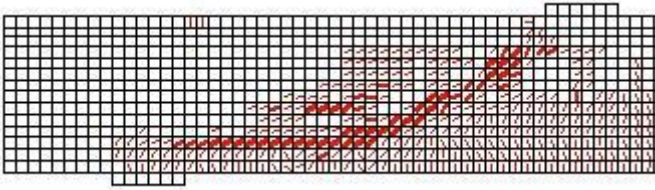


Figure 5.7. Experimental and FE-predicted shear force-deflection curves for strengthened beams

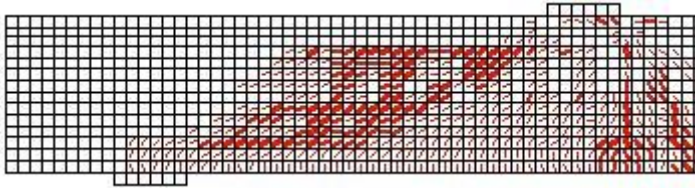
For the strengthened beams, the experimental crack patterns at failure were compared with those obtained from the numerical analysis, as depicted in Figure 5.8. Except for S/S/2.0/G6-325, an inclined crack appeared in the shear span resulting in a diagonal tension failure of the strengthened slender beams as observed during experimental tests. An inclined crack caused a shear-compression failure in S/D/2.7/G2-325 and S/D/2.7/C2-325.



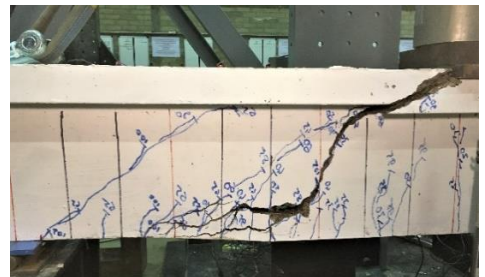
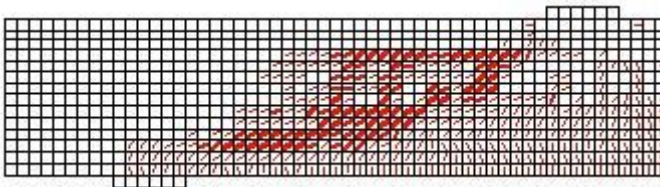
S/S/2.0/G3-325



S/S/2.7/G3-325

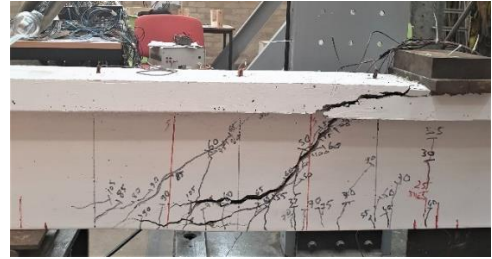
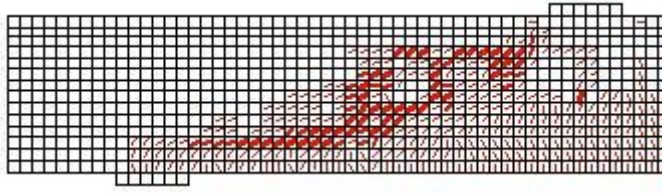


S/S/2.0/G6-325

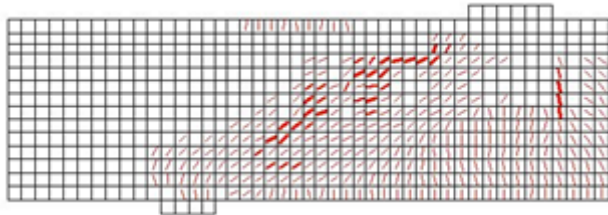


S/S/2.7/G6-325

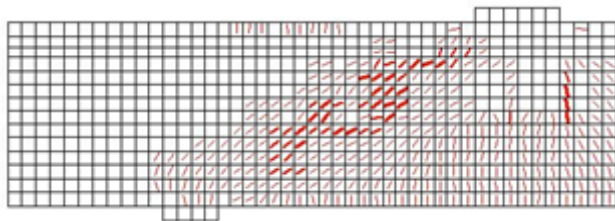
Figure 5.8. Continued



S/S/2.7/C3-325



S/D/2.7/G2-325



S/D/2.7/C2-325

Figure 5.8. Experimental and FE-predicted crack patterns at failure for the strengthened beams

5.4. FE modelling of beams in published literature

This section aims to validate the FE model against experimental results reported by Mofidi et al. (2012a) and Jemaa et al. (2015). A brief summary of these experimental studies is presented in the below subsection. These experimental programmes were included in this

section to conduct further investigation on effects of beam size and steel-to-FRP shear reinforcement ratio on the DE FRP-strengthened behaviour. As mentioned previously, the verified FE model was used to carry out the parametric studies reported in Chapter 6.

5.4.1. Experimental Programme

5.4.1.1. Mofidi et al. (2012a)

The RC T-beams tested by Mofidi et al. (2012a) were included in this chapter to verify the FE model with a view to conducting a parametric study. One beam, namely S1-CON, was a control beam whereas three beams, namely S1-9d260s, S1-12d260s and S1-9d260p, were strengthened in shear with embedded CFRP bars. As illustrated in Figure 5.9, each beam had a flange depth of 102 mm, flange width of 508 mm, web width of 152 mm and overall depth of 406 mm. All beams had an effective depth of about 350 mm and an a/d ratio of about 3.0. The steel shear reinforcement consisted of 8 mm diameter steel shear links spaced at 175 mm centre-to-centre (c/c), resulting in a steel shear reinforcement ratio of 0.38%. The DE shear strengthening system comprised 9.5 mm diameter sand-coated or plain CFRP bars spaced at 260 mm c/c for S1-9d260s and S1-9d260p, respectively. S1-12d260s was strengthened with 12.7 mm diameter sand-coated CFRP bars spaced at 260 mm (c/c). The beams strengthened with 9.5 mm diameter CFRP bars had an FRP shear reinforcement ratio of 0.18% whereas the beam strengthened with 12.7 mm diameter CFRP bars had an FRP shear reinforcement ratio of 0.32%. All beams were longitudinally reinforced in compression and tension with six 10 M steel bars (area of each bar 100 mm^2) and four 25 M steel bars (area of each bar 500 mm^2), respectively. Table 5.3 lists material properties of the concrete, steel and FRP shear reinforcement.

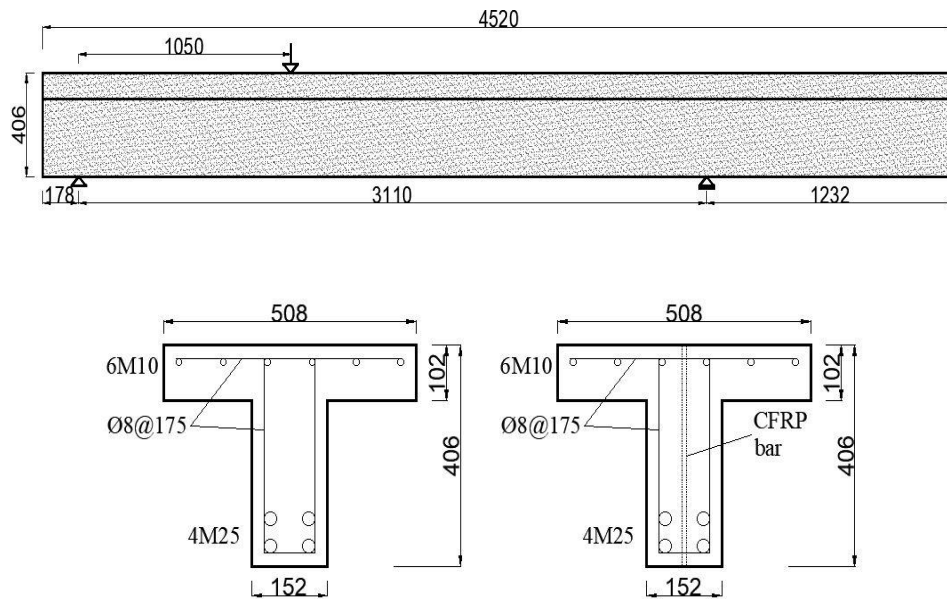


Figure 5.9. Elevation and cross-sections of the beams tested by Mofidi et al. (2012a)
(dimensions in millimetres)

Table 5.3. Material properties of the RC T-beams tested by Mofidi et al. (2012a)

Property	Concrete	10 M and 25 M steel bars	8 mm steel bars	Sand- coated CFRP bars	Plain surface CFRP bars
Elastic Modulus (MPa)	-	200000	200000	148000	155000
Concrete Strength (MPa)	29.6 ^{1,2}				
Ultimate Strain (mm/mm)	-	-	-	0.0127	0.018
Yield Strength (MPa)	-	470	540	-	-
Ultimate Strength (MPa)	-	-	-	1885	2800
¹ Concrete strength of S1-CON was 25 MPa.					
² Maximum aggregate size was 14 mm.					

5.4.1.2. Jemaa et al. (2015)

Two large-scale RC beams, an unstrengthened (control) and a DE GFRP-strengthened beam, were utilised to further validate the FE model. The experimental test setup together with geometrical details of the beams are shown in Figure 5.10. The total height, web width, flange depth and flange width of the large-scale beams were 650 mm, 150 mm, 125 mm and 400 mm, respectively. The beams had an a/d ratio of 3 and an effective depth of 600 mm. As shown in Figure 5.10, the beams were reinforced in compression with four 12 mm diameter steel bars, and the tension reinforcement consisted of four 25 mm diameter steel bars (area of each bar 491 mm²). The steel shear reinforcement comprised 8 mm diameter shear links spaced at 600 mm centre-to-centre (c/c), resulting in a steel shear reinforcement ratio of 0.11%. The DE shear strengthening scheme involved two 12 mm diameter sand-coated GFRP or CFRP bars spaced at 600 mm (c/c), resulting in a FRP shear reinforcement ratio of 0.25%. The material properties of the concrete, steel and DE FRP shear reinforcement are given in Table 5.4. It should be noted that the material properties and experimental results of the beam strengthened with CFRP bars were reported in Caro (2018) and are given here in the following subsection.

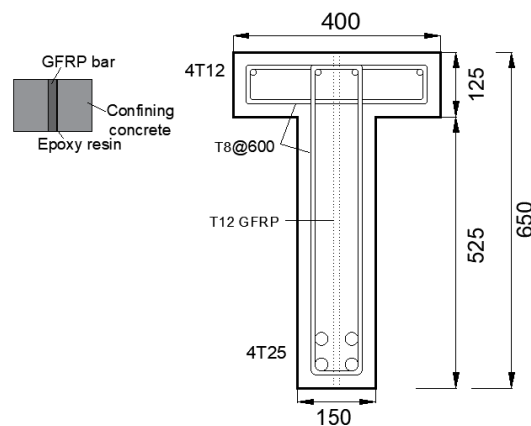


Figure 5.10. Continued

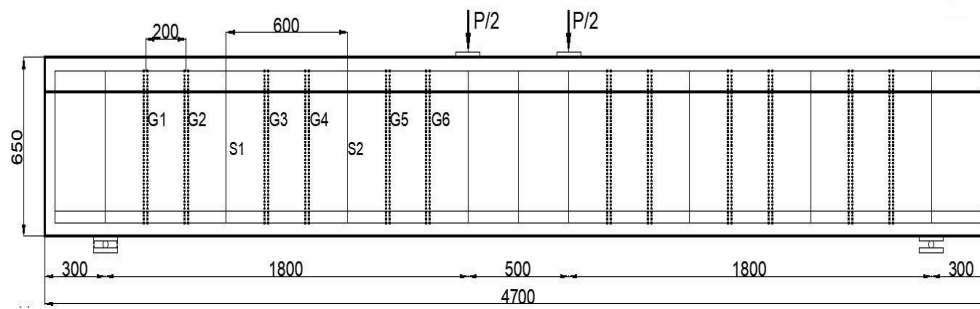


Figure 5.10. Cross-section and elevation of tested beams (Jemaa et al., 2015) (dimensions in millimetres)

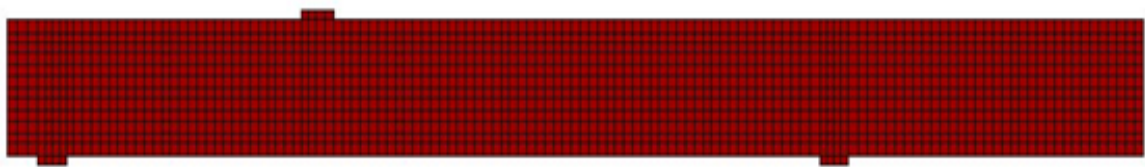
Table 5.4. Material properties of the RC T-beams tested by Jemaa et al. (2015)

Property	Concrete	12 mm and 25 mm steel bars	8 mm steel bars	Sand-coated GFRP bars
Elastic Modulus (MPa)	-	200000	200000	40000
Concrete Strength (MPa)	40.4 ¹			
Ultimate Strain (mm/mm)	-	-	-	0.0243
Yield Strength (MPa)	-	580	540	-
Ultimate Strength (MPa)	-	680	680	973
¹ Maximum aggregate size was 10 mm.				

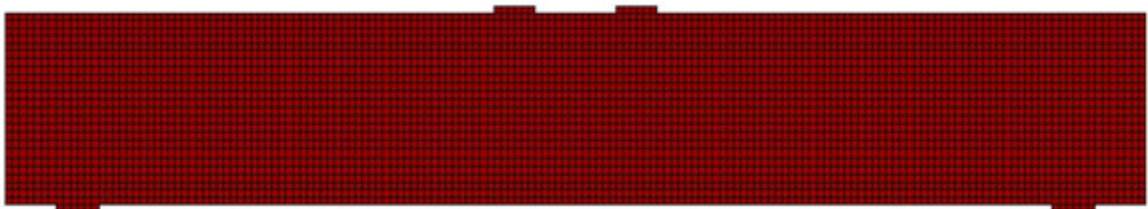
5.4.2. Validation

The FE predictions of the tested beams described above in terms of shear force at failure and deflection at peak load together with the corresponding experimental results are presented in Table 5.5. Table 5.5 also reports the predicted and experimental initial stiffness values.

It is worth noting that strain-hardening of the steel reinforcement in the beams reported by Mofidi et al. (2012a) was not modelled since the ultimate strength of the steel reinforcement was not reported. This assumption was also successfully implemented by Dirar et al. (2013b), Qapo (2016), and Qapo et al. (2016) for shear-deficient RC beams strengthened with FRP composites. The average mesh size was selected between $2.5d_a$ and $3d_a$. The typical FE models for the beams are depicted in Figure 5.11. The test results of the large-scale beam strengthened with CFRP bars can be found elsewhere (Caro, 2018). The sand-coated 12 mm diameter CFRP bars had the tensile strength of 2300 MPa, elastic modulus of 130 GPa, and ultimate strain of 1.7%.



(a)



(b)

Figure 5.11. FE modelling (a) Mofidi et al. (2012a) (b) Jemaa et al. (2015)

The FE results were in good correlation with the published experimental results in terms of predicting ultimate shear force capacity. The mean value of the predicted-to-experimental

shear force at failure is 1.01 with a standard deviation of 0.09, further demonstrating the accuracy of the FE model in terms of predicting ultimate shear force capacity. The corresponding values for the deflection at peak shear force were 0.58 and 0.14, respectively. The mean error of the predicted-to-experimental shear force at failure is calculated to be 7.3% whereas the corresponding mean error for the deflection at peak shear force is 42%. The standard deviation of 0.58 for the deflection can be explained by the stiffer response of FE results. This may be related to the experimental setup or microcracks. For example, the crack stiffness of S1-12d260s was well predicted, whereas the crack stiffness of S1-9d260s was not predicted well. This may be related to experimental results since the overall stiffness of S1-9d260s up to failure was lower than its control beam of S1-CON. The FE model also overestimated the cracked stiffness of large-scale control and DE GFRP-strengthened beams, whereas the overall stiffness of large-scale DE CFRP-strengthened beam was well predicted. As can also be seen in Table 5.5, the mean value for the predicted-to-experimental initial stiffness is 1.3 with a standard deviation of 0.29. The mean error for the predicted-to-experimental initial stiffness is 30.8%.

The comparison between experimental and FE-simulated shear force-deflection curves for the beams tested by Mofidi et al. (2012a) and Jemaa et al. (2015) is depicted in Figure 5.12. As shown in Figure 5.12, the elastic stiffness (i.e. prior to cracking) was reasonably predicted. Thereafter, cracking instigated stiffness deterioration and this deterioration caused a transition from linear to non-linear response. Upon further loading, the cracked stiffness continued to deteriorate up to failure. Finally, the brittle failure of the six beams accurately predicted. The large-scale DE CFRP-strengthened beam failed in shear after tension reinforcement yielded.

Table 5.5. Experimental results and FE predictions for the beams tested by Mofidi et al. (2012a) and Jemaa et al. (2015)

Beam	Shear force at failure (kN)			Deflection at peak shear force (mm)			Initial stiffness (kN/mm)		
	Experimental	FE Prediction	FE/Exp.	Experimental	FE Prediction	FE/Exp.	Experimental	FE Prediction	FE/Exp.
S1-CON	232.2	205.6	0.89	11.9	8.3	0.70	40	38.5	0.96
S1-9d260s	260.3	262.5	1.01	21.3	10.6	0.50	29.4	41.7	1.42
S1-12d260s	266.6	285.2	1.07	15.4	11.6	0.75	38.5	41.7	1.08
S1-9p260s	280.7	264.6	0.94	24.7	10.7	0.43	35.7	41.7	1.17
Control	149.5	165.6	1.11	18.8	12.2	0.65	23.3	38.9	1.67
GFRP strengthened	293	280.2	0.96	41.5	18.7	0.45	23.3	38.9	1.67
CFRP strengthened	318.1	353.7	1.11	>70*	>23	- *	35	38.9	1.11
Mean			1.01			0.58			1.3
Mean error			7.3%			42%			30.8%
Standard deviation			0.09			0.14			0.29
*Flexural failure									

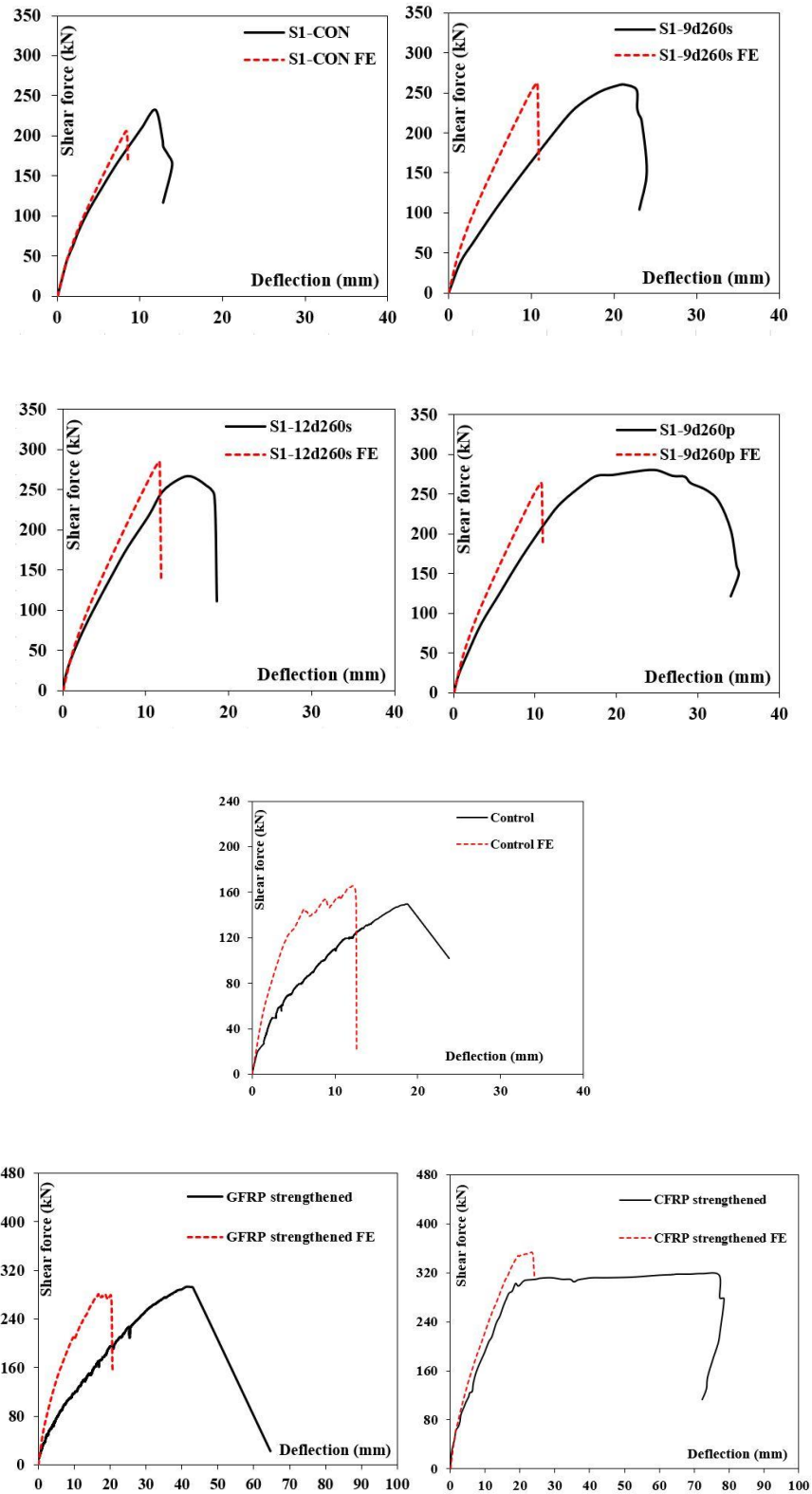


Figure 5.12. Experimental and FE-predicted shear force-deflection curves for the beams tested by Mofidi et al. (2012a) and Jemaa et al. (2015)

5.5. Summary and conclusions

This chapter addresses a two-dimensional FE model developed for the physically tested beams described in Chapter 3 as well as beams tested by Mofidi et al. (2012a) and Jemaa et al. (2015). The general knowledge on VecTor2 software, geometrical details consisting of element types and mesh density, constitutive material models and solution algorithm for the FE model were described in this chapter. The concrete was modelled using two-dimensional, four-node, rectangular plane stress elements with two degrees of freedom at each node. The steel reinforcing and FRP bars were modelled as discrete reinforcement using two-node truss elements with two degrees of freedom at each node.

The FE results presented in this chapter can be summarised as follows:

- The FE results for the beams described in Chapter 3 were in good agreement with the experimental results in terms of predicting ultimate shear force capacity. The mean value of the predicted-to-experimental shear force at failure was 1.03 with a standard deviation of 0.1. The corresponding values for the deflection at peak shear force were 0.87 and 0.23, respectively. The experimental crack patterns at failure were also compared with those obtained from the numerical analysis. The crack patterns at failure were well predicted.
- The FE model also gave accurate shear strength predictions for RC beams tested by Mofidi et al. (2012a) and Jemaa et al. (2015). For these beams, the mean value of the predicted-to-experimental shear force at failure was 1.01 with a standard deviation of 0.09. The corresponding values for the deflection at peak shear force, were 0.58 and 0.14, respectively.
- The validated FE model presented in this chapter is used to conduct parametric studies as reported in Chapter 6.

CHAPTER 6: PARAMETRIC STUDY AND DESIGN OF DE FRP-STRENGTHENED RC BEAMS

6.1. General

This chapter aims to present a FE parametric study of RC T-beams strengthened in shear with embedded FRP bars. The crucial parameters impacting the shear behaviour of DE FRP-strengthened RC beams were examined numerically. The investigated parameters were beam size, steel-to-FRP shear reinforcement ratio, tension reinforcement ratio and a/d ratio. Furthermore, the accuracy of existing design models to strengthen concrete beams with DE FRP reinforcement proposed by the Concrete Society's Technical Report 55 (TR55, 2012), Mofidi et al. (2012a), and Raicic (2019) was evaluated, and new design equations for DE FRP-strengthened RC beams were proposed.

This chapter is consisted of four sections. The parametric study is addressed in Section 6.2. The existing shear strengthening design models are evaluated in Section 6.3. New design equations offering predictions for the total shear force capacity of DE FRP-strengthened beams are also presented in Section 6.3. Section 6.4 summarises the key outcomes of this chapter.

6.2. Parametric study

A total of 67 FE analyses were conducted as part of this parametric study. Unless otherwise stated, all FE modelled beams stated in this chapter failed in shear. Each parameter was changed one at a time while other parameters were kept constant.

6.2.1. Size effect

The size effect in RC beams strengthened with embedded FRP bars is yet to be completely understood. This is mainly because the published literature mostly included a database on relatively small-scale DE FRP-strengthened beams (e.g., Valerio and Ibell, 2003; Mofidi et al., 2012a; Qin et al., 2015; Bui et al., 2020a). As stated in Section 4.3.4, the experimental results showed that embedded GFRP bars significantly mitigated size effect once the beam size increased. It is therefore crucial to further quantify size effect in DE FRP-strengthened RC beams. A FE parametric study on size effect in RC T-beams strengthened in shear with DE FRP bars was carried out to fill this knowledge gap.

The size effect in RC T-beams strengthened with embedded GFRP bars was studied by the development of FE models nominally identical to U/S/2.7 and S/S/2.7/G6-325 but with dimensions multiplied by 1.25, 1.5, 1.75, and 2. The cross-sectional area of the steel and DE FRP reinforcement was scaled by the above factors in order to keep the reinforcement ratios constant. It should be noted that all beams had a mesh size of 25 mm and were numerically tested under three-point bending. The details of the modelled beams together with the predicted shear stress at failure and shear force capacity are presented in Table 6.1.

Table 6.1. Details of RC T-beams

Beam	b_w (mm)	b_f (mm)	d (mm)	h (mm)	p_l %	p_f %	V_t, FE (kN)	$\frac{V_{tFE}}{b_w d}$ (MPa)
U/1.0	75	200	300	325	2.7	-	74.4	3.31
S/1.0	75	200	300	325	2.7	0.25	88.2	3.92
U/1.25	93.5	250	375	406	2.7	-	96.7	2.76
S/1.25	93.5	250	375	406	2.7	0.25	130.7	3.73
U/1.5	112.5	300	450	487.5	2.7	-	108.5	2.14
S/1.5	112.5	300	450	487.5	2.7	0.25	177.3	3.50
U/1.75	131	350	525	569	2.7	-	136.2	1.98
S/1.75	131	350	525	569	2.7	0.25	220.4	3.20
U/2.0	150	400	600	650	2.7	-	162	1.80
S/2.0	150	400	600	650	2.7	0.25	252	2.80

Similar to the experimental results, the results predicted by the FE model proved that the shear strength at failure in both unstrengthened and strengthened beams decreased with an increment in the effective depth from 300 to 600 mm. The shear stress at failure diminished from 3.31 to 2.14 MPa, and from 3.92 to 3.5 MPa with an increase in the effective depth from 300 to 450 mm for the unstrengthened and strengthened modelled beams, respectively. The shear stress further diminished from 2.14 to 1.8 MPa, and from 3.5 to 2.8 MPa, with an increment in the effective depth from 450 to 600 mm in the unstrengthened and strengthened modelled beams, respectively. The overall increase in the effective depth from 300 to 600

mm instigated a decrease in the overall shear stress of the control and strengthened beams by approximately 45.6 and 28.6%, respectively. This compares well with the corresponding experimental results of 50 and 18%, respectively. These results are also consistent with the numerical results of RC beams reported by Seo et al. (2015). The numerical results produced using VecTor2 software showed that shear stress at failure of RC beams diminished with an increase in the effective depth (Seo et al., 2015). The FE-predicted results together with the test results showed that embedded FRP bars mitigated size effect. Figure 6.1 demonstrates the variation in normalised shear stress (i.e., shear stress at failure divided by $\sqrt{f_c}$) with log (d). As can be seen in Figure 6.1, the normalised shear stress decreased with decreasing log (d).

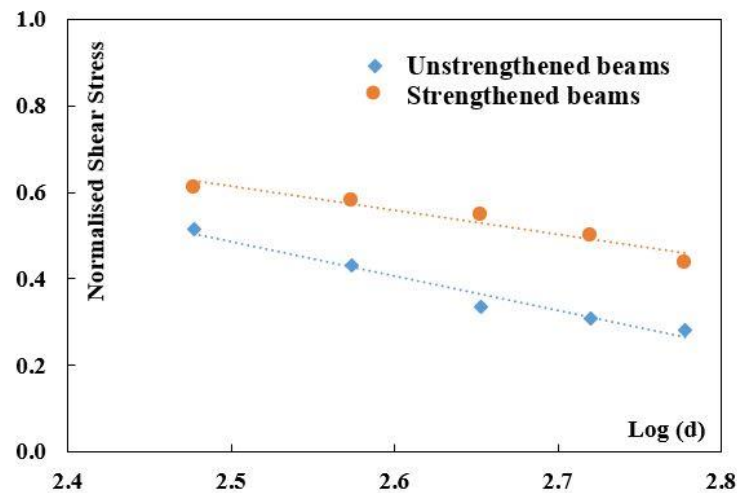


Figure 6.1. Normalised shear stress vs. log (d)

6.2.2. Tension reinforcement ratio

The effect of tension reinforcement ratio on the behaviour of DE FRP-strengthened beams has not yet been examined. The experimental results showed that tension reinforcement ratio

influenced failure mode but not gain due to DE FRP bars. The effect of tension reinforcement ratio on failure mode was further investigated by modelling DE FRP shear-strengthened beams nominally identical to S/S/2.0/G3-325, S/S/2.7/G3-325, S/S/2.0/G6-325, S/S/2.7/G6-325 and S/S/2.7/C3-325 but with tension reinforcement ratios in the range from 0.45 to 4.15%, obtained by changing the diameter of tension steel bars.

Figure 6.2 shows that the variation of normalised moment capacity (i.e., moment at failure (M_u) divided by flexural capacity (M_f) with tension reinforcement ratio is bilinear. A normalised moment capacity of 1.00 denotes flexural failure whereas M_u/M_f values less than 1.00 denote shear failure. All strengthened beam models with a tension reinforcement ratio less than 2.0% failed in flexure. On the other hand, all strengthened beam models with a tension reinforcement ratio more than 2.0% failed in shear. The experimental results reported in Chapter 4 also showed the DE FRP-strengthened beam with a tension reinforcement ratio of 2% failed in flexure, whereas the corresponding beam with a tension reinforcement ratio of 2.7% failed in shear. All these findings clarify the effect of tension reinforcement ratio on the failure mode of DE FRP shear-strengthened beams.

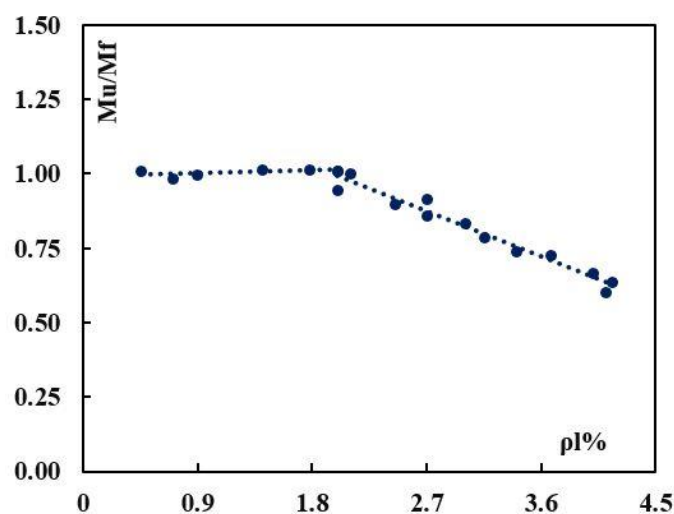


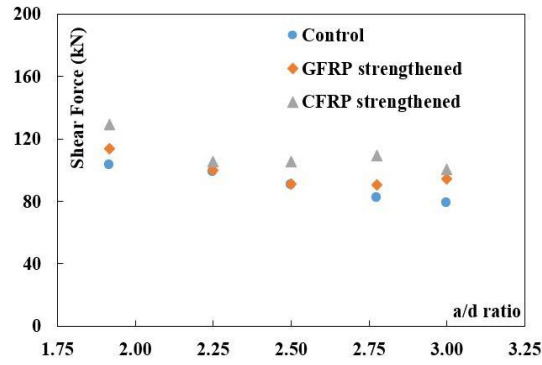
Figure 6.2. Effect of tension reinforcement ratio

6.2.3. Shear span-to-effective depth ratio (a/d)

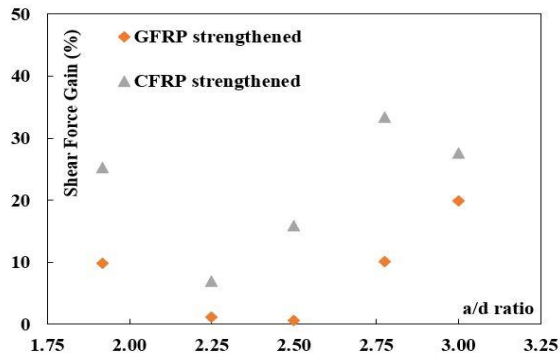
As mentioned in Chapter 2, the behaviour of RC beams is significantly controlled by the a/d ratio (Kani 1964; Kani 1967). However, research examining the impact of a/d ratio on the behaviour of DE FRP shear-strengthened RC beams has been limited (Dirar and Theofanous, 2017). A recent numerical investigation conducted by Caro (2018) concluded that shear force capacity together with DE FRP reinforcement contribution increased with a reduction in the a/d ratio from 2.5 to 1.9.

The effect of the a/d ratio was studied by the development of FE models nominally identical to U/D/2.7, S/D/2.7/G2-325, and S/D/2.7/C2-325 but with a/d ratios ranging between 1.9 and 3. Figure 6.3 (a) demonstrates the influence of the a/d ratio on the total shear force capacity. As can be seen in Figure 6.3 (a), the shear force capacity decreased with increasing the a/d ratio from 1.9 to 3. Such a result is consistent with the outcomes of Kani (1967), Caro (2018), Dirar and Theofanous (2017), and the experimental results reported in Chapter 4. The increment in a/d ratio from 1.9 to 3 caused a reduction of 23.8% in the unstrengthened shear force capacity. The corresponding reductions for DE GFRP and CFRP-strengthened beams were 16.8 and 22.4%, respectively.

Figure 6.3 (b) depicts the impact of a/d ratio on the percentage shear force gain obtained from embedded FRP bars. The percentage shear force gain provided by DE CFRP bars decreased from 25.3% to 15.9% with increasing a/d ratio from 1.9 to 2.5. The percentage shear force gain afterward increased from 15.9% to 27.6% with increasing a/d ratio from 2.5 to 3. The corresponding percentage shear force gain provided by GFRP bars decreased from 9.9% to 0.5% increasing a/d ratio from 1.9 to 2.5. This was followed by an increase in percentage shear force gain from 0.5% to 19.9% with increasing a/d ratio from 2.5 to 3.



(a)



(b)

Figure 6.3. Effect of a/d ratio on predicted (a) Shear force capacity (b) Shear force gain provided by FRP bars

6.2.4. Interaction between existing steel shear links and FRP bars

As the experimental results demonstrated, the interaction between existing steel shear links and FRP bars is one of the crucial parameters impacting the shear behaviour of RC T-beams strengthened with DE FRP bars. The experimental results also indicated that the total shear force capacity together with the shear resistance enhancement due to DE FRP reinforcement were inversely proportional to the steel-to-FRP shear reinforcement ratio ($E_s \cdot \rho_s / E_f \cdot \rho_f$).

An experimental programme conducted by Qin (2016) provided insight into the concrete contribution to shear resistance in beams with high steel shear reinforcement ratio. The details of the experimental programme are given in Chapter 2 and can be found elsewhere (Qin, 2016). Figure 6.4 shows the experimental components of shear resistance for the beams with a steel shear reinforcement ratio of 0.29% tested by Qin (2016). Similar to the experimental test results reported in Chapter 4, the strain values developed by the steel and FRP shear reinforcement were used to calculate the steel and FRP contributions (V_s and V_f) to the shear force capacity. The concrete contribution (V_c) was also calculated as the total shear force capacity (V_t) minus the sum of V_s and V_f . The results of the shear resistance components can be found elsewhere (Qin, 2016). The unstrengthened beams (N00, N07 and N15)) attained shear strengths of about 143, 148 and 155 kN, respectively. The strengthened beams (B00, B07, and B15) failed at a shear force of 142, 182, and 164 kN, respectively. Of note is that the experimental shear resistance components or strain readings for B00 were not reported. Therefore, the shear resistance components of B00 are not incorporated in Figure 6.4.

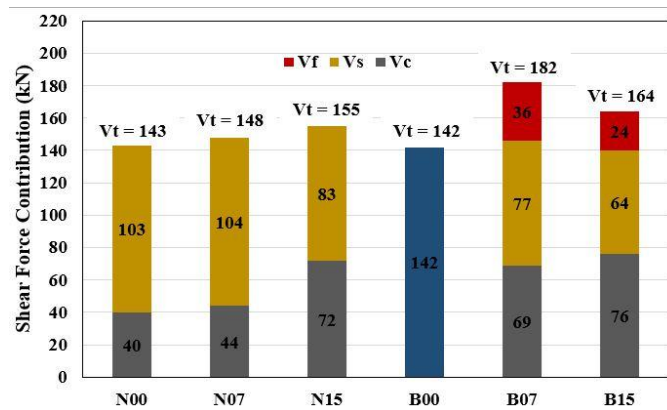


Figure 6.4. Components of shear resistance for the beams tested by Qin (2016)

Figure 6.4 clearly shows that the concrete contribution is significant and remains almost constant in the presence of DE FRP bars. V_c values for N07 and N15 were 44 and 72 kN, respectively; and increased to 69 and 76 kN, respectively, through the provision of additional

CFRP bars. This can be attributable to the reason that a high steel shear reinforcement ratio provides better confinement. Thus, the concrete contribution remains significant in beams with high steel shear reinforcement ratios.

Figure 6.5 depicts the variation in the experimental components of shear resistance for the experimentally tested beams. As can be seen in Figure 6.5, the presence of DE FRP bars instigated a significant decrease in the concrete contribution to the shear resistance. In contrast to beams with an existing steel reinforcement ratio of 0.29%, the concrete contribution can be insignificant in strengthened beams with a steel shear reinforcement ratio of 0.11%.

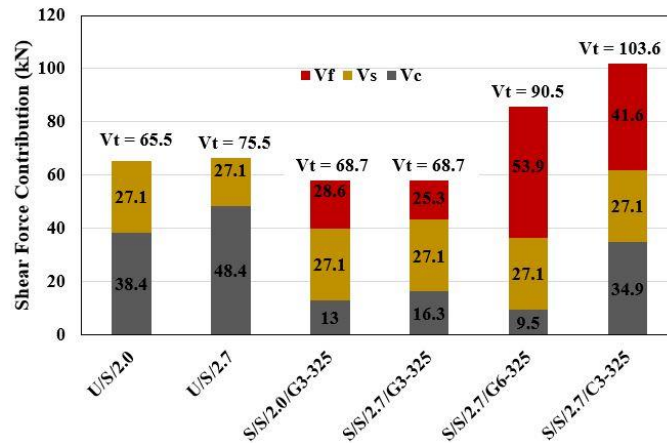


Figure 6.5. Components of shear resistance for the tested beams

Making use of the validated FE model, a parametric study was conducted to further examine the interaction between DE FRP bars and existing steel shear links. This interaction was separately investigated for beams with low and high existing steel shear reinforcement ratios.

The beams with low steel shear reinforcement ratio considered in the parametric study were nominally identical to the tested beams but had steel-to-FRP shear reinforcement ratios in the range from 0.17 to 4.35, obtained by changing the diameter and spacing of existing steel

shear links and/or the diameter, spacing and elastic modulus of DE FRP bar. All modelled beams failed in shear after yielding of the existing steel shear links.

Figure 6.6 shows that the variation of steel-to-FRP shear resistance ratio (V_s/V_f) with steel-to-FRP shear reinforcement ratio is bilinear. The DE FRP contribution far exceeds the steel contribution, resulting in V_s/V_f values in the range from 0.08 to 0.19, for steel-to-FRP shear reinforcement ratios in the range from 0.17 to 0.78. With increasing the steel-to-FRP shear reinforcement ratio from 0.78 to 2.75, the gap between the DE FRP and steel contributions decreases, resulting in V_s/V_f values in the range from 0.19 to 0.56. The steel-to-FRP shear resistance ratio remains almost constant for steel-to-FRP shear reinforcement ratios higher than 2.75. This implies that, for beams with low existing steel shear reinforcement ratios, the steel-to-FRP shear reinforcement ratio should be designed to be well below 2.75 in order to maximise the DE FRP contribution.

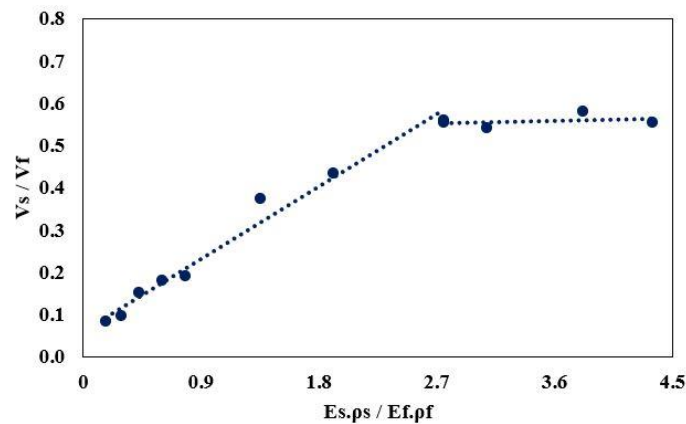


Figure 6.6. Effect of steel-to-FRP shear reinforcement ratio for DE FRP-strengthened beams with low existing steel shear reinforcement ratios

A FE parametric study was also carried out to provide insight into the interaction between DE FRP bars and high amounts of existing steel shear reinforcement. The beams incorporated in the parametric study were nominally identical to S1-9d260s, S1-12d260s

and S1-9p260s, tested by Mofidi et al. (2012a), but had steel-to-FRP shear reinforcement ratios ($E_s \rho_s / E_f \rho_f$) in the range from 0.64 to 4.62, obtained by changing the diameter and spacing of existing steel shear links and/or the diameter and spacing of DE FRP bar.

As forementioned, the contribution of concrete to the shear strength was insignificant in DE FRP strengthened RC T-beams with low amounts of steel shear reinforcement. On the other hand, the concrete contribution remained significant in DE FRP-strengthened RC T-beams with high amounts of steel shear reinforcement. Hence, the concrete contribution was considered as a shear component in the parametric study.

The variation between the sum of steel and concrete-to-FRP shear resistance ratio ($V_s + V_c / V_f$) and steel-to-FRP shear reinforcement ratio is also bilinear as shown in Figure 6.7. The shear resistance ratio ($V_s + V_c / V_f$) increased from 0.64 to 1.7 with the increase in steel-to-FRP shear reinforcement ratio from 0.64 to 2.72. The ($V_s + V_c / V_f$) ratio remained almost constant for values of steel-to-FRP shear reinforcement ratio higher than 2.72. This suggests that the contribution of DE FRP bars to the shear resistance can also be maximised by considering a steel-to-FRP shear reinforcement ratio below 2.72.

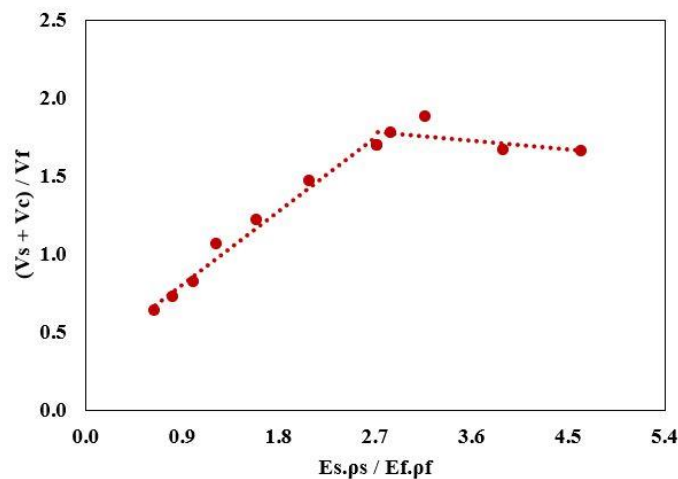


Figure 6.7. Effect of steel-to-FRP shear reinforcement ratio for DE FRP-strengthened beams with high existing steel shear reinforcement ratios

6.3. Design models

6.3.1. Existing design models

This section reviews the existing design models in the published literature for estimating the shear force capacity of RC slender beams strengthened with embedded FRP bars. In particular, the design models proposed by TR55 (2012), Mofidi et al. (2012a), and Raicic (2019) are considered. The details of these three models are presented in the following subsections.

TR55 design model

TR55 (2012) is currently the sole standard document covering design of DE FRP shear strengthening systems. TR55 ignores the concrete contribution and assumes that the total shear force capacity consists of the steel and DE FRP contributions as given in Equation 6.1.

$$V_t = V_s + V_f \quad (6.1)$$

The steel contribution is given by:

$$V_s = 0.78 \frac{A_{sw}}{s} d f_y \cot \theta \quad (6.2)$$

where d is the effective beam depth, f_y is the yield strength of the steel shear reinforcement and θ is the inclination angle of the concrete struts.

TR55 utilizes the truss analogy, with a shear crack inclination angle of 45 degrees, to give prediction for the contribution of embedded FRP reinforcement to the shear strength of RC slender beams.

The DE FRP contribution is given by:

$$V_f = \frac{\varepsilon_{fse} E_{fd} A_f}{S_f} W_{eff} \quad (6.3)$$

where ε_{fse} is the effective strain in the DE FRP bars (taken as 0.004 mm/mm), E_{fd} is the design Young's modulus of the DE FRP bars (MPa) and W_{eff} is the effective width (mm) over which the DE FRP bars may act and given by:

$$W_{eff} = (h - 2l_{b,max}) \quad (6.4)$$

where h is the strengthened depth (mm) and $l_{b,max}$ is the maximum anchorage length (mm) beyond which no additional capacity gain can be achieved, given by:

$$l_{b,max} = \frac{\varepsilon_{fse} E_{fd} A_f}{(\pi * d_b * \frac{\tau_b}{\gamma_A})} \quad (6.5)$$

where d_b , τ_b , and γ_A are the bar diameter of DE FRP reinforcement (mm), average bond stress (MPa) (can be taken as 15 MPa), and γ_A partial safety factor of adhesive material, respectively.

Design model proposed by Mofidi et al. (2012a)

An analytical design model, adopting 45 degrees truss analogy, was revealed by Mofidi et al. (2012a). The contribution of DE FRP reinforcement is expressed as given Equation 6.6.

$$V_f = k_L \cdot k_S \frac{A_{frp} \cdot E_{frp} \cdot \varepsilon_{frp} \cdot d_{frp} (\sin \alpha + \cos \alpha)}{s_{frp}} \quad (6.6)$$

where A_{frp} , E_{frp} , d_{frp} , α and s_{frp} are the cross-section area of FRP bars (mm^2), the Elastic modulus of DE FRP bars (MPa), the effective shear depth (mm), -which should be higher than either 0.72 multiplied by the overall height or 0.9 multiplied by the effective depth-, the inclination angle of FRP bar and FRP bar spacing (mm), respectively.

The effective strain (ε_{frp}) in FRP bars can be calculated for this model as stated in Equation 6.7.

$$\varepsilon_{frp} = \sqrt{\frac{8}{D_{frp} \cdot E_{frp}} \left(\frac{\tau_m \cdot s_m}{1 + \alpha_m} \right)} \leq 0.004 \quad (6.7)$$

where τ_m , s_m , α_m and D_{frp} are the maximum bond stress (MPa), corresponding slip at τ_m (mm), curve fitting parameter and diameter of FRP bar (mm), respectively.

The experimental results suggest that the bond-slip parameters of τ_m , s_m and, α_m can be taken as either 8.4 or 21.3 MPa, 0.08 or 0.176 mm, and 0.09 or 0.125 for either sand-coated or plain-surface FRP bars, respectively.

The parameter k_s stated in Equation 6.6 is a coefficient that considers the relationship between existing steel reinforcement and FRP bars. k_s is recommended to be equal to 0.6 for RC beams reinforced with shear links spaced at a distance of less than $2d/3$ (d is the effective depth). For other situations including RC beams without steel shear links, k_s can be taken as 1.

Another coefficient stated in Equation 6.6 is k_L , which considers the case where the FRP bar embedded length is smaller than the necessary minimum anchorage length (L_{eff}). k_L should

be between 0 and 1, depending on the relationship between d_{frp} and L_{eff} . k_L and L_{eff} can be calculated according to following equations;

$$k_L = \begin{cases} 1 & \frac{d_{frp}}{2} \geq L_{eff} \\ \frac{d_{frp}}{\sqrt{\frac{E_{frp} \cdot D_{frp} \cdot s_m}{2 \tau_m} \frac{1 + \alpha_m}{(1 - \alpha_m)^2}}} & \frac{d_{frp}}{2} < L_{eff} \end{cases} \quad (6.8)$$

$$L_{eff}(s_m) = \frac{f(s_m) \cdot D_{frp}}{4 \tau_m} \frac{1 + \alpha_m}{1 - \alpha_m} \quad (6.9)$$

where $f(s_m)$ is the stress of FRP bar at maximum slip. This stress can be calculated based on Equation 6.10 (Cosenza et al., 2002).

$$f(s_m) = \sqrt{\frac{8 E_{frp} \cdot \tau_m \cdot s_m}{D_{frp} \cdot (1 + \alpha_m)}} \quad (6.10)$$

Design model proposed by Raicic (2019)

Raicic (2019) demonstrated that the shear strength predictions of TR55 design model for DE FRP strengthened RC beams were conservative. One reason for the conservative predictions of TR55 design model is that it assumes the effective strain in DE FRP bars to be equal to 0.004 mm/mm. Raicic (2019) performed experimental tests on push-off specimens and RC beams strengthened with embedded FRP bars. The experimental results confirmed that the strain values exceeded the effective strain value of 0.004 mm/mm recommended by TR55

design model. This is broadly consistent with the experimental results reported in Chapter 4 where the experimentally measured strain values in DE FRP bars ranged from 0.005 to 0.015 mm/mm.

It is therefore that the effective strain value proposed by TR55 design model was modified by Raicic (2019). Raicic (2019) recommended that the average effective strain value be taken as 1% and 0.7% for DE GFRP and CFRP bars, respectively to improve TR 55 design model predictions.

6.3.2. Proposed design models

To overcome the shortcomings of existing design models, new design models based on steel-to-FRP shear reinforcement ratio are proposed in this section. The shortcomings of these models are discussed in Section 6.3.3. The new models distinguish between the design of DE FRP-strengthened RC slender beams with low (i.e., 0.1%) and high (i.e., higher than 0.2%) existing steel shear reinforcement ratios. The existing steel shear reinforcement ratios of 0.1 and 0.2% were chosen because they are representative of pre-1980 and post-1980 concrete shear design in the UK, respectively (BA 44/96, 1996; BS 8110-1, 1997; Concrete Society, 2009; Qin et al., 2015; Sogut et al., 2021).

6.3.2.1 Proposed design framework

A new design framework developed for DE FRP-strengthened RC slender beams is provided in this section. Based on the discussion presented in section 6.2.4, two approaches may be adopted for calculating the total shear force capacity of slender beams strengthened with DE FRP bars. For DE FRP-strengthened beams with high existing steel shear reinforcement ratios, contribution of the concrete to the total shear force capacity can be important and

should be considered in the design. Thus, the overall shear force capacity can be determined as given in Equation 6.11.

$$V_t = V_c + V_s + V_f \quad (6.11)$$

Equation 6.11 can be written in the following form;

$$\frac{V_t}{V_c + V_s} = \frac{V_c + V_s + V_f}{V_c + V_s} \quad (6.12)$$

Equation 6.13 can finally be derived from Equation 6.12 as follows;

$$V_t = (V_c + V_s)\left(1 + \frac{V_f}{V_c + V_s}\right) \quad (6.13)$$

For DE FRP-strengthened beams with low existing steel shear reinforcement ratios (i.e., 0.1%), the concrete contribution can be ignored, and hence Equation 6.14 can give the overall shear force capacity.

$$V_t = V_s + V_f \quad (6.14)$$

Similar to Equation 6.12, Equation 6.14 can be re-written as follows;

$$\frac{V_t}{V_s} = \frac{V_s + V_f}{V_s} \quad (6.15)$$

After the derivation of Equation 6.15, Equation 6.16 can be obtained as follows;

$$V_t = (V_s)\left(1 + \frac{V_f}{V_s}\right) \quad (6.16)$$

The contributions of the concrete (V_c) and/or steel (V_s) can be calculated based on codes of practice (e.g., ACI 318-14 (2014), EN 1992-1-1 (2004)) (Mofidi and Chaallal, 2011; Perera and Ruiz, 2012; TR55, 2012). Equations to calculate the shear resistance ratios (V_f/V_s) and (V_f/V_{s+V_c}) are given in the following section.

6.3.2.2. Proposed shear design equations for beams with low existing steel shear reinforcement ratios

Figure 6.6 may be re-drawn to present the relation between V_f/V_s (FRP-to-steel shear resistance ratio) and $E_{s,\rho_s}/E_{f,\rho_f}$. As shown in Figure 6.8, FRP-to-steel shear resistance ratio is in inverse proportion to steel-to-FRP shear reinforcement ratio ($R^2 = 0.98$).

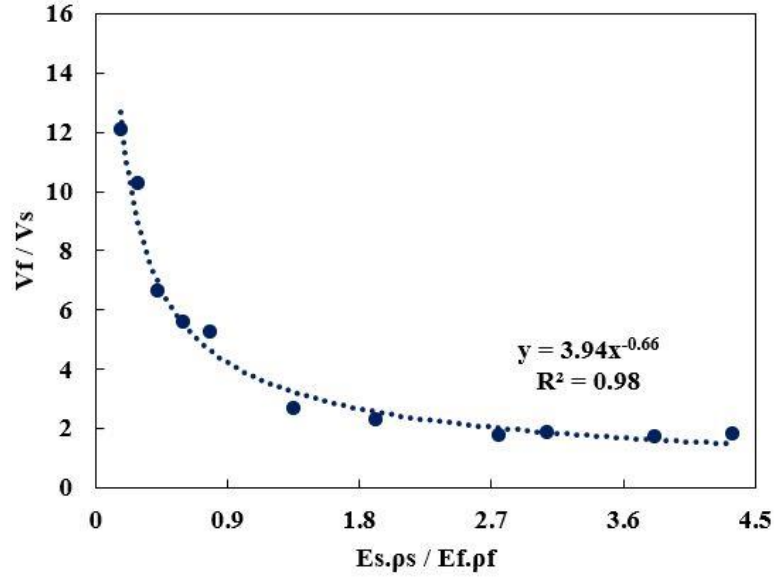


Figure 6.8. FRP-to-steel shear resistance ratio vs. steel-to-FRP shear reinforcement ratio for DE FRP-strengthened beams with low existing steel shear reinforcement ratios

The relation between V_f/V_s and $E_s \cdot \rho_s / E_f \cdot \rho_f$ can be modelled as follows;

$$\frac{V_f}{V_s} = 3.94 * (E_s \cdot \rho_s / E_f \cdot \rho_f)^{-0.66} \quad (6.17)$$

By substituting Equation 6.17 into Equation 6.16, the total shear force capacity for DE FRP strengthened RC slender beams with low existing steel shear reinforcement ratios can be calculated as follows;

$$V_t = (V_s)(1 + (3.94 * (E_s \cdot \rho_s / E_f \cdot \rho_f)^{-0.66})) \quad (6.18)$$

The total shear force capacity can finally be written by substituting Equation 6.2 into Equation 6.18 as follows;

$$V_t = (0.78 \frac{A_{sw}}{s} df_y \cot \theta) (1 + (3.94 * (E_s \cdot \rho_s / E_f \cdot \rho_f)^{-0.66})) \quad (6.19)$$

where the inclination angle (θ) of the shear crack is 21.8° . It is worth noting that when the concrete strut capacity ($V_{Rd,max}$) with $\cot \theta$ equal to 2.5 is higher than the design shear stress (V_{Ed}), it is not required to determine θ , as recommended by EN 1992-1-1 (2004).

6.3.2.3. Proposed shear design equations for beams with high existing steel shear reinforcement ratios

Figure 6.9 may be redrawn from Figure 6.7 to present the variation of $V_f / (V_c + V_f)$ with steel-to-FRP shear reinforcement ratio. As can be seen in Figure 6.9, $V_f / (V_c + V_f)$ is also inversely proportional to steel-to-FRP shear reinforcement ratio ($R^2 = 0.95$).

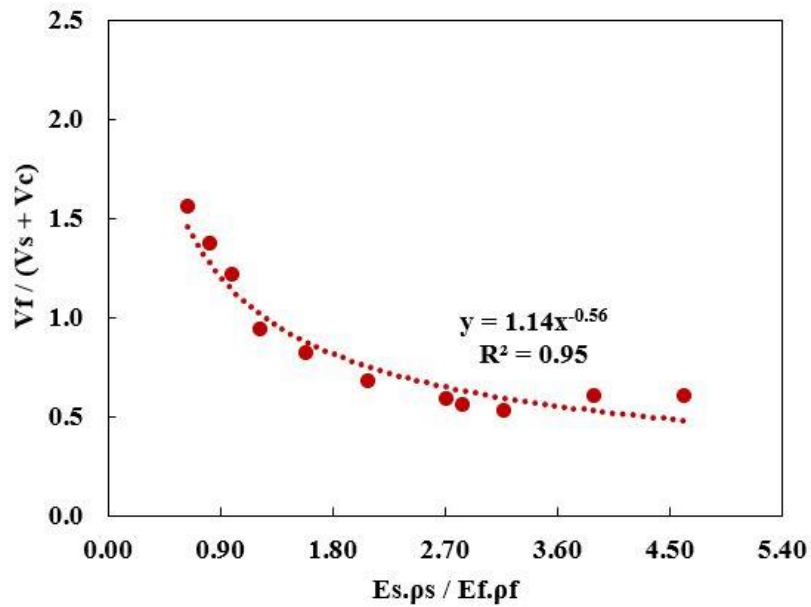


Figure 6.9. $V_f / (V_c + V_f)$ vs. steel-to-FRP shear reinforcement ratio for DE FRP-strengthened beams with high existing steel shear reinforcement ratios

The relation between $V_f / (V_c + V_f)$ and $E_s \cdot \rho_s / E_f \cdot \rho_f$ can be defined as follows;

$$\frac{V_f}{V_s + V_c} = 1.14 * (E_s \cdot \rho_s / E_f \cdot \rho_f)^{-0.56} \quad (6.20)$$

The total shear force capacity for DE FRP strengthened RC beams with high existing steel shear reinforcement ratios may be calculated by substituting Equation 6.21 into Equation 6.13 as follows;

$$V_t = (V_c + V_s) \left(1 + \left(1.14 * \left(E_s \cdot \frac{\rho_s}{E_f} \cdot \rho_f \right)^{-0.56} \right) \right) \quad (6.21)$$

V_c and V_s may be calculated based on the recommendations of ACI 318 (2014) and the total shear force capacity is given as follows;

$$V_t = \left(0.17 \sqrt{f_c} b_w d + \frac{A_{sw}}{s} d f_y \cot \theta \right) \left(1 + \left(1.14 * (E_s \cdot \rho_s / E_f \cdot \rho_f)^{-0.56} \right) \right) \quad (6.22)$$

where the inclination angle (θ) of the shear crack is 45° .

6.3.3. Comparison between existing and proposed design models

A database involving 15 DE FRP shear-strengthened RC beams with low existing steel shear reinforcement ratios is reported in Table 6.2. All considered RC beams failed in shear. The

given steel contribution was calculated according to Equation 6.2 and the total shear force capacity consisted of the sum of the steel and DE FRP contributions.

The comparison between the proposed and existing design models in terms of predicted total shear force capacity ($V_{t, \text{Eq.6.19}}$, $V_{t, \text{TR55}}$, $V_{t, \text{Raicic (2019)}}$ and $V_{t, \text{Mofidi et al. (2012a)}}$) is presented in Table 6.3. The mean value of the predicted-to-experimental shear force capacity was used to measure the accuracy of the models. The most accurate shear design model for DE FRP-strengthened RC beams is the model proposed in this study (Equation 6.19). The mean value and standard deviation of the proposed model were 1.10 and 0.37, respectively. The remaining three models proposed by TR55 (2012), Raicic (2019) and Mofidi et al. (2012a) significantly underestimated the total shear force capacity. The mean values of $V_{t, \text{TR55}} / V_{t, \text{exp}}$, $V_{t, \text{Raicic (2019)}} / V_{t, \text{exp}}$ and $V_{t, \text{Mofidi et al. (2012a)}} / V_{t, \text{exp}}$ are 0.41, 0.48, and 0.36, respectively, with a standard deviation of 0.08. Of note is that Equation 6.19 overestimated the shear force capacity of tested beams tested by Breveglieri et al. (2015), while the shear force capacity of the tested beams by Bui et al. (2020a) was underestimated by the proposed model. The overestimation of the beams tested by Breveglieri et al. (2015) can be attributable to the failure modes of beams. Breveglieri et al. (2015) stated that the DE FRP shear strengthening system failed due to debonding of CFRP bars and no deterioration at the flange of the beams was observed. The underestimation of the beams tested by Bui et al. (2020a) can be explained by the relatively low yield strength of steel shear links (i.e., 240 MPa). Bui (2018) stated that the yield strength of the steel shear links was determined in accordance with the recommendation of Thai Industrial Standards Institute (TIS 24-2548, 2003).

Table 6.4 shows a database of ten DE FRP shear-strengthened RC beams with high existing steel shear reinforcement ratios. All considered beams in the database failed in shear. The steel and concrete contributions were calculated based on the recommendations of ACI 318 (2104) for the design models proposed in this study and the design model proposed by

Mofidi et al. (2012a). The steel contribution was calculated based on Equation 6.2, assuming a shear crack inclination angle of 45 degrees, for the design models proposed by TR55 and Raicic (2019). As recommended by these two design models, the concrete contribution was ignored.

Table 6.5 compares the total shear force capacity calculated by the proposed design model (V_t , Eq. 6.22) and the existing design models in the literature (V_t , TR55, V_t , Raicic (2019) and V_t , Mofidi et al. (2012a)) with experimental results. The predictions of the design models proposed by TR55 (2012), Raicic (2019) and Mofidi et. al (2012a) significantly underestimated the total shear force capacity with a mean predicted-to-experimental ratio of 0.38, 0.35 and 0.58 and a standard deviation of 0.11, 0.05 and 0.13, respectively. The model proposed by Raicic (2019) could not be employed to calculate the shear force capacity of S1-12d260s. This can be attributable to the high strain values in CFRP bars which resulted in an increase of $l_{b, \max}$. The design model proposed in this study (Equation 6.22) accurately predicted the total shear force capacity of DE FRP shear-strengthened RC beams with high existing steel shear reinforcement ratios. Equation 6.22 predicted the total shear force capacity with a mean value of 0.87, and a standard deviation of 0.23. The proposed model underestimated the shear force capacity of the tested beams by Bui et al. (2020a). This can also be attributable to the relatively low yield strength of steel shear links.

One reason for the conservative predictions of TR55 design model is that it takes the effective strain in the DE FRP bars as 0.004 mm/mm. However, the experimentally measured strain values in the DE FRP bars intersected by the main shear cracks ranged from 0.005 to 0.015 mm/mm. Although Raicic (2019) improved the predictions of TR55 by proposing effective strain values, TR55 assumes a fixed value for average bond stress, whereas Caro et al. (2017) demonstrated that it depends on many variables (e.g., concrete strength, DE FRP bar diameter and elastic modulus, adhesive type, and embedded length).

A further shortcoming of the TR55 design model is that it does not consider the effect of steel-to-FRP shear reinforcement ratio. As previously mentioned, Raicic (2019) only modified the effective strain value proposed by TR55 (2012).

One of the reasons for the conservative predictions of the model proposed by Mofidi et al. (2012) can also be that the effective strain in the DE FRP bars is limited by 0.004 mm/mm. It also assumes relatively low bond-slip parameters (i.e., 8.4 MPa and 0.08 mm for sand-coated FRP bars). The interaction between existing steel shear links and DE FRP bars is considered in this model. However, the consideration of this interaction is limited by a coefficient equal to either 0.6 or 1.

It is worth noting that the proposed equations give significantly improved predictions. The main reason for this is that the proposed equations consider the interaction between existing steel shear links and DE FRP bars. However, these equations are based on the numerical analysis. It is acknowledged that the proposed equations are valid in the case where the failure mode of tested beams was not governed by bond failure. Further experimental tests are needed to confirm the accuracy of the proposed equations.

6.4. Summary and conclusions

This chapter presents results of FE investigations on the structural behaviour of RC T-beams strengthened in shear with embedded FRP bars. Moreover, it provides insight into the influence of beam size, steel-to-FRP shear reinforcement ratio, tension reinforcement ratio and a/d ratio on the structural behaviour of DE-FRP-strengthened beams. Furthermore, this chapter evaluates the accuracy of existing design models for DE FRP shear-strengthened RC beams and proposes new design models. Based on the numerical results, the following conclusions are drawn:

- With increasing the effective depth from 300 to 600 mm, the overall decrease in shear stress at failure for unstrengthened and strengthened beams was 45.6 and 28.6%, respectively. These results revealed that embedded FRP bars could mitigate the size effect.
- The tension reinforcement ratio had a clear effect on failure mode. Similar to the experimental results, FE modelled strengthened beams with a tension reinforcement ratio equal to or less than 2.0% failed in flexure whereas FE modelled strengthened beams with higher tension reinforcement ratios failed in shear. However, the tension reinforcement ratio did not influence the gain due to FRP bars.
- An increment in the a/d ratio from 1.9 to 3 instigated a reduction of 23.8% in the unstrengthened shear force capacity. The corresponding reductions for DE GFRP and CFRP-strengthened beams were 16.8 and 22.4%, respectively. When the a/d ratio was increased from 1.9 to 2.5, the percentage shear force gain due to DE CFRP bars decreased from 25.3% to 15.9%. This was followed by an increase in the percentage shear force gain from 15.9% to 27.6%, with an increase in the a/d ratio from 2.5 to 3. Similar to DE CFRP bars, the percentage shear force gain due to GFRP bars decreased from 9.9% to 0.5% once the a/d ratio was increased from 1.9 to 2.5. This was also followed by an increase in percentage shear force gain from 0.5% to 19.9% when the a/d ratio was increased from 2.5 to 3.
- Similar to experimental results, the contribution of DE FRP reinforcement to the shear resistance was observed to be inversely proportional to steel-to-FRP shear reinforcement ratio. DE FRP bars should be designed in such a way that the steel-to-FRP shear reinforcement ratio is less than 2.70 in order to exploit DE FRP shear strengthening systems.

- Existing design models proposed by TR55 (2012), Raicic (2019) and Mofidi et al. (2012a) significantly underestimates the total shear force capacity of DE FRP-strengthened beams. The proposed design equations in this study offer improved predictions compared with existing design models.

Table 6.2. Details of DE FRP shear-strengthened RC beams with low existing steel shear reinforcement ratios

RC Beam	Reference	b _w (mm)	d (mm)	h (mm)	a/d	d _s (mm)	s (mm)	f _y (MPa)	E _s (GPa)	ρ _s (%)	FRP material	d _f (mm)	s _f (mm)	α°	E _f (GPa)	ρ _f (%)	E _s ·ρ _s / E _f ·ρ _f	V _s (kN)
2S-C180-90	Breveglieri et al. (2015)	180	360	400	2.5	6	300	574	200	0.105	Carbon	8	180	90	160	0.155	0.84	76
2S-C180-45	Breveglieri et al. (2015)	180	360	400	2.5	6	300	574	200	0.105	Carbon	8	180	45	160	0.219	0.60	76
S/3.0	Dirar and Theofanous (2017)	150	600	650	3	8	600	540	200	0.112	Glass	12	300	90	40	0.251	2.22	105.9
S/2.0/G3.82	This study	75	300	325	3	4	300	540	200	0.112	Glass	6	300	90	46	0.126	3.86	26.5
S/2.7/G3.82	This study	75	300	325	3	4	300	540	200	0.112	Glass	6	300	90	46	0.126	3.86	26.5
S/2.7/G1.91	This study	75	300	325	3	4	300	540	200	0.112	Glass	6	150	90	46	0.251	1.93	26.5
S/2.7/C1.35	This study	75	300	325	3	4	300	540	200	0.112	Carbon	6	300	90	130	0.126	1.37	26.5
C150	Raicic (2019)	150	320	350	3	4	150	660	200	0.112	Carbon	6	150	90	124	0.126	1.43	69
G150	Raicic (2019)	150	320	350	3	4	150	660	200	0.112	Glass	6	150	90	46	0.126	3.86	69
C150 ∠	Raicic (2019)	150	320	350	3	4	150	660	200	0.112	Carbon	6	150	45	124	0.177	1.02	69
G150 ∠	Raicic (2019)	150	320	350	3	4	150	660	200	0.112	Glass	6	150	45	46	0.177	2.74	69
B1-2Sd6-5ETS FRP d10(90)	Bui et. al (2020a)	180	360	400	2.5	6	300	240	200	0.105	Glass	10	180	90	50	0.242	1.73	31.8
B2-2Sd6-5ETS FRP d10(45)	Bui et. al (2020a)	180	360	400	2.5	6	300	240	200	0.105	Glass	10	180	45	50	0.342	1.23	31.8
MBDE	Brindley (2018)	225	450	540	3.5	6	270	434	217	0.10	Carbon	2*10	270	90	124	0.259	0.68	79.8
LBDE	Brindley (2018)	300	600	720	3.5	8	360	336	210	0.10	Carbon	2*12	360	90	124	0.209	0.81	109.8

Table 6.3. Comparison between existing and proposed design models for DE FRP shear-strengthened RC beams with low existing steel shear reinforcement ratios

RC Beam	Reference	$V_{t, \text{exp}}$ (kN)	$V_{t, \text{Eq.6.19}}$ (kN)	$V_{t, \text{TR55}}$ (kN)	$V_{t, \text{Raicic (2019)}}$ (kN)	$V_{t, \text{Mofidi et al. (2012a)}}$ (kN)	$V_{t, \text{Eq.6.19}} / V_{t, \text{exp}}$	$V_{t, \text{TR55}} / V_{t, \text{exp}}$	$V_{t, \text{Raicic (2019)}} / V_{t, \text{exp}}$	$V_{t, \text{Mofidi et al. (2012a)}} / V_{t, \text{exp}}$
2S-C180-90	Breveglieri et al. (2015)	222.3	410.7	116.9	107.6	104.4	1.85	0.53	0.48	0.47
2S-C180-45	Breveglieri et al. (2015)	320.8	495.9	146.3	158.9	116.1	1.55	0.46	0.50	0.36
S/3.0	Dirar and Theofanous (2017)	293	352.1	141.2	179.7	132	1.20	0.48	0.61	0.45
S/2.0/G3.82	This study	68.7	69.2	31.5	36.6	31.1	1.01	0.46	0.53	0.45
S/2.7/G3.82	This study	68.7	69.2	31.5	36.6	31.1	1.01	0.46	0.53	0.45
S/2.7/G1.91	This study	90.5	94	36.5	46.7	35.8	1.04	0.40	0.52	0.40
S/2.7/C1.35	This study	103.6	111.3	37.3	38.7	34.8	1.07	0.36	0.37	0.34
C150	Raicic (2019)	209	283.3	92.5	97.9	79.4	1.36	0.44	0.47	0.38
G150	Raicic (2019)	200	180.4	79.9	91.4	75	0.90	0.40	0.46	0.37
C150 \angle	Raicic (2019)	222	337.9	105.9	121.3	83.7	1.52	0.48	0.55	0.38
G150 \angle	Raicic (2019)	193	208.8	84.8	103.8	77.5	1.08	0.44	0.54	0.40
B1-2Sd6-5ETS FRP d10(90)	Bui et. al (2020a)	272.3	119	60.8	82.7	54	0.44	0.22	0.30	0.20
B2-2Sd6-5ETS FRP d10(45)	Bui et. al (2020a)	288.9	141.2	75.2	118.4	63.2	0.49	0.26	0.41	0.22
MBDE	Brindley (2017)	482	486.4	187.9	206.3	138	1.01	0.39	0.43	0.29
LBDE	Brindley (2017)	605	607.4	272.3	313.1	186.4	1.00	0.45	0.52	0.31
Mean Value							1.10	0.41	0.48	0.36
Standard Deviation							0.37	0.08	0.08	0.08

Table 6.4. Details of DE FRP shear-strengthened RC beams with high existing steel shear reinforcement ratios

RC Beam	Reference	b _w (mm)	d (mm)	h (mm)	a/d	f _c (MPa)	d _s (mm)	s (mm)	f _y (MPa)	E _s (GPa)	ρ _s (%)	FRP material	d _f (mm)	s _f (mm)	α°	E _f (GPa)	ρ _f (%)	E _s ρ _s / E _f ρ _f	V _s (kN)	V _c (kN)	V _s , Eq.6.2 (kN)
S1-9d260s	Mofidi et al. (2012a)	152	350	406	3	29.6	8	175	540	200	0.378	Carbon	9.5	260	90	148	0.179	2.85	108.6	49.2	84.7
S1-12d260s	Mofidi et al. (2012a)	152	350	406	3	29.6	8	175	540	200	0.378	Carbon	12.7	260	90	148	0.321	1.59	108.6	49.2	84.7
S1-9d260p	Mofidi et al. (2012a)	152	350	406	3	29.6	8	175	540	200	0.378	Carbon	9.5	260	90	155	0.179	2.72	108.6	49.2	84.7
4S-C180-90	Breveglieri et al. (2015)	180	360	400	2.5	32.3	6	180	574	200	0.175	Carbon	8	180	90	160	0.155	1.41	64.9	62.6	50.6
4S-C180-45	Breveglieri et al. (2015)	180	360	400	2.5	32.3	6	180	574	200	0.175	Carbon	8	180	45	160	0.219	1.00	64.9	62.6	50.6
R00	Qin et al. (2015)	125	295	360	3.05	17.4	8	275	542	186	0.292	Carbon	10	275	90	124	0.228	1.92	58.5	26.1	45.6
R07	Qin et al. (2015)	125	295	360	3.05	29.6	7.7	275	522	186	0.271	Carbon	10	275	90	124	0.228	1.78	52.2	34.1	40.7
R12	Qin et al. (2014)	125	295	360	3.05	29.6	7.5	275	510	186	0.257	Carbon	10	275	90	124	0.228	1.69	48.3	34.1	37.7
B3-2Sd9-5ETS FRP d10(90)	Bui et. al (2020a)	180	360	400	2.5	38	9	300	240	200	0.236	Glass	10	180	90	50	0.242	3.89	36.6	67.9	28.6
B4-2Sd9-5ETS FRP d10(45)	Bui et. al (2020a)	180	360	400	2.5	38	9	300	240	200	0.236	Glass	10	180	45	50	0.342	2.76	36.6	67.9	28.6

Table 6.5. Comparison between existing and proposed design models for DE FRP shear-strengthened RC beams with high existing steel shear reinforcement ratios

RC Beam	Reference	$V_{t, exp}$ (kN)	$V_{t, Eq.6.22}$ (kN)	$V_{t, TR55}$ (kN)	$V_{t, Raicic (2019)}$ (kN)	$V_{t, Mofidi et al. (2012a)}$ (kN)	$V_{t, Eq.6.22} / V_{t, exp}$	$V_{t, TR55} / V_{t, exp}$	$V_{t, Raicic (2019)} / V_{t, exp}$	$V_{t, Mofidi et al. (2012a)} / V_{t, exp}$
S1-9d260s	Mofidi et al. (2012a)	260.3	257.9	120	106.7	172.1	0.99	0.46	0.41	0.66
S1-12d260s	Mofidi et al. (2012a)	266.6	296.3	129.5	N/A*	179.9	1.11	0.49	N/A*	0.67
S1-9d260p	Mofidi et al. (2012a)	280.7	260.5	120.1	103.1	189.7	0.93	0.43	0.37	0.68
4S-C180-90	Breveglieri et al. (2015)	226.1	247.6	91.6	82.3	144.6	1.10	0.41	0.36	0.64
4S-C180-45	Breveglieri et al. (2015)	370.1	273.1	120.9	133.6	151.6	0.74	0.33	0.36	0.41
R00	Qin et al. (2015)	142	151.5	73.2	63.1	103.4	1.07	0.52	0.44	0.73
R07	Qin et al. (2015)	182	157.5	68.3	58.2	105	0.87	0.38	0.32	0.58
R12	Qin et al. (2015)	164	152.6	65.3	55.2	101.2	0.93	0.40	0.34	0.62
B3-2Sd9-5ETS FRP d10(90)	Bui et. al (2020a)	309.1	160.3	57.7	79.5	126.8	0.52	0.19	0.26	0.41
B4-2Sd9-5ETS FRP d10(45)	Bui et. al (2020a)	353.9	172.1	72	115.3	135.9	0.49	0.20	0.33	0.38
Mean Value							0.87	0.38	0.35	0.58
Standard Deviation							0.23	0.11	0.05	0.13

CHAPTER 7: CONCLUSIONS AND RECOMMENDATIONS

7.1. General

The fifteen RC T-beams that comprised the experimental programme were designed, fabricated, and tested at the University of Birmingham Structural Engineering Laboratory. The test parameters were steel-to-FRP shear reinforcement ratio, embedded length of FRP bars, presence of existing holes, a/d ratio, and tension reinforcement ratio. The effect of beam size on the behaviour of DE FRP-strengthened RC T-beams was also investigated. A two-dimensional nonlinear FE model was developed using VecTor2 software package and validated against test results. The beams tested by Modifi et al. (2012a) and Jemaa et al. (2015) were also included in this thesis to verify the FE model. Based on the good correlation between experimental and numerical results in terms of predicting ultimate shear force capacity, a FE parametric study was conducted to explore the impacts of beam size, steel-to-FRP shear reinforcement ratio, tension reinforcement ratio, and a/d ratio. Moreover, it was demonstrated that current shear strengthening design guidance and design models in the published literature significantly underestimated the overall shear force capacity of strengthened beams with embedded FRP bars. New design models were, therefore, proposed and demonstrated to give accurate predictions. This chapter aims to briefly present findings from experimental and numerical research. The main findings obtained from experimental results and FE simulations are presented in Section 7.2. Recommendations in support of future work are addressed in Section 7.3.

7.2. Conclusions

The following conclusions are derived from the experimental findings:

1. The behaviour of RC beams strengthened in shear with DE FRP bars was governed by the interaction between existing steel shear links and DE FRP bars. The total shear force capacity of strengthened slender beams decreased by up to 33.7% with increasing steel-to-FRP shear reinforcement ratio from 1.35 to 3.82. The DE FRP and concrete contributions to the shear resistance of slender beams also decreased by up to 39.2% and 62.8%, respectively, when steel-to-FRP shear reinforcement ratio was increased from 1.35 to 3.82. Thus, calculating the DE FRP shear resistance as the difference between strengthened and unstrengthened shear force capacities can lead to erroneous results. Moreover, the total shear capacity of the strengthened deep beam decreased by about 15% with increasing steel-to-FRP shear reinforcement ratio from 1.37 to 3.86. The DE FRP contribution to the shear resistance of the strengthened deep beam also diminished by about 69.5% once steel-to-FRP shear reinforcement ratio was increased, whereas the concrete contribution to the shear resistance of the strengthened deep beam was almost constant.
2. The failure mode was clearly affected by the tension reinforcement ratio. The DE FRP-strengthened beams with a tension reinforcement ratio of 2.0% failed in flexure whereas corresponding strengthened beams with 2.7% tension reinforcement ratio failed in shear. However, the strength enhancement due to FRP bars was not affected by the tension reinforcement ratio.
3. The effect of beam size on DE FRP-strengthened beams was clearly observed. The size effect was significantly mitigated by embedded FRP bars. The reduction in shear stress at failure for the unstrengthened slender beams was 50%, whereas the

reduction in shear stress at failure for DE FRP-strengthened slender beams was 18%.

The corresponding values for deep beams were 26% and 10%, respectively.

4. The a/d ratio played an important role in governing the behaviour of strengthened beams. The total shear force capacity of the DE CFRP-strengthened beam increased by 30% when the a/d ratio was decreased from 3 to 1.9. The corresponding increase for the DE GFRP-strengthened beam was about either 26% or 66%. The contribution of DE FRP bars to the shear resistance decreased with a reduction in the a/d ratio, whereas the contribution of concrete to the shear resistance increased with decreasing the a/d ratio. The contribution of DE CFRP bars decreased by about 21% with the decrease in the a/d ratio. The corresponding reduction for DE GFRP bars was about either 81% or 60%.
5. Existing holes instigated premature shear failure in RC T-beams prior to reaching their nominal shear force capacity. The shear strength reduction due to existing holes ranged from 7 to 22%.
6. The embedded length of FRP bars had a clear impact on the DE FRP-strengthened behaviour. Both the shear strength enhancement obtained from embedded FRP bars and shear force capacity increased by up to 197.8% and 91.1%, respectively, with increasing embedded length from 262.5 to 300 mm.

Based on the numerical simulations, the following conclusions are drawn:

1. An increasing effective beam depth instigated a decrease in shear stress at failure for control and DE FRP-strengthened beams. The reductions were 45.6% and 28.6%, respectively. The FE-predicted results also showed that embedded FRP bars mitigated size effect.

2. FE modelled strengthened beams with a tension reinforcement ratio equal to or less than 2.0% failed in flexure whereas FE modelled strengthened beams with higher tension reinforcement ratios failed in shear. However, the tension reinforcement ratio did not impact the shear strength enhancement due to FRP bars.
3. An increment in a/d ratio from 1.9 to 3 resulted in a decrease the shear force capacity of the control beam by 23.8%. The corresponding reductions in shear force capacity of DE GFRP and CFRP-strengthened beams were 16.8% and 22.4%, respectively. The percentage shear force gain due to DE FRP bars decreased by up to 0.5% with an increase in the a/d ratio from 1.9 to 2.5. This was followed by an increase of up to 27.6% in the percentage shear force gain with a further increase in the a/d ratio from 2.5 to 3.
4. The shear resistance gain achieved by embedded FRP bars was inversely correlated with steel-to-FRP shear reinforcement ratio. DE FRP bars should be designed in such a way that the steel-to-FRP shear reinforcement ratio is less than 2.70 in order to exploit the DE FRP shear strengthening system.
5. Existing design models significantly underestimated the shear force capacity of strengthened beams. Design equations proposed in this study offer improved predictions compared with existing design models.

7.3. Recommendations in support of future work

This PhD research experimentally and numerically examined the DE FRP-strengthened behaviour of RC beams with a focus on information gaps in the current literature. However, it would be useful for future studies to focus on the following issues to gain a deeper understanding of DE FRP-strengthened behaviour.

- Further experimental tests are necessary to examine structural behaviour of large-scale RC beams strengthened with embedded FRP bars.
- Further experimental tests are also essential to explore how the a/d ratio influences the strengthened behaviour. Thus, the number of experimental tests for strengthened deep beams with embedded FRP bars can be increased, and design models can be proposed for the strengthened deep beams.
- Shear strengthening of existing RC beams with DE FRP bars has great potential to eliminate the shortcomings of external shear strengthening techniques. The prestressed FRP bars can be considered to improve the effectiveness of DE FRP shear strengthening technique.
- The design equations were proposed to present improved predictions for DE FRP-strengthened slender RC beams. Nevertheless, further experimental research is essential to measure the accuracy of equations by expanding the database of strengthened slender beams.
- The behaviour of DE strengthened RC beams under monotonic loading was investigated. However, the long-term behaviour (i.e., under fatigue loading) of DE FRP-strengthened beams has not yet been investigated. Therefore, further experimental research is essential to investigate the performance of the DE technique under cyclic loading.
- Shear-strengthened continuous beams with DE FRP bars have received little experimental attention. Further experimental studies should be carried out to examine the strengthened behaviour of continuous slender and deep beams.

REFERENCES

Abbood, I.S., Odaa, S.A., Hasan, K.F. and Jasim, M.A. (2021) Properties Evaluation of Fiber Reinforced Polymers and Their Constituent Materials Used in Structures – A Review. *Materials Today: Proceedings*, 43 (2): 1003-1008.

ACI Committee 318 (2014) *Building Code Requirements for Structural Concrete (ACI 318-14) and Commentary (ACI 318R-14)*. American Concrete Institute, Farmington Hills, USA.

ACI Committee 426 on Shear and Diagonal Tension (1973) The Shear Strength of Reinforced Concrete Members. *Journal of the Structural Division*, 99(6): 1091-1187.

ACI Committee 440 (2017) *Guide for the Design and Construction of Externally Bonded FRP Systems for Strengthening Concrete Structures*. ACI 440.2R-17, American Concrete Institute, Farmington Hills, USA.

ACI Committee 445 on Shear and Torsion (1998) Recent Approaches to Shear Design of Structural Concrete. *Journal of Structural Engineering*, 124(12): 1375-1417.

Amaechi, C.V., Agbomerie, C.O., Orok, E.O. and Ye, J. (2020) Economic Aspects of Fiber Reinforced Polymer Composite Recycling. In *Encyclopedia of Renewable and Sustainable Materials*, Elsevier BV: Oxford, UK.

BA 44/96 (1996) *The Assessment of Concrete Highway Bridges and Structures*. The Highways Agency, UK.

Bažant, Z. P. (1997) Fracturing Truss Model: Size Effect in Shear Failure of Reinforced Concrete. *Journal of Engineering Mechanics*, 123 (12): 1276-1288.

Bažant Z.P. and Oh B.H. (1983) Crack band theory for fracture of concrete. *Matériaux et Constructions*, 16(3): 155-177.

Bažant Z.P. and Kim J.K. (1984) Size Effect in Shear Failure of Longitudinally Reinforced Beams. *ACI Journal Proceedings*, 81 (5): 456-468.

Benzeguir, Z.E.A., El-Saikaly, G. and Chaallal, O. (2019) Size Effect in RC T-Beams Strengthened in Shear with Externally Bonded CFRP Sheets: Experimental Study. *ASCE Journal of Composites for Construction*, 23(6): 04019048.

Belarbi, A., Bae, S.W. and Brancaccio, A. (2012) Behavior of Full-scale RC T-beams Strengthened in Shear with Externally Bonded FRP Sheets. *Construction and Building Materials*, 32: 27–40.

Bentz, E.C. (2005) Explaining the Riddle of Tension Stiffening Models for Shear Panel Experiments. *ASCE Journal of Structural Engineering*, 131(9): 1422–1425.

Bentz, E.C., Vecchio F.J. and Collins M.P. (2006) The Simplified MCFT for Calculating the Shear Strength of Reinforced Concrete Elements, *ACI Structural Journal*, 103(4): 614–624

Bhanugoban, M., Yapa, H.D. and Dirar, S. (2021) Efficient Shear Retrofitting of Reinforced Concrete Beams using Prestressed Deep Embedded Bars. *Engineering Structures*, 246: 113053.

Breveglieri, M., Aprile, A. and Barros, J.A. (2015) Embedded Through-Section Shear Strengthening Technique Using Steel and CFRP Bars in RC beams of Different Percentage of Existing Stirrups. *Composite Structures*, 126: 101-113.

Bircher, D.B., Tuchscherer, R.G., Huizinga, M. and Bayrak O. (2014) Depth Effect in Deep Beams. *ACI Structural Journal*, 111(4): 731-740.

Brindley, M. (2017) Shear Assessment and Strengthening of Reinforced Concrete T-beams with Externally Bonded CFRP Sheets. PhD Thesis, University of Bath.

BS 4449 (2005) Steel for the Reinforcement of Concrete-Weldable Reinforcing Steel-Bar, Coil and Decoiled Product-Specification. British Standards Institution.

BS 8110-1 (1997) Structural Use of Concrete-Part 1: Code of Practice for Design and Construction. British Standard Institution, London.

BS EN 12390-3 (2019) Testing Hardened Concrete-Compressive strength of test specimens. British Standards Institution.

BS EN 1992-1-1. (2004) Eurocode 2: Design of Concrete Structures-Part 1-1: General Rules and Rules for Buildings. British Standards Institution.

Bui, L.V.H. (2018) Mechanical Performances of Concrete Beams with Hybrid Usage of Steel and FRP Reinforcement. PhD Thesis, Chulalongkorn University.

Bui, L.V.H., Stitmannathum, B. and Ueda, T. (2020a) Experimental Investigation of Concrete Beams Strengthened with Embedded Through-Section Steel and FRP Bars. *ASCE Journal of Composites for Construction*, 24 (5): 04020052.

Bui, L.V.H., Stitmannathum, B. and Ueda, T. (2020b) Simulation of Concrete Beams Strengthened by Embedded Through-section Steel and GFRP Bars with Newly Developed Bond Model. *Journal of Advanced Concrete Technology*, 18(7): 364-385.

Byars, E.A., Waldron, P., Dejke, V., Demis, S. and Heddadin, S. (2003) Durability of FRP in Concrete-Deterioration Mechanisms. *International Journal of Materials and Product Technology*, 19 (1-2): 28-39.

Caro, M., Jemaa, Y., Dirar, S. and Quinn, A. (2017) Bond Performance of Deep Embedment FRP Bars Epoxy Bonded into Concrete. *Engineering Structures*, 147: 448-457.

Caro, M. (2018) Shear Strengthening of Concrete Beams with Embedded FRP Bars. PhD Thesis, University of Birmingham.

Caro, M., Dirar, S., Quinn, A. and Yapa, H. (2021) Shear Strengthening of Existing Reinforced Concrete Beams with Embedded Bars-An Overview. *Proceedings of the Institution of Civil Engineers - Structures and Buildings*, doi.org/10.1680/jstbu.20.00169.

CEB-FIP (1993) CEB-FIP Model Code 1990. Thomas Telford Services Ltd., London.

Concrete Society (2009) Historical Approaches to the Design of Concrete Buildings and Structures. Technical Report No. 70, Crowthorne, UK.

Concrete Society (2012) Design Guidance for Strengthening Concrete Structures using Fibre Composite Materials. Technical report TR55, Camberley, UK.

Chaallal, O., Mofidi, A., Benmokrane, B. and Neale, K. (2011) Embedded Through-Section FRP Rod Method for Shear Strengthening of RC Beams: Performance and Comparison with Existing Techniques. *ASCE Journal of Composites for Construction*, 15 (3): 374-383.

Collins, M.P. (1978) Towards a Rational Theory for RC Members in Shear. *Journal of the Structural Division, ASCE*, 104(ST4): 649-66.

Collins, M.P., and Kuchma, D.A. (1999) How Safe Are Our Large, Lightly Reinforced Concrete Beams, Slabs, and Footings? *ACI Structural Journal*, 96(4): 482-490.

Cosenza, E., Manfredi, G. and Realfonzo, R. (2002). Development Length of FRP Straight Rebars. *Composites Part B: Engineering*, 33(7): 493-504.

CSA A23.3 (2019) Design of Concrete Structures. Canadian Standards Association, Canada.

D'Ambrisi, A., Feo, L. and Focacci, F. (2013) Experimental Analysis on Bond between PBO-FRCM Strengthening Materials and Concrete. *Composites Part B: Engineering*, 44 (1): 524-532.

De Lorenzis, L. and Nanni, A. (2001) Shear Strengthening of Reinforced Concrete Beams with Near-surface Mounted Fiber-reinforced Polymer Rods. *Structural Journal*, 98(1): 60-68.

De Lorenzis, L. and Teng, J.G. (2007) Near-surface Mounted FRP Reinforcement: An Emerging Technique for Strengthening Structures, *Composites Part B: Engineering*, 38(2): 119-143.

Diab, H.M. and Sayed, A.M. (2020) An Anchorage Technique for Shear Strengthening of RC T-Beams Using NSM-BFRP Bars and BFRP Sheet. *International Journal of Concrete Structures and Materials*, 14:49.

Dias, S.J.E. and Barros, J.A.O. (2008) Shear Strengthening of T-cross Section Reinforced Concrete Beams by Near-surface Mounted Technique. *ASCE Journal of Composites for Construction*, 12(3): 300–311.

Dias, S.J.E. and Barros, J.A.O. (2012) NSM Shear-strengthening Technique with CFRP Laminates Applied in High-strength Concrete Beams with or without Pre-cracking. *Composites Part B: Engineering*, 43(2): 290–301.

Dias, S.J.E. and Barros, J.A.O. (2013) Shear Strengthening of RC Beams with NSM CFRP Laminates: Experimental Research and Analytical Formulation. *Composite Structures*, 99: 477-490.

Dirar, S., Lees, J. and Morley, C. (2012) Precracked Reinforced Concrete T-beams Repaired in Shear with Bonded Carbon Fiber-reinforced Polymer Sheets. *ACI Structural Journal*, 109(2): 215-224.

Dirar, S., Lees, J.M. and Morley, C.T. (2013a) Precracked RC T-beams Repaired in Shear with Prestressed CFRP Straps. *ACI Structural Journal*, 110(5): 855-866.

Dirar S, Lees, J.M. and Morley, C.T. (2013b) Phased nonlinear finite-element analysis of precracked RC T-beams repaired in shear with CFRP sheets. *ASCE Journal of Composites for Construction*, 17(4): 476-487.

Dirar, S. and Theofanous, M. (2017) Large-scale Reinforced Concrete T-beams Strengthened in Shear with Embedded GFRP Bars. In: *Proceedings of the 8th International Conference on Advanced Composites in Construction (ACIC 2017)*, Sheffield, UK, pp.114-119.

Elanchezhian, C., Ramnath, B.V. and Hemalatha J. (2014) Mechanical Behaviour of Glass and Carbon Fibre Reinforced Composites at Varying Strain Rates and Temperatures. *Procedia Materials Science*, 6: 1405-1418.

Emmons, P.H., Vaysburd, A.M. and Thomas, J. (1998) Strengthening Concrete Structures. Part II. *Concrete International*, 20 (3): 56-60.

Fenwick, R.C. (1966) The Shear Strength of Reinforced Concrete Beams. PhD Thesis, University of Canterbury.

Godat, A., Qu, Z., Lu., X.Z., Labossière, P., Ye, L.P. and Neale, K.W. (2010) Size Effects for Reinforced Concrete Beams Strengthened in Shear with CFRP Strips. *ASCE Journal of Composites for Construction*, 14 (3):260–271.

Godat, A., Chaallal, O. and Neale, K.W. (2013) Nonlinear Finite Element Models for the Embedded Through-section FRP Shear-strengthening Method. *Computers & Structures*, 119: 12-22.

Gonzalez-Libreros, J.H., Sneed, L.H., D'Antino, T. and Pellegrino, C. (2017) Behavior of RC Beams Strengthened in Shear with FRP and FRCM Composites. *Engineering Structures*, 150: 830-842.

Hawkins, N.M., Kuchma, D.A., Mast, R.F., Marsh, M.L. and Reineck, K.H. (2005) Simplified Shear Design of Structural Concrete Members Appendixes. NCHRP Web-Only Document 78, Transportation Research Board, The National Academies, Washington.

He, X.G. and Kwan, A.K.H. (2001). Modeling Dowel Action of Reinforcement Bars for Finite Element Analysis of Concrete Structures. *Computers & Structures*, 79 (6): 595-604.

Ianniruberto, U. and Imbimbo, M. (2004) Role of Fiber Reinforced Plastic Sheets in Shear Response of Reinforced Concrete Beams: Experimental and Analytical Results. *ASCE Journal of Composites for Construction*, 8 (5):415–424.

ISIS Canada (2007), Reinforcing Concrete Structures with Fibre Reinforced Polymers. Design Manual No. 3, ISIS Canada Corporation. Canada.

Jemaa, Y., Jones, C. and Dirar, S. (2015) Deep Embedment Strengthening of Full-scale Shear Deficient Reinforced Concrete Beams. In *Proceedings of the 12th International Symposium on Fiber Reinforced Polymers for Reinforced Concrete Structures (FRPRCS-12)*, Nanjing, China, pp. 1-6.

Jeong, C.Y., Kim, H.G., Kim, S.W., Lee, K.S. and Kim, K.H. (2017) Size effect on Shear Strength of Reinforced Concrete Beams with Tension Reinforcement Ratio. *Advances in Structural Engineering*, 20(4):582-594.

JSCE (2002) Standard Specifications for Concrete Structures, Materials and Construction, Japan Society of Civil Engineers.

Kani, G.N.J. (1964) The Riddle of Shear Failure and Its Solution. ACI Journal Proceedings, 61 (4): 441-468.

Kani, G.N.J. (1967) How Safe are Our Large Reinforced Concrete Beams? ACI Journal Proceedings, 64 (3): 128-141.

Kim, H.G., Jeong, C.Y., Kim, M.J., Lee, Y.J. and Park, J.H. and Kim, K.H. Prediction of Shear Strength of Reinforced Concrete Beams without Shear Reinforcement Considering Bond Action of Longitudinal Reinforcements. Advances in Structural Engineering, 21(1):30-45.

Kotsovos, M.D., Bobrowski, J. and Eibl, J. (1987) Behaviour of Reinforced Concrete T-beams in Shear. The Structural Engineer, 65B (1): 1-9.

Krauklis, A.E., Karl, C.W., Gagani, A.I. and Jørgensen, J.K. (2021) Composite Material Recycling Technology-State-of-the-Art and Sustainable Development for the 2020s. Journal of Composites Science, 5 (1), 28.

Kuchma, D.A. and Collins, M. P. (1998) Advances in Understanding Shear Performance of Concrete Structures. Progress in Structural Engineering and Materials, 1(4): 360-369.

Machida, A. (1993) State-of-the-art Report on Continuous Fiber Reinforcing Materials. Society of Civil Engineers (JSCE), Tokyo.

Mitchell, D. and Collins M.P. (1974) Diagonal Compression Field Theory-A Rational Model for Structural Concrete in Pure Torsion. ACI Journal, Proceedings 71(8):396–408.

Mofidi, A. and Chaallal, O. (2011) Shear Strengthening of RC Beams with EB FRP: Influencing Factors and Conceptual Debonding Model. ASCE Journal of Composites for Construction, 15(1): 62-74.

Mofidi, A., Chaallal, O., Benmokrane, B. and Neale, K. (2012a) Experimental Tests and Design Model for RC Beams Strengthened in Shear Using the Embedded Through-section FRP Method. *ASCE Journal of Composites for Construction*, 16 (5): 540-550.

Mofidi, A., Chaallal, O., Benmokrane, B. and Neale, K. (2012b) Performance of End-Anchorage Systems for RC Beams Strengthened in Shear with Epoxy-Bonded FRP. *ASCE Journal of Composites for Construction*, 16 (3): 322-331.

Mofidi, A., Chaallal, O., Cheng, L. and Shao, Y. (2016) Investigation of Near-surface-Mounted Method for Shear Rehabilitation of Reinforced Concrete Beams Using Fiber Reinforced-polymers Composites. *ASCE Journal of Composites for Construction*, 20(2): 04015048.

Mohamed, K., Abdalla, J.A. and Hawileh R.A. (2020) Experimental and Analytical Investigations of the Use of Groove-Epoxy Anchorage System for Shear Strengthening of RC Beams Using CFRP Laminates. *Materials*, 13 (19): 4350.

Mostofinejad, D., Esfahani, M. R., & Shomali, A. (2019). Experimental and Numerical Study of the RC Beams Shear-strengthened with NSM Technique. *Journal of Composite Materials*, 53 (17): 2377–2389.

Mostofinejad, D., Hosseini, S.A. and Razavi, S.B. (2016) Influence of Different bonding and Wrapping Techniques on Performance of Beams Strengthened in Shear using CFRP Reinforcement. *Construction and Building Materials*, 116: 310-320.

Mostofinejad, D. and Tabatabaei Kashani, A. (2013) Experimental Study on Effect of EBR and EBROG Methods on Debonding of FRP Sheets Used for Shear Strengthening of RC Beams. *Composites Part B: Engineering*, 45 (1): 1704-1713.

Mörsch, E. (1909) *Der Eisenbetonbau, seine Theorie und Anwendung (Reinforced Concrete Theory and Application)*, 3rd edition. Verlag Konrad Wittner, Stuttgart.

Park, R. and Paulay, T. (1975) Reinforced Concrete Structures. John Wiley & Sons Inc., Canada.

Perera, R. and Ruiz, A. (2012) Design Equations for Reinforced Concrete Members Strengthened in Shear with External FRP Reinforcement Formulated in An Evolutionary Multi-objective Framework. Composites Part B: Engineering, 43(2): 488-496.

Pešić, N. and Pilakoutas, K. (2003) Concrete Beams with Externally Bonded Flexural FRP-Reinforcement: Analytical Investigation of Debonding Failure. Composites Part B: Engineering, 34 (4): 327-338.

Prince-Lund Engineering, (Access date: 22/12/2021), <https://www.princelund.com/frp-reinforcement.html>.

Qapo, M., Dirar, S. and Jemaa, Y. (2016) Finite Element Parametric Study of Reinforced Concrete Beams Shear-strengthened with Embedded FRP bars. Composite Structures, 149: 93-105.

Qin, S. (2016) Shear Behaviour of Corroded Reinforced Concrete T-Beams Repaired with Fibre Reinforced Polymer Systems. PhD Thesis, University of Birmingham.

Qin, S., Dirar, S., Yang, J., Chan, A.H.C. and Elshafie, M. (2015) CFRP Shear Strengthening of Reinforced Concrete T-beams with Corroded Shear Links. ASCE Journal of Composites for Construction, 19(5): 04014081.

Rahal, K.N. and Rumaih, H.A. (2011) Tests on Reinforced Concrete Beams Strengthened in Shear Using Near Surface Mounted CFRP and Steel Bars. Engineering Structures, 33(1): 53-62.

Raicic, V. (2018) Deep embedment shear strengthening of reinforced concrete continuous T-beams, PhD Thesis, University of Bath.

Raicic, V., Ibell, T., Darby, A., Evernden, M. and Orr, J. (2017) Effectiveness of the Deep Embedment (DE) Technique for Shear Strengthening of Reinforced Concrete Continuous Beams. In: Proceedings of the 8th International Conference on Advanced Composites in Construction (ACIC 2017), Sheffield, 5-7 September 2017. pp. 6.

Reineck, K.H. (1991) Ultimate Shear Force of Structural Concrete Members without Transverse Reinforcement Derived from a Mechanical Model. *ACI Structural Journal*, 88 (5): 592-602.

Ritter, W. (1899) Die Bauweise Hennebique. *Schweizerische Bauzeitung*, 33 (7): 59–61.

Rizzo, A. and De Lorenzis, L. (2009) Behavior and Capacity of RC Beams Strengthened in Shear with NSM FRP Reinforcement. *Construction and Building Materials*, 23 (4): 1555-1567.

Saribiyik, A., Abodan, B. and Balci, M.T. (2021) Experimental Study on Shear Strengthening of RC Beams with Basalt FRP Strips using Different Wrapping Methods. *Engineering Science and Technology, an International Journal*, 24(1): 192-204.

Seo, J., Lee, J. and Lopez, M. M. (2015) Parametric Study on Shear Performance for Steel Fiber Reinforced Concrete Beams. *Advances in Structural Engineering*, 18 (7): 1115–1127.

Schlaich, J., Schäfer, K. and Jennewein, M. (1987) Toward a Consistent Design of Structural Concrete. *PCI Journal*, 32 (3): 74-150.

Schmidt, M., Schmidt, P.; Wanka, S. and Classen, M. (2021) Shear Response of Members without Shear Reinforcement—Experiments and Analysis Using Shear Crack Propagation Theory. *Applied Sciences*, 11 (7): 3078.

Smith, K.N. and Fereig S.M. (1977) Mechanism of Shear Transfer in Reinforced Concrete Beams. *Canadian Journal of Civil Engineering*, 4(2): 145-152.

Subramanian, N. (2013) Design of Reinforced Concrete Structures. Oxford University Press, India.

Sogut, K., Dirar, S., Theofanous, M. and Faramarzi, A. (2022). Effect of FRP Bar Type on the Behaviour of Shear-strengthened Reinforced Concrete T-beams. In: Ilki, A., Ispir, M., Inci, P. (eds), 10th International Conference on FRP Composites in Civil Engineering, CICE 2021, Lecture Notes in Civil Engineering, vol 198.

Sogut, K., Dirar, S., Theofanous, M., Faramarzi, A. and Nayak, A. N. (2021) Effect of Transverse and Longitudinal Reinforcement Ratios on the Behaviour of RC T-beams Shear Strengthened with Embedded FRP Bars. Composite Structures, 113622.

Sogut, K., Dirar, S., Theofanous, M. and Faramarzi, A. (2019a). Effect of Existing Steel-to-Embedded FRP Shear Reinforcement Ratio on the Behaviour of Reinforced Concrete T-beams. In: Proceedings of the 9th International Conference on Advanced Composites in Construction, (ACIC 2019), Birmingham, UK, September 3-5, 2019.

Sogut, K., Dirar, S., Theofanous, M. and Faramarzi, A. (2019b). Size Effect in Shear-deficient Reinforced Concrete T-beams Strengthened with Embedded FRP Bars. In: Proceedings of the 14th International Symposium on Fiber-Reinforced Polymer Reinforcement for Concrete Structures, (FRPRCS-14), Belfast, UK, June 4-7, 2019.

Sonnenberg, A.M.C. and Al-Mahaidi, R. (2007) Investigation of Dowel Shear in RC Beams using Photogrammetry. Magazine of Concrete Research, 59 (9): 621-626.

Taylor, H.P.J. (1971) Fundamental Behaviour in Bending and Shear of Reinforced Concrete. PhD Thesis, City, University of London.

Taylor, H.P.J. (1974) The Fundamental Behavior of Reinforced Concrete Beams in Bending and Shear. ACI Special Publication, 42: 43-78.

Teng, J.G., Chen, J.F., Smith, S.T. and Lam, L. (2003) Behaviour and Strength of FRP-Strengthened RC Structures: A State-of-the-art Review. *Proceedings of the Institution of Civil Engineers - Structures and Buildings*, 156 (1): 51-62.

Tetta, Z.C., Koutas, L.N. and Bournas, D.A. (2018) Shear Strengthening of Concrete Members with TRM Jackets: Effect of Shear Span-to-Depth Ratio, Material and Amount of External Reinforcement. *Composites Part B: Engineering*, 137: 184-201.

Tetta, Z.C., Koutas, L.N. and Bournas D.A. (2015) Textile-reinforced Mortar (TRM) versus Fiber-reinforced Polymers (FRP) in Shear Strengthening of Concrete Beams. *Composites Part B: Engineering*, 77: 338-348.

Thermou, G.E., Papanikolaou, V.K., Lioupis, C. and Hajirasouliha, I. (2019) Steel-Reinforced Grout (SRG) Strengthening of Shear-critical RC Beams. *Construction and Building Materials*, 216: 68-83.

Thorenfeldt, E., Tomaszewicz, A. and Jensen, J.J. (1987) Mechanical Properties of High-Strength Concrete and Applications in Design. In: *Proceedings of the Symposium on Utilization of High Strength Concrete*, Stavanger, 15–18 June 1987. p. 149–159.

TIS 24-2548 (2003). Steel Bars for Reinforced Concrete: Deformed bars. Thai Industrial Standards Institute (TISI), Thailand.

Triantafillou, T.C. (1998) Shear Strengthening of Reinforced Concrete Beams Using Epoxy-Bonded FRP Composites. *ACI Structural Journal*, 95(2): 107-115.

Triantafillou, T.C. and Papanicolaou, C.G. (2006) Shear Strengthening of Reinforced Concrete Members with Textile Reinforced Mortar (TRM) Jackets. *Materials and Structures*, 39: 93-103.

Valerio, P. and Ibell, T.J. (2003) Shear Strengthening of Existing Concrete Bridges. Proceedings of the Institution of Civil Engineers, Structures and Buildings, 156(1):75-84.

Valerio, P., Ibell, T.J. and Darby, A.P. (2009) Deep Embedment of FRP for Concrete Shear Strengthening. Proceedings of Institution of Civil Engineers: Structures and Buildings, 162(5): 311-321.

Vecchio, F.J. (2000) Disturbed Stress Field Model for Reinforced Concrete: Formulation. ASCE Journal of Structural Engineering, 126(9): 1070-1077.

Vecchio, F.J. and Collins M.P. (1986) The Modified Compression Field Theory for Reinforced Concrete Elements Subjected to Shear. ACI Structural Journal, 83(2) 219–231.

Vecchio, F.J. and Collins, M.P. (1993) Compression Response of Cracked Reinforced Concrete. ASCE Journal of Structural Engineering, 119(12): 3590-3610.

Wagner (1929) Ebene Blechwandträger mit sehr dünnem Stegblech. Zeitschrift für Flugtechnik und Motorluftschiffahrt, Berlin, Volume 20; Translation into English: Flat sheet metal girders with very thin metal web, NACA Technical Memorandum No. 604.

Wang, P. T., Shah, S. P. and Naaman, A. E. (1978) Stress-strain Curves of Normal and Lightweight Concrete in Compression. ACI Journal Proceedings, 75(11): 603–611.

Walraven, J.C. and Reinhardt, H.W. (1981) Theory and Experiments on the Mechanical Behaviour of Cracks in Plain and Reinforced Concrete Subjected to Shear Loading. Heron, 26 (1).

Wong, P.S., Vecchio, F.J. and Trommels, H. (2013) VecTor2 & FormWorks user's manual (second edition). Toronto: University of Toronto.

Wu, H.C. and Eamon C.D. (2017) Strengthening of Concrete Structures Using Fiber Reinforced Polymers (FRP): Design, Construction and Practical Applications. Woodhead Publishing, UK.

Yu, Q. and Bažant P. (2011) Can Stirrups Suppress Size Effect on Shear Strength of RC Beams? ASCE Journal of Structural Engineering, 137 (5): 607-617.

Zhang, N. and Tan, K.H. (2007) Size Effect in RC Deep Beams: Experimental Investigation and STM Verification. Engineering Structures, 29 (12): 3241-3254.

Zhang, Z., Thomas Hsu., C.T. and Moren, J. (2004) Shear Strengthening of Reinforced Concrete Deep Beams using Carbon Fiber Reinforced Polymer Laminates. ASCE Journal of Composites for Construction, 8 (5):403–414.